UNIVERSITY OF CALIFORNIA SAN DIEGO

Selective targeting of WNT receptor FZD7 in human pluripotent stem cells and ovarian cancer

A dissertation submitted in partial satisfaction of the requirements for the degree
Doctor of Philosophy

in

Biomedical Sciences

by

Myan Do

Committee in charge:

Professor Karl Willert, Chair
Professor Steven Dowdy
Professor Dan Kaufman
Professor Jill Mesirov
Professor Tannishtha Reya

2021

The dissertation of Myan Do is approved, and it is acceptable in quality and form for publication on microfilm and electronically.

University of California San Diego

2021

DEDICATION

For my parents, who sacrificed everything for my education and opportunities, and for coffee, which got me out of bed and into lab each morning.

TABLE OF CONTENTS

LIST OF FIGURES

ACKNOWLEDGEMENTS

I would like to acknowledge Professor Karl Willert, my committee chair, for his support and trust in my science and my writing, and for tolerating my stubbornness.

Chapter 1, in full, is a reprint of the material as it appears in *eLife*, 2020. Gumber, D.*, Do, M.*, Suresh Kumar, N., Sonavane, P.R., Wu, C.C.N., Cruz, L.S., Grainger, S., Carson, D., Gaasterland, T., Willert, K. The dissertation author was a co-primary investigator and co-author of this paper.

Chapter 2, in full, is currently being prepared for submission for publication of the material. Do, M., Wu, C.C.N., Sonavane, P.R., Juarez, E.F., Adams, S.R., Ross, J., Rodriguez y Baena, A., Patel, C., Mesirov, J.P., Carson, D.A., Advani, S.J., Willert, K. The dissertation author was the primary investigator and author of this paper.

I would like to acknowledge UC San Diego (UCSD) Transgenic Mouse Services for technical assistance with generating the *Fzd7*$^{hF7/hF7}$ mouse line; UCSD Tissue Technology Shared Resource for performing hematoxylin and eosin (H&E) and immunohistochemistry (IHC) staining; Dr. Nissi Varki (UCSD) for IHC analyses; Jesus Olvera and Cody Fine of the UCSD Human Embryonic Stem Cell Core Facility for technical assistance with flow cytometry experiments; and UCSD Nikon Imaging Center for technical assistance with confocal imaging. I am grateful to Dr. Dina Hingorani and Maria Fernanda Camargo (UCSD) for initial help with antibody-drug conjugate synthesis and tumor xenograft mouse models. I am also grateful to Drs. Sundaram Ramakrishnan (University of Miami) and Dan Kaufman (UCSD) for kindly providing the MA-148 cell line, Dr. Michael Boutros (Heidelberg University) for the HEK293T FZD1,2,7-KO cell line, Dr. Mark Mercola (Stanford University) for the H9 T-GFP cell line, Dr. Seung Kim (Stanford University) for the H9 SOX17:GFP cell line, Dr. Dan Kaufman for induced pluripotent stem cell lines, Dr. Chad Cowan (Harvard Stem Cell Institute) for Cas9 and guide RNA plasmids, and Drs. Ian Huggins and Steven Dowdy for the pLVX-Luciferase-PuroR plasmid.

VITA

2011 Bachelor of Arts, University of California Berkeley

2015-2021 Graduate Student Researcher, University of California San Diego

2021 Doctor of Philosophy, University of California San Diego

PUBLICATIONS

Gumber, D.*, **Do, M.***, Suresh Kumar, N., Sonavane, P.R., Wu, C.C.N., Cruz, L.S., Grainger, S., Carson, D., Gaasterland, T., Willert, K. “Selective activation of FZD7 promotes mesendodermal differentiation of human pluripotent stem cells.” *eLife*. 9:e63060 (2020).

Do, M., Wu, C.C.N., Sonavane, P.R., Juarez, E.F., Adams, S.R., Ross, J., Rodriguez y Baena, A., Patel, C., Mesirov, J.P., Carson, D.A., Advani, S.J., Willert, K. “A FZD7-specific antibody-drug conjugate induces solid tumor regression in preclinical models.” (In preparation) (2021).

FIELDS OF STUDY

Major Field: Biomedical Sciences

ABSTRACT OF THE DISSERTATION

Selective targeting of WNT receptor FZD7 in human pluripotent stem cells and ovarian cancer

by

Myan Do

Doctor of Philosophy in Biomedical Sciences

University of California San Diego, 2021

Professor Karl Willert, Chair

WNT signaling is a highly conserved pathway with dual roles in development and disease. In human pluripotent stem (hPS) cells, an *in vitro* model of mammalian development, low-level WNT signaling maintains the self-renewal state, but carefully timed increases in WNT can induce terminal differentiation. While the WNT receptor Frizzled-7 (FZD7) is an established regulator of pluripotency in hPS cells, it is unclear if FZD7 or additional FZD receptors mediate the WNT signal that promotes stem cell differentiation. To address whether FZD7 is required for this process, my co-authors and I engineered bispecific antibody F7L6, which acts as a WNT signaling agonist by

selectively heterodimerizing FZD7 and its coreceptor, LRP6. F7L6 treatment of hPS cells elicited a transcriptional response similar to that observed for Wnt3a treatment, thus establishing that FZD7 signaling is sufficient to promote mesendodermal differentiation.

Though WNT signaling is required for normal embryonic development, it can be dysregulated in diseases such as cancer. Targeting WNT signaling in solid tumors has been historically challenging due to the WNT requirement for bone homeostasis. Clinical pan-WNT inhibitors frequently induce bone-related adverse events, creating a need for more specific WNT-pathway targeting strategies. We identified elevated RNA expression of *FZD7* in aggressive subtypes of ovarian serous cystadenocarcinoma (OV) in The Cancer Genome Atlas and confirmed high FZD7 protein expression in OV, but low FZD7 in normal ovary tissues, indicating that FZD7 is a tumor-specific antigen. We developed novel antibody-drug conjugate (F7-ADC), septuximab vedotin, a chimeric human-mouse IgG1 antibody to human FZD7 conjugated to antimitotic payload drug MMAE. The F7-ADC specifically binds FZD7, potently kills ovarian cancer cells *in vitro*, and induces regression of ovarian tumor xenografts in nude mouse models. To evaluate F7-ADC toxicity *in vivo*, we engineered immunocompetent *Fzd7*$^{hF7/hF7}$ mice to express Fzd7^{P188L} receptors reactive with our human-targeting F7-ADC. F7-ADC treatment did not induce adverse effects on *Fzd7*$^{hF7/hF7}$ mouse health or histopathological changes at the tissue level. Overall, our data suggest that the F7-ADC approach may be a powerful strategy to combat FZD7-expressing ovarian cancers in the clinic.

INTRODUCTION

Wnt signaling is a critical and evolutionarily conserved regulator of embryogenesis and adult tissue homeostasis. Wnts were first identified as Wingless (Wg) proteins in *Drosophila melanogaster* [1]. Mutations in the *wingless* (*wg*) gene resulted in flies lacking wings and various thoracic structures, establishing a requirement for Wg/Wnt signaling during early development. *wg* homolog, *int-1* (*Wnt1*) was later identified as a proto-oncogene in mice [2,3]. This suggested that Wnt signaling was necessary for normal development, but deregulated Wnt signaling could give rise to pathologies such as cancer.

A powerful *in vitro* platform to study the early stages of embryonic development are human pluripotent stem (hPS) cells. Endogenous, low-level WNT signaling maintains hPS cells in a self-renewing state [4–7], but carefully timed increases in WNT can induce cell differentiation towards the mesendoderm and definitive endoderm lineages [8–10]. WNT proteins activate cell signaling by engaging numerous WNT receptors, including but not limited to Frizzleds (FZDs), LRP5 and 6, ROR1 and 2 (reviewed in [11]). The mammalian genome encodes 10 FZDs and the function of each during development is not well understood, due to the ability of WNTs to bind and activate multiple FZDs. WNT receptor FZD7 was previously demonstrated to regulate pluripotency in hPS cells, and its downregulation induced differentiation and exit from the pluripotent stem cell state [12,13]. However, it is unclear if FZD7 or additional FZDs mediate the WNT signal that promotes stem cell differentiation [14]. To address whether FZD7 is required for this process, my co-authors and I engineered bispecific antibody F7L6, which acts as a WNT signaling agonist by selectively heterodimerizing FZD7 and its coreceptor, LRP6 [15]. Treatment of hPS cells with F7L6 elicited a transcriptional response similar to that observed for Wnt3a treatment, thus establishing that FZD7 signaling is sufficient to promote mesendodermal differentiation.

While FZD7 is highly expressed during early development, it is downregulated in most adult tissues. However, many types of solid tumors can aberrantly overexpress FZD7, including breast cancer, ovarian cancer, hepatocellular carcinoma, Wilms tumor, gastric cancers, colon

cancer, and melanoma [16–22], which has led to the proposal that targeting FZD7 is a viable option to treat multiple cancers (reviewed in [23,24]). Targeting WNT signaling in solid tumors has been historically challenging due to the requirement of endogenous WNT signaling for bone homeostasis [25–27]. Most WNT-targeting drugs inhibit global WNT signaling and frequently cause bone-related adverse events in patients, despite showing anti-tumor efficacy. Specifically drugging FZD7 may therefore be an alternative strategy to alleviate the bone toxicities caused by pan-WNT inhibitors. To this end, my co-authors and I developed novel antibody-drug conjugate (F7-ADC), septuximab vedotin, a chimeric human-mouse IgG1 antibody to human FZD7 conjugated to antimitotic payload drug, monomethyl auristatin E (MMAE). We demonstrate that the F7-ADC selectively and potently kills human ovarian cancer cells that express high levels of FZD7 *in vitro*, as well as FZD7-high ovarian tumor xenografts *in vivo*. Additionally, we did not observe toxicities following F7-ADC treatment in *Fzd7*$^{hF7/hF7}$ mice, which we engineered to react with our human-targeting F7-ADC. Taken together, our F7-ADC approach to targeting FZD7 may be a powerful strategy to combat a variety of aggressive solid tumors in the clinic.

CHAPTER 1:

SELECTIVE ACTIVATION OF FZD7 PROMOTES MESENDODERMAL DIFFERENTIATION OF HUMAN PLURIPOTENT STEM CELLS

1.1 INTRODUCTION

WNTs are highly conserved, lipid-modified secreted proteins with a broad range of activities throughout development and during adult tissue homeostasis (reviewed in [28]). Deregulated WNT activity is associated with many pathologies, including degenerative and age-related diseases and cancer (reviewed in [29]). With the human genome encoding 19 WNTs and an equally large number of WNT receptors (Frizzled [FZD]1-10, LRP5 and 6, ROR1 and 2, RYK, PTK7 and more; reviewed in [11]), relatively little is known about signaling specificities between WNT ligands and their receptors. In experimental settings, activation of WNT signaling with either purified recombinant WNT proteins, such as Wnt3a, or with small molecule agonists, such as GSK3 inhibitors, frequently elicits the desired downstream transcriptional effect. Such observations have led to the prevailing and oversimplified view that specific WNT-receptor interactions are not as critical as the ensuing downstream signaling event. Because of the lack of selectivity between WNTs and their receptors in vitro and the paucity of purified and biologically active WNT proteins, it has not been possible to address whether engagement of a single WNT receptor is sufficient to elicit the complex biological processes affected by WNT.

Human pluripotent stem (hPS) cells provide a powerful in vitro system to study early processes of human development. The role of WNT signaling in the regulation of pluripotency is dependent on both the developmental stage of the cells and on the level of signaling. Experiments in mouse embryonic stem cells, which reside in the naïve state (reviewed in [30]), have indicated a role for WNT/β-catenin signaling in self renewal and maintenance of pluripotency. In contrast, in hPS cells, which reside in the primed state and resemble epiblast-derived stem cells [31], WNT/β-

catenin signaling drives mesendodermal lineage specification, and an analysis of transcriptome-wide gene expression changes over a time-series treatment of hPS cells with Wnt3a reveals a transcriptional response reminiscent of primitive streak formation and ensuing gastrulation [14]. This is consistent with observations that short-term activation of Wnt/β-catenin signaling, via addition of Wnt3a, promotes differentiation towards definitive endoderm [32]. Furthermore, a low level of endogenous WNT activity is detectable in undifferentiated hPS cells [33,34] and is required for reprogramming of human fibroblasts to an induced pluripotent stem (iPS) cell state [35].

The WNT receptor FZD7 plays a prominent role in the regulation of pluripotency of hPS cells, and its downregulation accompanies differentiation and exit from the pluripotent stem cell state. However, since hPS cells express several WNT receptors, including FZD2, 3 and 5 [12,14], it is unclear whether Wnt3a promotes mesendodermal differentiation through FZD7 or whether other FZDs are required.

Here, we describe the development and characterization of a highly specific antibody and derivative single chain variable fragment (scFv) to FZD7. Fusing this FZD7-specific scFv to an LRP6-directed scFv creates a bi-specific binder, called F7L6, with potent WNT signaling activities that require FZD7 expression. Treatment of hPS cells with F7L6 elicits a transcriptional response similar to that observed for Wnt3a treatment, establishing that signaling through FZD7 is sufficient to promote mesendodermal differentiation.

1.2 RESULTS

Design, specificity, and expression of F7L6.

WNT/β-catenin signaling is initiated by WNT binding to and heterodimerizing the cell surface receptors FZD and either LRP5 or LRP6. To study the role of one specific FZD protein, FZD7, which is highly expressed in hPS cells [12,13], we developed a bi-specific binder to human FZD7 and LRP6, called F7L6. We generated a single chain variable fragment (scFv) to FZD7 by repurposing the variable region of our FZD7-targeting antibody (F7-Ab), a chimeric human/mouse IgG1. This antibody was derived from a bacterially produced antigen binding fragment (Fab) described in a previous study [12]. In parallel, we engineered an scFv to the third □-propeller domain of LRP6 based on previously published LRP6 antibodies [36]. We then engineered F7L6 by conjugating the FZD7-scFv and LRP6-scFv to a human IgG1 Fc to create the FZD7-specific Wnt mimetic F7L6 (complete amino acid sequence is provided in **Figure 1**). Additionally, we generated a FZD7-scFv-Fc (F7) and an LRP6-scFv-Fc (L6) (**Figure 2A**). We confirmed secretion of F7-Ab, F7, L6, and F7L6 from CHO cells by SDS-PAGE and Coomassie Blue staining and immunoblotting (**Figure 2B**). Using a dot blot with lysates of HEK293T cells carrying loss of function mutations in FZD1, 2 and 7 (F127-KO) (Voloshanenko et al., 2017) or in LRP6 (LRP6-KO) [37] confirmed binding specificity of each of these molecules. FZD7-specific binders (F7 and F7L6) only reacted with lysates upon FZD7 overexpression (note that endogenous FZD7 expression in LRP6 KO is below the level of detection), whereas LRP6 specific binders (L6 and F7L6) only reacted with lysates of cells expressing LRP6 (**Figure 2C**).

To further characterize the specificity of F7-Ab, we mapped its binding site to the “neck” region between the cysteine rich domain (CRD) and the first transmembrane domain of FZD7 (**Figure 2D**). Despite the high degree of homology between human and mouse Fzd7 (hFZD7 and mFzd7, respectively), F7-Ab only reacts with hFZD7 (**Figure 2E**). Protein alignment (**Figure 2D**) indicated that this neck region was the only extracellular portion harboring differences between

hFZD7 and mFzd7 (disregarding the amino-terminal signal sequence). A single amino acid change at position 188 from leucine to proline (P188) renders hFZD7 non-reactive to F7-Ab, whereas the corresponding amino acid change in mFzd7 (L188) restores F7-Ab reactivity (**Figure 2E**). Using fusion proteins between glutathione S-transferase (GST) and the FZD7 neck region followed by sequential shortening of the neck region, we mapped the F7-Ab epitope to an 8 amino acid stretch containing L188 (**Figure 2F**). Since FZD proteins are highly conserved and several available FZD antibodies react with multiple FZD proteins (for example, OMP-18R5/Vantictumab reacts with FZD1, 2, 5, 7 and 8), we confirmed that F7-Ab does not cross-react with the other nine human FZD receptors (FZD1-6, 8-10) (**Figure 2G**). To rule out the possibility that some FZDs fail to react with F7-Ab because they do not reach the cell surface, we performed confocal microscopy. This analysis confirmed that all FZD proteins were expressed on the cell surface (**Figure 3**). Taken together, F7-Ab, and hence F7 and F7L6, are specific to hFZD7 and do not cross-react with any of the other 9 human FZD proteins or with mFzd7.

Amino acid #	Domain
2-21	Ig kappa chain signal peptide
22-27	His tag
28-148	Heavy chain variable anti-FZD7
149-163	GS linker
164-270	Light chain variable anti-FZD7
271-284	GS linker
285-392	Light chain variable anti-LRP6 Bp3
393-412	GS linker
413-531	Heavy chain variable anti-LRP6 Bp3
532-762	Human IgG1 Fc

```
1   METDTLLLWV LLLWVPGSTG DHHHHHHGEV QLVESGGGLV QPKGSLKLSC
51  AASGFTFNTY AMHWVRQAPG KGLEWVARIR SKSNNYAKNY DDSVKDRFTI
101 SRDDSQSMLY LQMNNLKTED TAMYYCVREN YGGRFDYWGQ GTLVTVSSGG
151 GGSGGGGSGG GGSDIVMTQS PKSMSMSVGE RVTLRCKASE NVLNYVSWYQ
201 QKPEQSPKLL IYGASNRYTG VPDRFTGSGS ATDFTLTISS VQAEDLADYH
251 CGQSYRYPTF GAGTKLELKY GGGGSGGGGS GGGGDIVLTQ SPATLSLSPG
301 ERATLSCRAS QFIGSRYLAW YQQKPGQAPR LLIYGASNRA TGVPARFSGS
351 GSGTDFTLTI SSLEPEDFAT YYCQQYYDYP QTFGQGTKVE IKGGGGSGGG
401 GSGGGGSGGG GSQVQLKESG PALVKPTQTL TLTCTFSGFS LSNRGGGVGW
451 IRQPPGKALE WLAWIDWDDD KSYSTSLKTR LTISKDTSKN QVVLTMTNMD
501 PVDTATYYCA RFHLPLVFDS WGQGTLVTVS SMVRSDKTHT CPPCPAPELL
551 GGPSVFLFPP KPKDTLMISR TPEVTCVVVD VSHEDPEVKF NWYVDGVEVH
601 NAKTKPREEQ YNSTYRVVSV LTVLHQDWLN GKEYKCKVSN KALPAPIEKT
651 ISKAKGQPRE PQVYTLPPSR EEMTKNQVSL TCLVKGFYPS DIAVEWESNG
701 QPENNYKTTP PVLDSDGSFF LYSKLTVDKS RWQQGNVFSC SVMHEALHNH
751 YTQKSLSLSP GK
```

Figure 1.
Complete amino acid sequence of His-tagged F7L6.

Figure 2. Design, specificity and expression of F7L6.
(**A**) Schematic of FZD7- and LRP6-specific binders. Red blocks depict the variable light (V_L) and heavy (V_L) antibody domains that recognize FZD7 and were fused to form the single-chain variable fragment (scFv) in F7 and F7L6. Purple blocks depict the scFv that recognizes LRP6 and is used in L6 and F7L6. (**B**) Expression of FZD7- and LRP-specific binders. Transgenes encoding F7-Ab, F7, L6 and F7L6 were stably transduced in CHO cells. Recombinant proteins were harvested and purified from conditioned media and detected by Coomassie Blue staining (upper) and anti-human-Fc immunoblot (lower). (**C**) Binding specificity of F7, L6, and F7L6. HEK293T carrying mutations in FZD1, 2, and 7 (F127-KO) or in LRP6 (LRP6-KO) were transfected with FZD7 and LRP6, respectively, and whole cell lysates were probed in a dot blot format with conditioned media containing F7, L6, or F7L6. As a negative control (Mock), blots were incubated with CM from untransfected CHO cells. (**D**) Schematic of FZD7 and amino acid alignment of the extracellular "neck" region of hFZD7 and mFzd7. The dashed oval indicates the neck region. The red box in the amino acid sequences indicates amino acid position 188. (**E**) HEK293T cells were transiently transfected with the indicated V5-tagged transgenes, and cell lysates were probed with either F7-Ab or V5 antibody (α-V5). Mock = untransfected cells. (**F**) Mapping F7-Ab epitope to an 8 amino acid sequence. Bacterial lysates containing fusion proteins between GST and the FZD7 peptide sequences indicated in the table were detected by Coomassie staining (top) or by immunoblotting with F7-Ab (bottom). Abbreviations in table: aa188, amino acid at position 188; aa#, number of amino acids in FZD7 peptide; L, leucine; P, proline. (**G**) F7-Ab is specific to human FZD7 and does not cross-react with the other nine FZDs (1-6, 8-10). F127-KO were transfected with expression constructs carrying the indicated human FZD cDNAs tagged with an intracellular V5 sequence. Non-permeabilized cells were stained with F7-Ab for cell-surface FZD expression, and then permeabilized and stained for V5 expression. All FZD receptors were expressed as revealed by anti-V5 antibody staining.

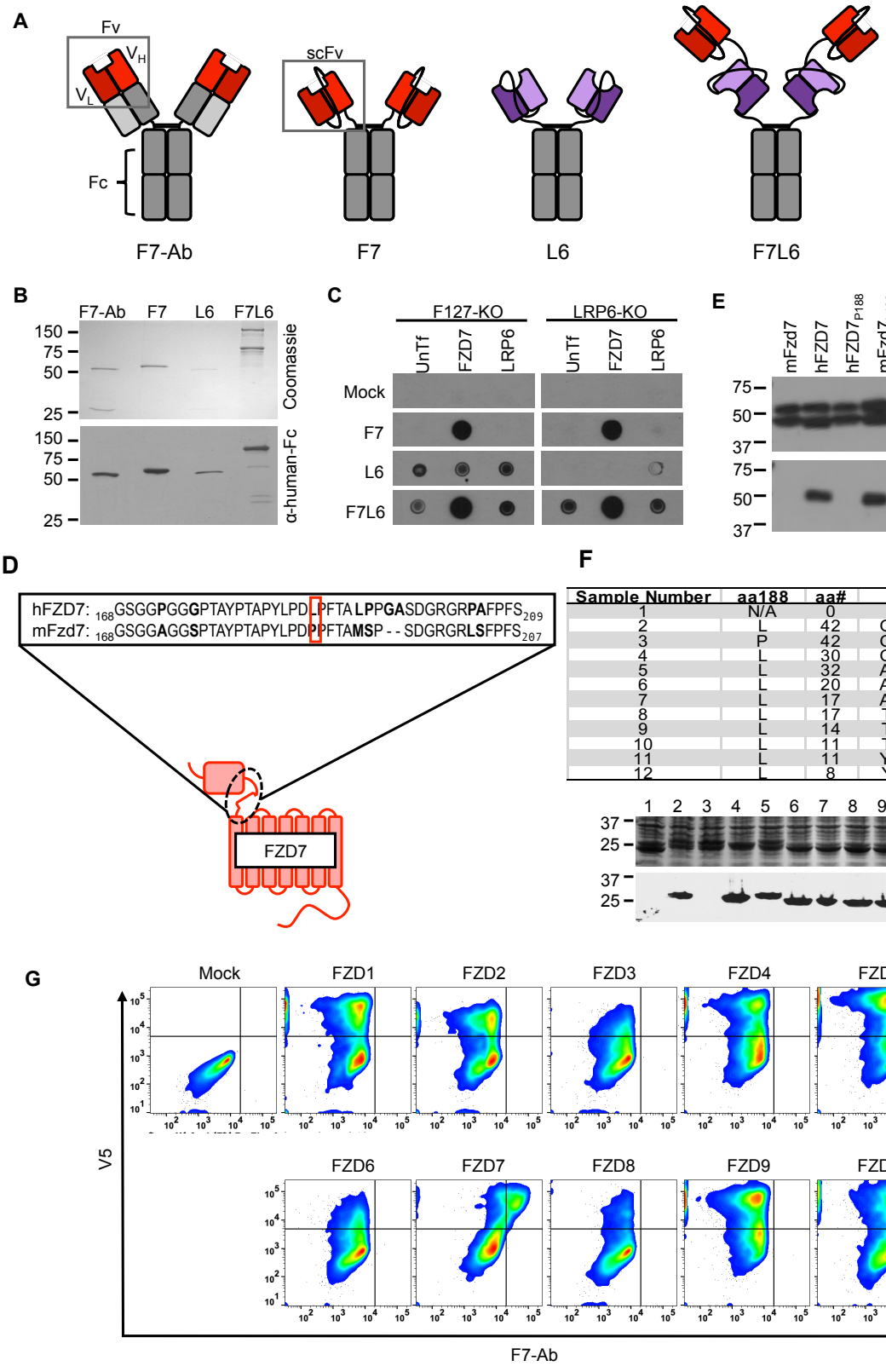
A
Fv
V_H
V_L
Fc
scFv
F7-Ab
F7
L6
F7L6
B
F7-Ab F7 L6 F7L6
150
75
50
25
Coomassie
α-human-Fc
C
F127-KO
LRP6-KO
UnTf
FZD7
LRP6
Mock
F7
L6
F7L6
E
mFzd7
hFZD7
$hFZD7_{P188}$
$mFzd7_{L188}$
Mock
α-V5
F7-Ab
D
hFZD7: $_{168}$GSGGPGGGPTAYPTAPYLPDLPFTALPPGASDGRGRPAFPFS$_{209}$
mFzd7: $_{168}$GSGGAGGSPTAYPTAPYLPDPPFTAMSP - - SDGRGRLSFPFS$_{207}$
FZD7
F
Sample Number | aa188 | aa# | Epitope
1 | N/A | 0 | N/A (GST)
2 | L | 42 | G168 -> S209
3 | P | 42 | G168 -> S209
4 | L | 30 | G168 -> A197
5 | L | 32 | A178 -> S209
6 | L | 20 | A178 -> A197
7 | L | 17 | A178 -> P194
8 | L | 17 | T181 -> A197
9 | L | 14 | T181 -> P194
10 | L | 11 | T181 -> T191
11 | L | 11 | Y184 -> P194
12 | L | 8 | Y184 -> T191
1 2 3 4 5 6 7 8 9 10 11 12
37
25
G
Mock
FZD1
FZD2
FZD3
FZD4
FZD5
FZD6
FZD7
FZD8
FZD9
FZD10
V5
F7-Ab

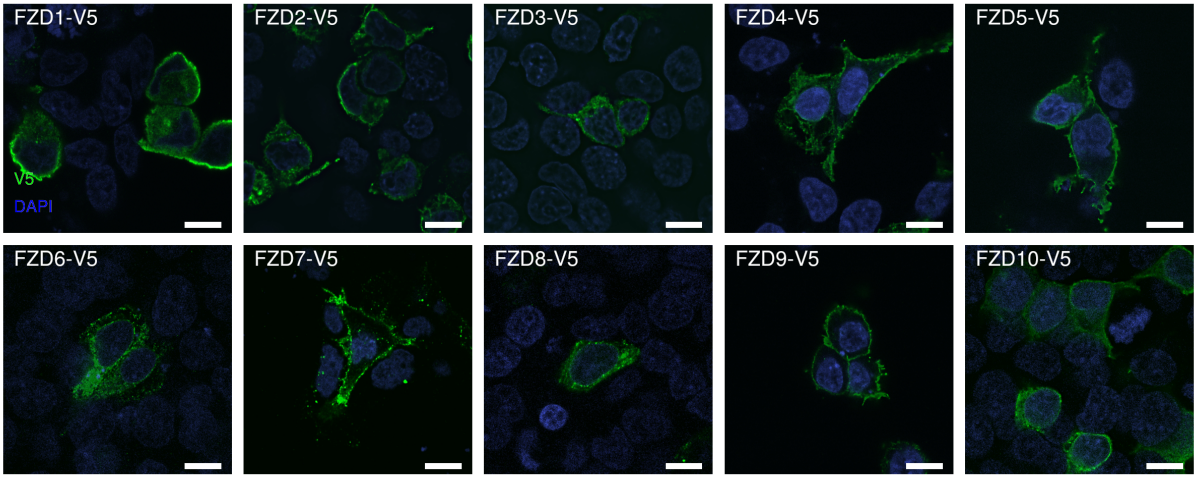

Figure 3.
Immunofluorescent detection of V5-tagged FZD1-10 demonstrates cell surface localization. Scale bar = 10 µm.

F7L6 activates Wnt/β-catenin signaling.

The bi-specific binder, F7L6, activates WNT/ β-catenin signaling by heterodimerizing FZD7 and LRP6 (**Figure 4A**). We confirmed F7L6 signaling activity using HEK293T cells stably transfected with the WNT reporter Super TOP-Flash (STF) [38] (**Figure 4B**). As expected, single binders to FZD7 (F7) or LRP6 (L6) did not activate signaling. As is the case with native WNT proteins, activity of F7L6 is potently augmented by addition of R-Spondin1 (RSPO1) [39] (**Figure 4C**) with potency in the single digit nano-molar range. Interestingly, addition of RSPO1 increased F7L6 activity approximately 10-fold, but only augmented the activities of Wnt3a or FLAg F^{P+P}-L^{1+3}, a previously published WNT mimetic [40], by 2-fold (**Figure 5**). A possible reason for this distinction is that F7L6 is selective for FZD7, whereas Wnt3a and FLAg F^{P+P}-L^{1+3} are capable of interacting with multiple FZDs. Furthermore, both Wnt mimetics retain significant activity at sub nano-molar concentrations whereas Wnt3a's activity is undetectable at such concentrations.

In contrast to WNT, which binds to the CRD of FZD [41], F7L6 binds to the neck region between the CRD and first transmembrane domain, allowing us to assess the requirement of the CRD in signaling. Interestingly, FZD7 lacking the CRD (CRD-less FZD7) activates signaling when heterodimerized to LRP6 with F7L6 while Wnt3a does not (**Figure 4D**), indicating that the CRD is dispensable for signaling. Furthermore, appending the F7-Ab epitope of 8 amino acids (see **Figure 4F**) onto another FZD, FZD2, is sufficient for F7L6 to activate WNT/β-catenin signaling through FZD2 (**Figure 4E**). These data establish that heterodimerization of FZD7 or FZD2 with LRP6 is sufficient for pathway activation.

Treatment of mouse L-cells with Wnt3a activates downstream signaling, as assayed by cytoplasmic β-catenin stabilization [42], whereas treatment with F7L6 does not (**Figure 4F**), consistent with the lack of reactivity of F7-Ab with mouse Fzd7 (see **Figure 2E**). However, overexpression of human FZD7 in these cells is sufficient to activate signaling by F7L6 (**Figure 4F**), thus confirming F7L6 signaling specificity through FZD7. The kinetics of β-catenin

stabilization in L-cells is similar for Wnt3a and F7L6, being first detectable between 15 and 30 minutes after stimulation (**Figure 4G**). Lastly, using reverse transcription quantitative PCR (RT-qPCR), we demonstrated that F7L6, like Wnt3a, activates expression of the WNT target gene, *SP5*, in hPS cells, which express FZD7, in a dose-dependent manner (**Figure 4H, Figure 6**). In sum, F7L6 potently induces WNT/β-catenin signaling through FZD7.

F7L6 is a bi-specific bivalent (or tetravalent) molecule, potentially capable of simultaneously engaging two FZD7 and two LRP6 molecules, thus leading to receptor oligomerization, which has been proposed to promote intracellular signalosome formation [43]. To address whether FZD7-LRP6 heterodimerization alone is sufficient for signaling, we deleted the Fc portion to generate a single chain F7L6 (F7L6-sc) that is predicted to engage one FZD7 and one LRP6 receptor. F7L6-sc activated Wnt signaling, albeit to a lesser extent than the tetravalent F7L6 protein (**Figure 4I**). Interestingly, the maximal response in the STF assay for F7L6 was approximately twice that for F7L6-sc. Size exclusion chromatography confirmed that F7L6-sc is monomeric in solution and does not form larger oligomers (**Figure 7).** These data demonstrate that a 1:1 association of FZD7 and LRP6 is sufficient to activate downstream signaling.

Figure 4. F7L6 activates Wnt/B-catenin signaling.
(**A**) Schematic of the proposed mechanism of action of F7L6 through the heterodimerization of FZD7 and LRP6 at the cell surface. (**B**) F7L6 activation of the WNT signaling pathway was evaluated using a luciferase-based WNT reporter (Super TOP-Flash, STF) assay. HEK293T stably transduced with the WNT reporter Super TOP-Flash (STF) were treated with indicated conditioned media for 24 hours and then assayed for luciferase activity. (**C**) F7L6 signaling activity is augmented by RSPO1. HEK293T:STF cells were treated with the indicated concentrations of F7L6 in the presence or absence of RSPO1 (100 ng/mL) for 24 hours and then assayed for luciferase activity (RLU = relative light units). (**D**) F7L6 activates signaling independently of the WNT-binding cysteine-rich domain (CRD). F127-KO cells carrying the STF reporter were transfected with expression plasmids carrying wildtype FZD7 or CRD-less FZD7, treated with Wnt3a or F7L6 for 24 hours and then assayed for luciferase activity. Inset illustrates FZD7 lacking the CRD. (**E**) F7L6 activates FZD2 tagged with the 8-amino acid epitope of FZD7. F127-KO cells carrying the STF reporter were transfected with expression plasmids carrying wildtype FZD2 or FZD2-8aa, treated with Wnt3a or F7L6 for 24 hours and then assayed for luciferase activity. Inset illustrates FZD2 (blue) with the 8-amino acid FZD7 tag (red). (**F**) F7L6 leads to β-catenin stabilization in mouse L-cells expressing human FZD7. Untransfected (L) or FZD7-expressing (L-FZD7) L-cells were treated with 10 nM F7L6 or Wnt3a for 3 hours. Cell lysates were immunoblotted for β-catenin and FZD7. Blotting for β-actin served as a loading control. (**G**) F7L6 leads to β-catenin stabilization in a time-dependent manner. L and L-FZD7 cells were treated with 10 nM Wnt3a or F7L6 for the indicated times, and cell lysates were immunoblotted for β-catenin. Blotting for β-actin served as a loading control. (**H**) F7L6 activates *SP5* expression in hPS cells in a dose-dependent manner. H1/WA01 cells were treated with the indicated doses of F7L6 or Wnt3a for 24 hours. RNA was analyzed by qRT-PCR. Data represented as mean ± SEM for three technical replicates, with a nonlinear regression curve. All samples were normalized to the 0 nM (buffer) control. (**I**) Bivalent and tetravalent Wnt mimetics activate Wnt signaling. HEK293T:STF cells were treated with indicated concentrations of either F7L6 (tetravalent) or F7L6-sc (bivalent) in the presence of RSPO1 (100 ng/mL) for 24 hours and then assayed for luciferase activity (RLU = relative light units). For all statistical analyses: one-way ANOVA and Tukey's multiple comparisons test: ****$p \leq 0.0001$, *$p \leq 0.05$.

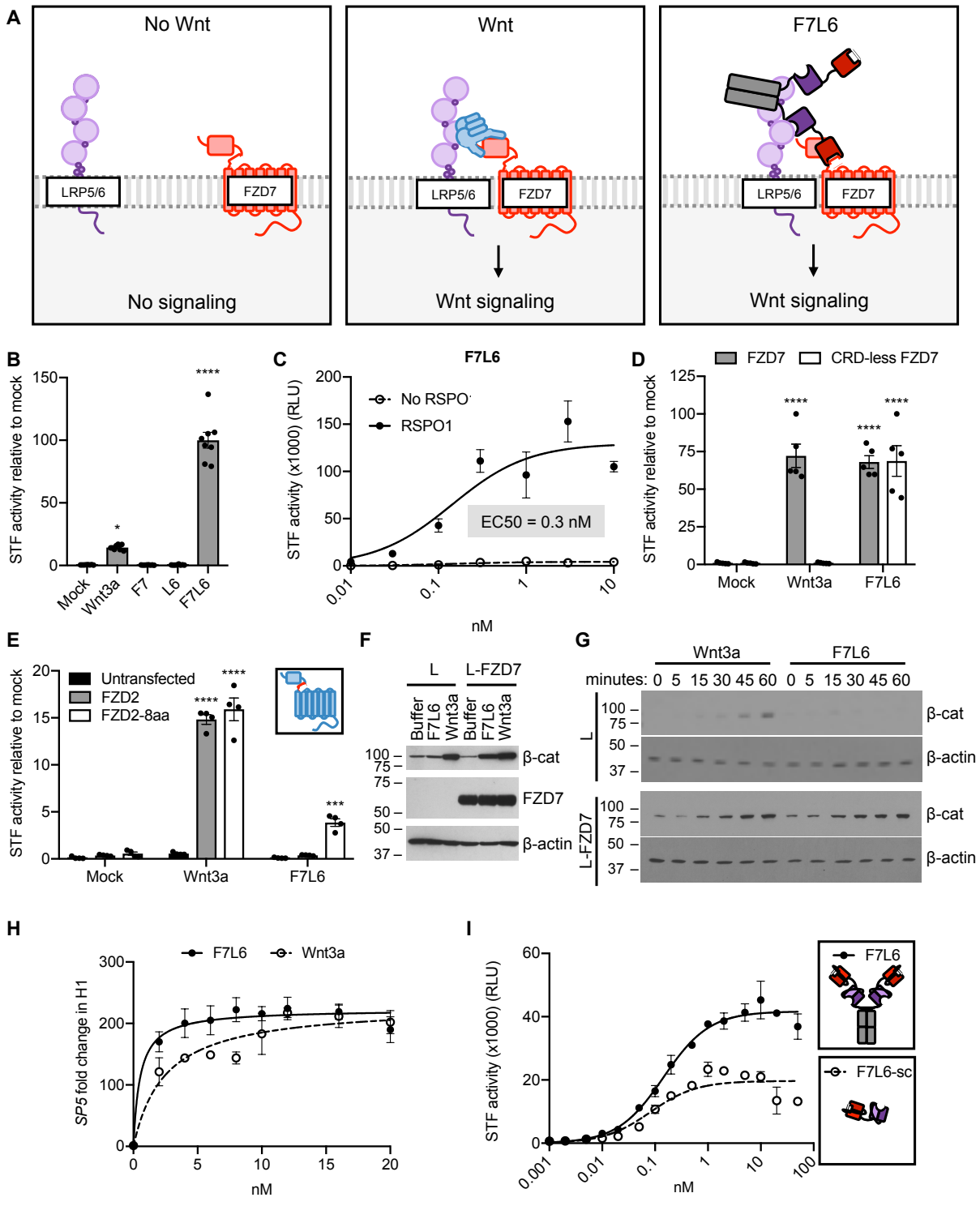
A
No Wnt
LRP5/6
FZD7
No signaling
Wnt
LRP5/6
FZD7
Wnt signaling
F7L6
LRP5/6
FZD7
Wnt signaling
B
STF activity relative to mock
Mock
Wnt3a
F7
L6
F7L6
C
F7L6
No RSPO
RSPO1
STF activity (x1000) (RLU)
EC50 = 0.3 nM
nM
D
FZD7
CRD-less FZD7
STF activity relative to mock
Mock
Wnt3a
F7L6
E
Untransfected
FZD2
FZD2-8aa
STF activity relative to mock
Mock
Wnt3a
F7L6
F
L
L-FZD7
Buffer
F7L6
Wnt3a
β-cat
FZD7
β-actin
G
Wnt3a
F7L6
minutes: 0 5 15 30 45 60 0 5 15 30 45 60
L
L-FZD7
β-cat
β-actin
H
F7L6
Wnt3a
SP5 fold change in H1
nM
I
F7L6
F7L6-sc
STF activity (x1000) (RLU)
nM

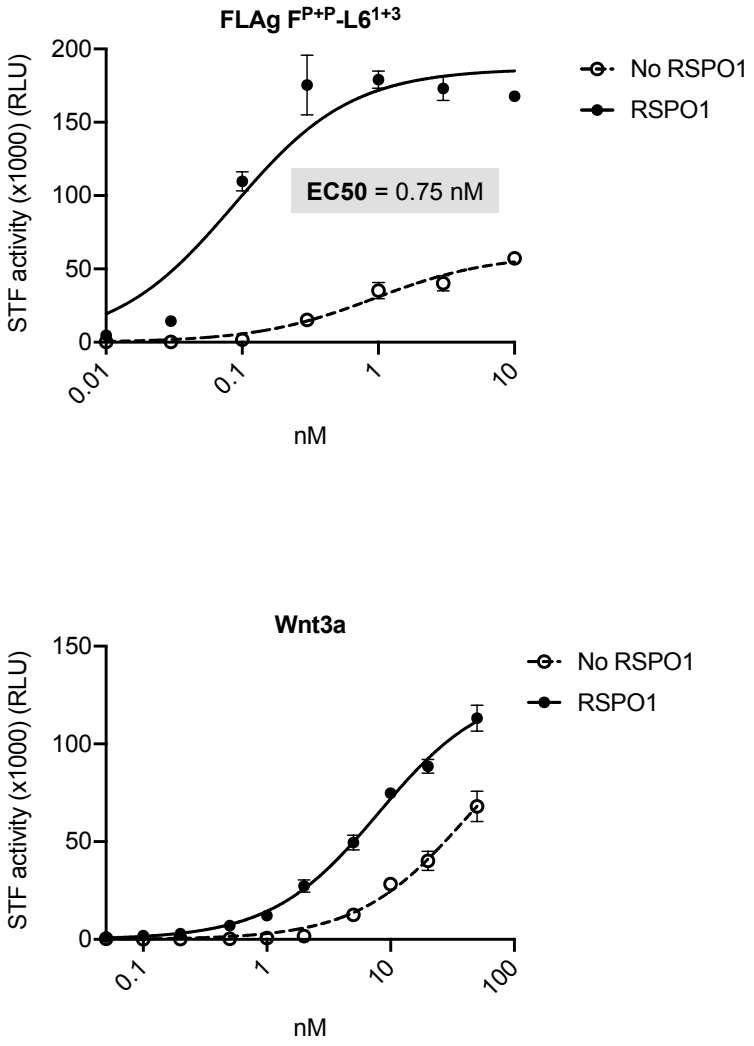

Figure 5. Dose response curves for FLAgP+P-L61+3 and Wnt3a.
HEK293T:STF cells were treated with the indicated concentrations of FLAgP+P-L61+3 or Wnt3a in the presence or absence of RSPO1 (100 ng/mL) for 24 hours and then assayed for luciferase activity (RLU = relative light units).

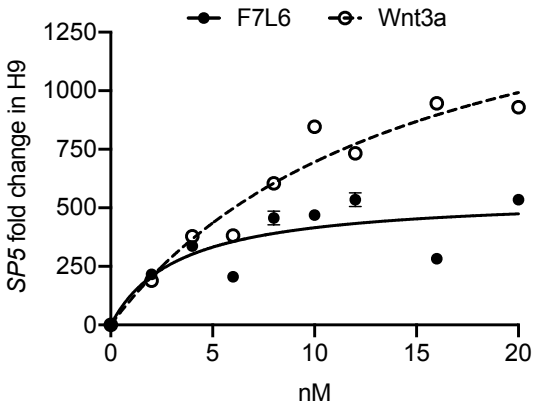

Figure 6. F7L6 activates Wnt target gene SP5 in human pluripotent stem cells in a dose-dependent manner.
H9/WA09 cells were treated with the indicated doses of F7L6 or Wnt3a for 24 hours. RNA was analyzed by qRT-PCR. Data represented as mean ± SEM for three technical replicates, with a nonlinear regression curve. All samples were normalized to the 0 nM (buffer) control.

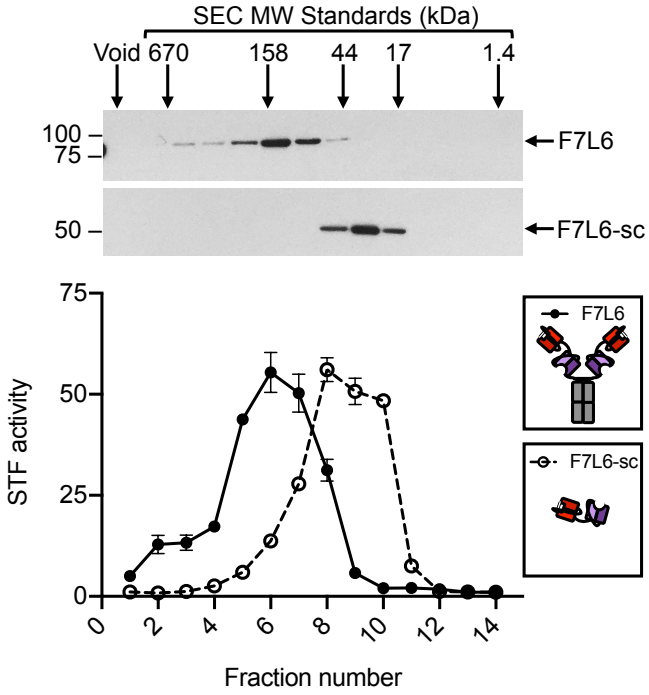

Figure 7. Size exclusion chromatography of F7L6 and F7L6-sc.
Purified Wnt mimetics F7L6 and F7L6-sc were fractionated on a Superdex 200 column. Fractions were assayed by SDS-PAGE followed by Coomassie staining and by activation of the STF reporter in HEK293T cells.

Differential effects of F7L6, Wnt3a, and CHIR on gene expression in hPS cells.

Previous studies have shown that modulating WNT/β-catenin signaling is crucial for differentiation of hPS cells into mesendoderm and definitive endoderm (DE) [14,32,34,44,45]. Wnt3a and GSK3-inhibitors (e.g. CHIR99021, CHIR98014, BIO, Li) [4,46–48] are frequently used interchangeably as WNT pathway activators in these differentiation protocols [49–54]. While Wnt3a is an established activator of WNT/β-catenin signaling, relatively little is known about the receptors that promote WNT-driven differentiation of hPS cells. We hypothesized that FZD7 mediates this process, since it transduces the Wnt3a signal [55,56] and regulates the pluripotent state. Here, we used F7L6 to selectively activate FZD7 signaling in hPS cells and analyzed global changes in gene expression by RNA sequencing (RNA-seq). We also examined the temporal kinetics of gene expression changes in response to a single, continuous dose of F7L6, Wnt3a, or CHIR98014 (CHIR) treatment.

Clustering of significantly differentially expressed genes (1,814 genes, **Figure 8**) according to change in percent maximum reads per kilobase per million mapped reads (RPKM) revealed distinct waves and classes of gene expression, including activation of many known Wnt pathway genes (**Figure 9A**), activation of mesendodermal and endodermal genes, and downregulation of pluripotency- and ectoderm-associated genes (**Figure 9B**).

Gene expression changes in response to Wnt3a and F7L6 were overall highly similar, with robust activation of classic markers of mesendoderm (i.e. *GSC*, *MIXL1*, *SP5* and *T*) and DE (i.e. *LEFTY1*, *EOMES*, *CER1*, *FOXA2*, *CXCR4*, and *SOX17*) and downregulation of pluripotency markers, such as *POU3F1*, *FZD7*, and *PODXL* (TRA-1-81). However, there were some notable differences between Wnt3a and F7L6 treatments. For example, induction of established WNT target genes, such as *DKK1*, *AXIN2*, *WLS*, *WNT3*, and *NKD1*, was more potent with Wnt3a than with F7L6. Also, induction of genes, such as *T*, *SP5*, *GSC*, and *FOXA2*, was slightly delayed for F7L6 relative to Wnt3a. These differences are potentially due to F7L6 solely engaging FZD7 and

LRP6 to promote downstream signaling, while Wnt3a, in contrast, promotes signaling through multiple FZD-LRP5/6 heterodimers.

In contrast to Wnt3a and F7L6, CHIR treatment produced significantly different gene expression profiles, both in kinetics and amplitude (**Figure 9A,B**). For example, while all three treatments activated known WNT target genes (e.g. *AXIN2*, *DKK1*, *LEF1* and *SP5*) and mesendodermal genes (e.g. *T*, *MIXL1*, *GATA4* and *EOMES*), CHIR did so more robustly than Wnt3a or F7L6. Such differences are likely attributable to the fact that CHIR acts downstream of the receptor complexes and hence is not restricted by receptor availability. Furthermore, while all three treatments activated expression of Wnt pathway and mesendodermal genes, CHIR failed to activate expression of certain genes, in particular the DE markers *FOXA2* and *SOX 17* (and to a lesser extent *CER* and *GSC*), an effect we validated using RT-qPCR (**Figure 10**). Interestingly, expression of other DE markers, such as *CXCR4*, which encodes a cell surface receptor commonly used to enrich DE populations using flow cytometry [57,58], was activated by CHIR (**Figure 9B**). These results indicate that sustained activation of WNT/β-catenin signaling by GSK3 inhibition with CHIR produces significant differences compared to selective pathway activation with either Wnt3a or F7L6.

F7L6, Wnt3 and CHIR treatment significantly altered expression of 525, 708, and 1,646 genes, respectively (**Figure 11**). A majority of genes (428 of 805 genes) in the F7L6 and Wnt3a lists overlapped, whereas expression changes of a large number of genes was unique to CHIR (1,009 genes), highlighting the substantial differences when the pathway is activated at the level of receptor rather than at the level of GSK3 inhibition. Using Gene Set Enrichment Analysis (GSEA) [59,60] of the 391 genes that changed in response to all three treatments indicated enrichment of diverse developmental processes, including Animal Organ Morphogenesis (Gene Ontology [GO]:0009887), Anatomical Structure Formation Involved In Morphogenesis

(GO:0048646), Tube Development (GO:0035295), Circulatory System Development (GO:0072359), and Neurogenesis (GO:0022008) (**Figure 11**).

Importantly, GSEA of all genes altered by CHIR indicated enrichment in Neurogenesis (GO:0022008) and Neuron Differentiation (GO:0030182), both categories that were not among the top five GO terms for F7L6 and Wnt3a (**Figure 11**), indicating that CHIR treatment additionally promotes differentiation into ectodermal lineages. The 1,009 differentially expressed genes unique to CHIR were additionally enriched in processes such as Biological Adhesion (GO:0022610), Locomotion (GO:0040011), Cell Junction (GO:0030054), and Positive Regulation Of Multicellular Organismal Process (GO:0051240). In summary, our RNA-seq analyses confirmed that activation of FZD7 signaling by F7L6 was sufficient to modulate WNT target genes and induce expression of mesendoderm and DE differentiation in hPS cells. Overall, F7L6 and Wnt3a treatments induced similar (though not identical) patterns and temporal kinetics of gene expression, while CHIR caused much wider changes in global gene expression.

Figure 8. Heat map of 1,814 significantly differentially expressed genes in response to F7L6, Wnt3a, and/or CHIR98014.

Heat map of 1,814 significantly differentially expressed genes in response to F7L6, Wnt3a, and/or CHIR98014 (CHIR) treatments in hPS cells (H1/WA01). Cells were treated with 5 nM F7L6 or Wnt3a, or 250 nM CHIR98014 (CHIR) for the indicated hours, and RNA was isolated and analyzed by RNA-seq. Data are represented as percent maximum RPKM (0, white; 100, blue; ≥100, pink).

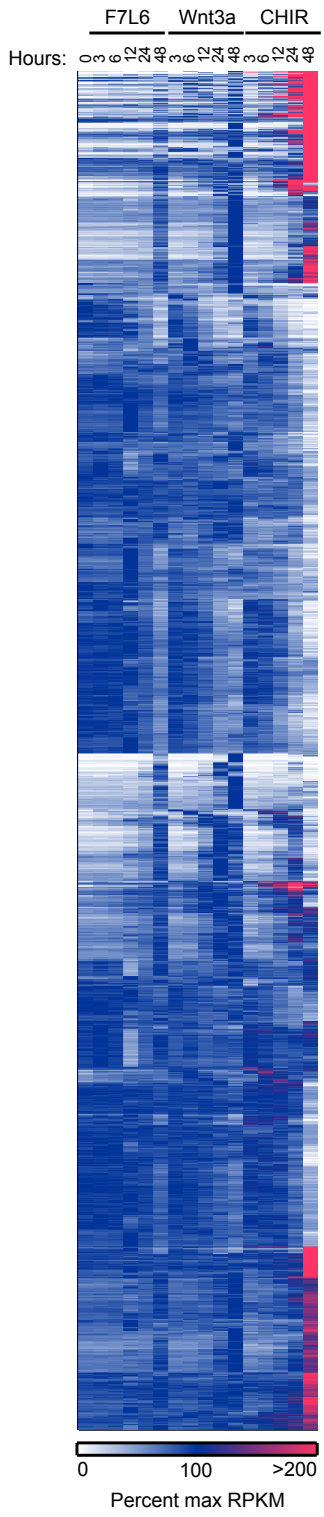
F7L6
Wnt3a
CHIR
Hours:
0 3 6 12 24 48 3 6 12 24 48 3 6 12 24 48
0
100
>200
Percent max RPKM

Figure 9. F7L6, Wnt3a, and CHIR differentially alter the transcriptome of human pluripotent stem cells.

HPS cells (H1/WA01) were treated with 5 nM F7L6 or Wnt3a, or 250 nM CHIR98014 (CHIR) for the indicated hours. RNA was isolated and analyzed by RNA-seq. Significant differential gene expression was defined as a 1.75-fold increase or decrease in RPKM compared to the 0-hour (buffer) control. Expression is represented as percent maximum RPKM (0, white; 100, blue; ≥100, pink). RPKM for each gene was normalized to the maximum RPKM across F7L6 and Wnt3a treatment groups. (**A**) Heat map of Wnt target genes changed in response to F7L6, Wnt3a, or CHIR. (**B**) Heat map of changed genes associated with mesendoderm and primitive/definitive endoderm differentiation, and pluripotency and neural differentiation. F7L6 promotes mesendodermal differentiation, similarly to Wnt3a.

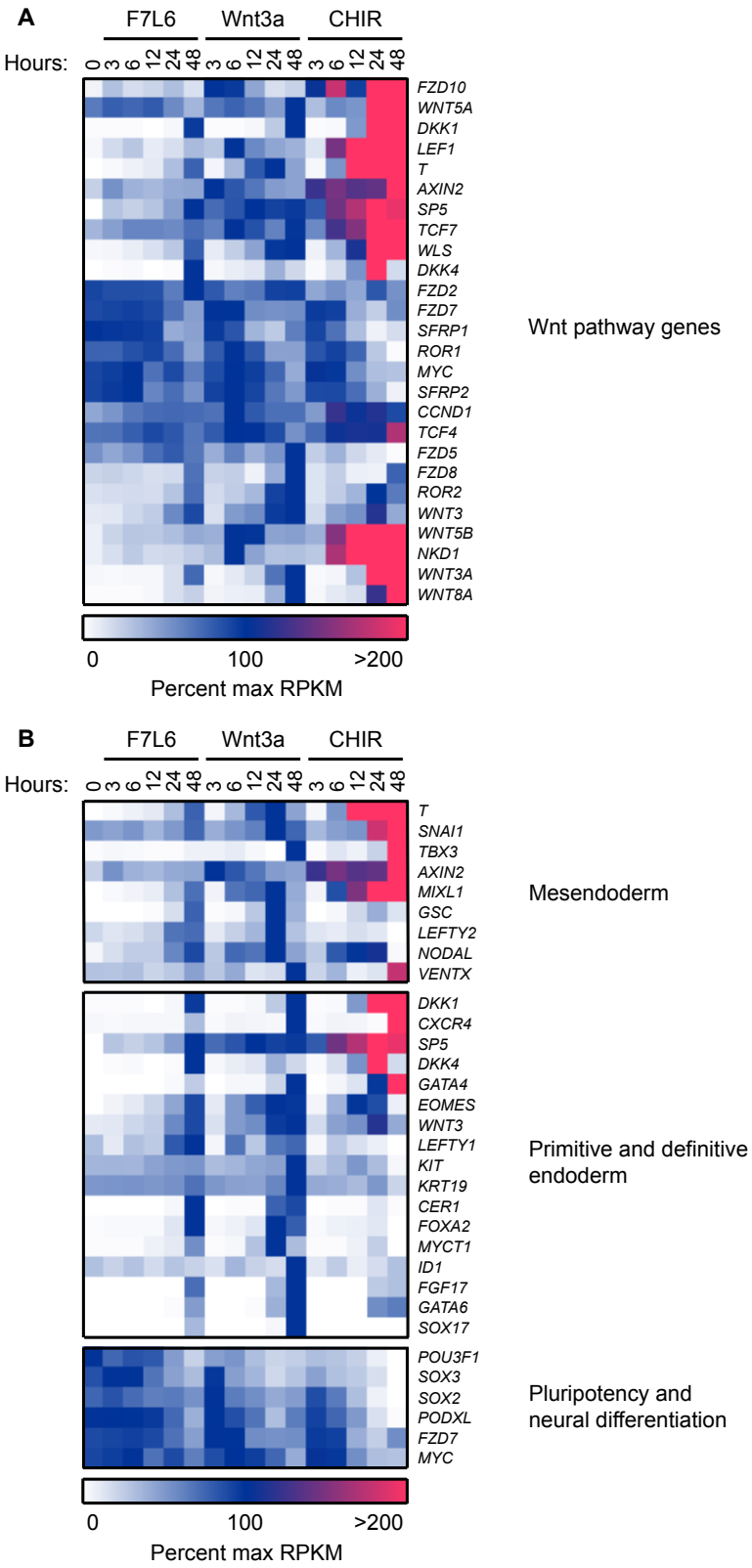
A
F7L6
Wnt3a
CHIR
Hours:
0 3 6 12 24 48 3 6 12 24 48 3 6 12 24 48
FZD10
WNT5A
DKK1
LEF1
T
AXIN2
SP5
TCF7
WLS
DKK4
FZD2
FZD7
SFRP1
ROR1
MYC
SFRP2
CCND1
TCF4
FZD5
FZD8
ROR2
WNT3
WNT5B
NKD1
WNT3A
WNT8A
Wnt pathway genes
0
100
>200
Percent max RPKM
B
F7L6
Wnt3a
CHIR
Hours:
0 3 6 12 24 48 3 6 12 24 48 3 6 12 24 48
T
SNAI1
TBX3
AXIN2
MIXL1
GSC
LEFTY2
NODAL
VENTX
Mesendoderm
DKK1
CXCR4
SP5
DKK4
GATA4
EOMES
WNT3
LEFTY1
KIT
KRT19
CER1
FOXA2
MYCT1
ID1
FGF17
GATA6
SOX17
Primitive and definitive endoderm
POU3F1
SOX3
SOX2
PODXL
FZD7
MYC
Pluripotency and neural differentiation
0
100
>200
Percent max RPKM

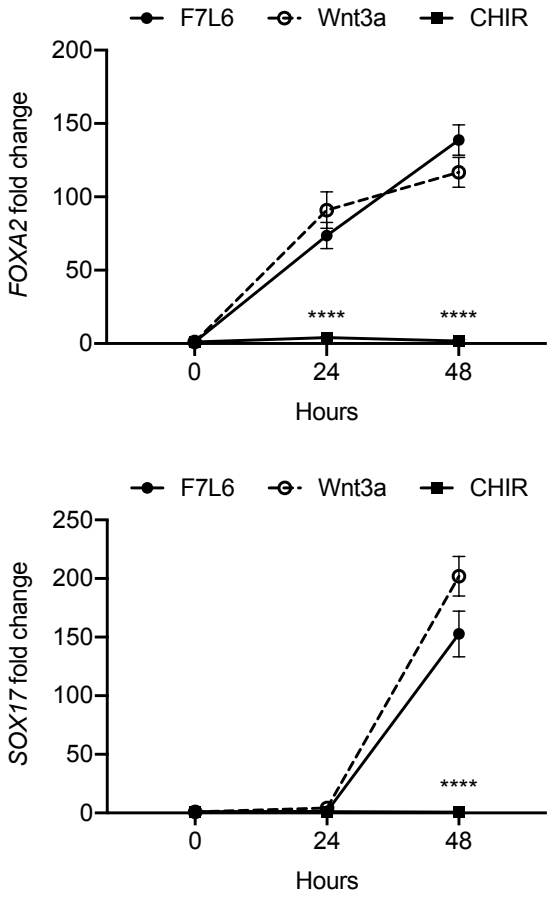

Figure 10. CHIR does not activate select definitive endoderm markers in undirected differentiation of human pluripotent stem cells.
H1/WA01 cells were treated with 5 nM F7L6 or Wnt3a, or 250 nM CHIR for the indicated hours. RNA was isolated and analyzed by RT-qPCR for FOXA2 and SOX17. Data represented as mean ± SEM for two independent experiments, three technical replicates each. All samples were normalized to the 0-hour (buffer) control. For statistical analyses: one-way ANOVA and Tukey's multiple comparisons test for significance of CHIR against F7L6 and Wnt3a at each time point: ****$p \leq 0.0001$.

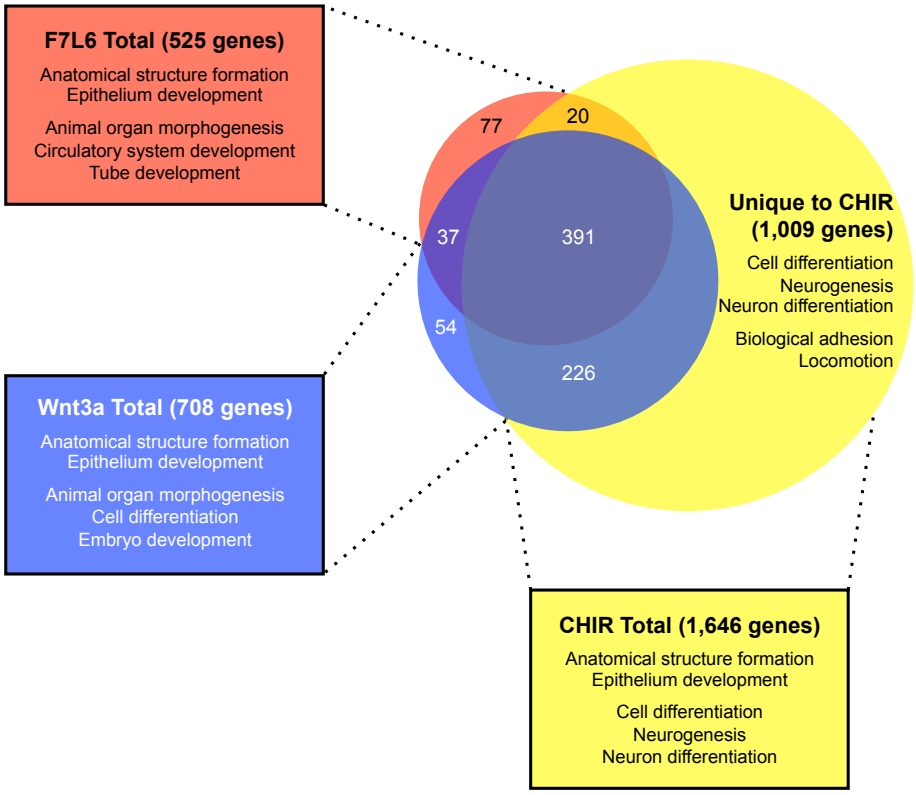

Figure 11. GSEA analyses of transcriptome changes induced by F7L6, Wnt3a, and CHIR. Venn diagram and GSEA analyses of genes differentially expressed in response to F7L6, Wnt3a, and CHIR98014 treatments in human pluripotent stem cells (H1). The top five GSEA gene set hits for each treatment group are listed by commonality among the groups and alphabetical order.

Early WNT target gene activation by F7L6 and Wnt3a in hPS cells.

As revealed by our RNA-seq analysis, selective FZD7 pathway activation elicits a complex program of gene expression. Recent studies have provided evidence that certain Wnts recruit additional receptors to the Fzd-Lrp5/6 complex to increase signaling specificity. For example, the cell surface proteins Reck and Gpr124 promote Wnt7 signaling through Fzd [61,62]. Furthermore, Egfr promotes a specific interaction of Wnt9a with Fzd9 and Lrp5/6 [37]. Likewise, Wnt3a may recruit additional, and currently unknown, co-receptors to activate signaling in hPS cells. In contrast, owing to its design, our Wnt mimetic F7L6 only recruits FZD7 and LRP6. To confirm that Wnt3a and F7L6 promote similar downstream signaling events, we more closely examined early WNT target gene activation and identified groups of genes with maximal activation at 3 hours and at 6 hours upon Wnt3a treatment (**Figure 12A,B**). We used RT-qPCR to validate changes in expression of several genes within these clusters in response to Wnt3a and F7L6 over a six-hour time course in hPS cells. Both Wnt3a and F7L6 activated these early target genes with similar kinetics, with expression of *AXIN2*, *SOX9*, and *ARL4A* at 3 hours (**Figure 12C-E**) and *NKX1-2*, *NKD1* and *FGF18* at 6 hours (**Figure 12F-H**). These findings support that heterodimerization of FZD7 and LRP6 by F7L6 is sufficient to elicit a transcriptional response in hPS cells similar to that elicited by Wnt3a and likely does not involve the recruitment of additional receptors.

Figure 12. Early Wnt target genes activated by F7L6 and Wnt3a in hPS cells.
RNA-seq profiles of genes significantly activated at 3 hours **(A)** and 6 hours **(B)** in response to Wnt3a (5nM) in H1/WA01 cells. Validation of three target genes (*AXIN2*, *SOX9* and *ARL4A*) maximally activated at 3 hours (**C-E**) and of three genes (*NKX1-2*, *NKD1* and *FGF18*) maximally activated at 6 hours (**F-G**). H1 cells were treated with F7L6 or Wnt3a (each at 10nM) for the indicated time and total RNA was analyzed by RT-qPCR. Gene expression was normalized to the expression of *RPL13A*. Data represented as mean ± SEM for two independent experiments, three technical replicates each. All samples were normalized to the 0-hour (buffer) control. For statistical analyses: one-way ANOVA and Tukey's multiple comparisons test for significance between F7L6 and Wnt3a treatments at each time point: ****p≤0.0001, ***p≤0.001, **p≤0.01, *p≤0.05.

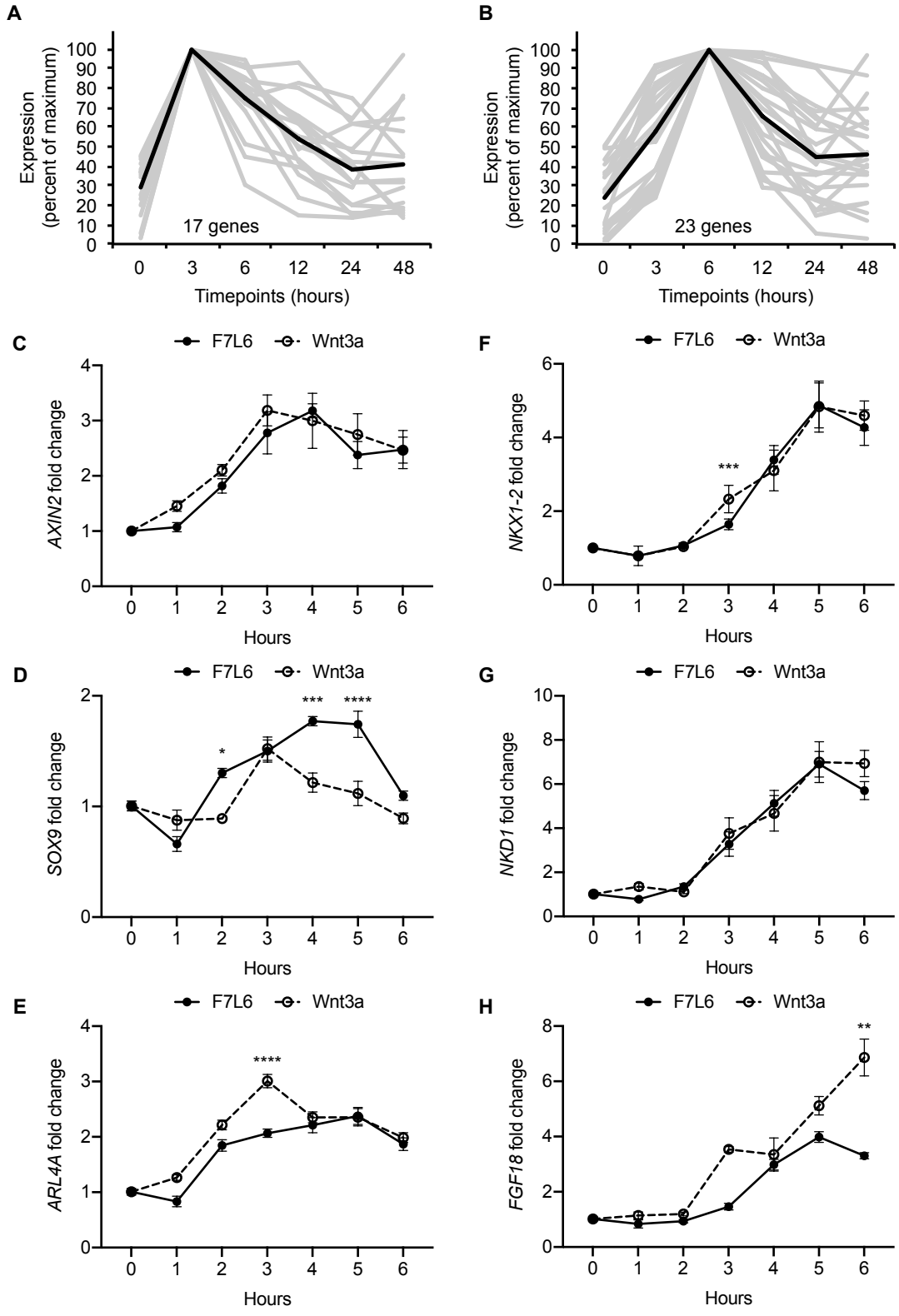
A
Expression (percent of maximum)
17 genes
Timepoints (hours)
B
23 genes
C
F7L6
Wnt3a
AXIN2 fold change
Hours
F
NKX1-2 fold change
***
D
SOX9 fold change
*
***
****
G
NKD1 fold change
E
ARL4A fold change
****
H
FGF18 fold change
**

FZD7 activation promotes differentiation of hPS cells.

Our RNA-Seq analysis indicated that F7L6, like Wnt3a, promotes mesendodermal differentiation. To monitor differentiation in real time, we employed human embryonic stem (hES) cells (H9/WA09) carrying reporter genes that mark meso- and endo-dermal differentiation: (1) for mesodermal differentiation, TBXT(T)-GFP, which harbors the gene encoding enhanced green fluorescent protein (eGFP) under control of the *TBXT* (T) promoter [63], and (2) for endodermal differentiation, SOX17-eGFP, which carries the eGFP gene in the *SOX17* locus [64]. We treated these reporter cell lines with a single, continuous dose of F7L6, Wnt3a or CHIR and monitored GFP expression for 5 days (**Figure 13A**). F7L6 potently activated expression of both reporters (**Figure 13B,C**), with T-GFP expression first detectable at 24 hours (**Figure 13B, D**) and SOX17-eGFP at 36 hours (**Figure 13C, E**). Wnt3a likewise activated expression of both transgenes with similar temporal kinetics, however, their induction was significantly lower than with F7L6 (**Figure 13B-E**). This difference in potency between F7L6 and Wnt3a is likely due to the fact that Wnt3a is more unstable than F7L6 in these culture conditions. Treatment with CHIR yielded reporter gene expression distinct from both F7L6 and Wnt3a, with an early peak in T-GFP expression that subsequently declines (**Figure 13B, D**) and no induction of the SOX17-eGFP reporter (**Figure 13C, E**). This is consistent with our RNA-Seq (**Figure 9B**) and RT-qPCR results (**Figure 10**), again highlighting the distinct effects on differentiation of GSK3 inhibition versus FZD7 activation with either Wnt3a or F7L6.

Figure 13. Activation of FZD7 with F7L6 promotes differentiation of hPS cells.
(**A**) Schematic of live cell imaging experiment. Abbreviations: E8, essential 8 medium; Tx, treatment. H9/WA09 cells carrying a T-GFP (**B, D**) or a SOX17-eGFP (**C, E**) reporter gene were treated with the indicated compounds, and fluorescence was imaged every 3 hours for a total of 120 hours on an IncuCyte® Life Cell Analysis System. Fluorescence was quantified by total green object integrated intensity (GCU x μm^2/image).

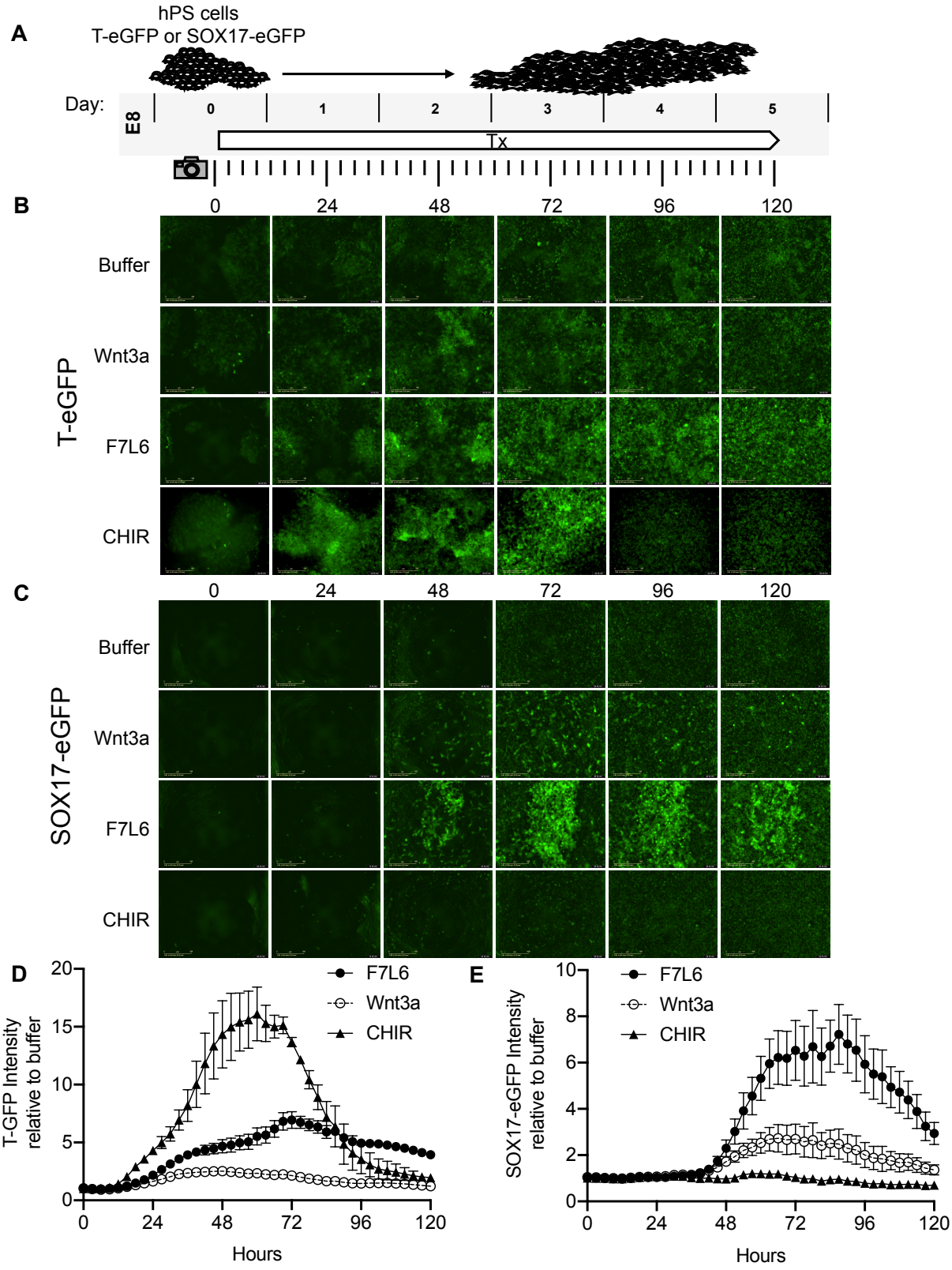
A
hPS cells
T-eGFP or SOX17-eGFP
Day:
E8
0
1
2
3
4
5
Tx
B
0
24
48
72
96
120
Buffer
Wnt3a
F7L6
CHIR
T-eGFP
C
SOX17-eGFP
D
T-GFP Intensity relative to buffer
F7L6
Wnt3a
CHIR
Hours
E
SOX17-eGFP Intensity relative to buffer

FZD7 activation directs endodermal differentiation.

Protocols to differentiate hPS cells specifically towards definitive endoderm (DE) have been established and are widely used to generate mature endodermally derived cell populations, such as pancreas, liver [65], and intestine [66]. DE differentiation of hPS cells is induced by Activin/Nodal signaling, and Wnt3a addition on day 1 of differentiation increases the efficiency of mesendoderm specification and subsequent DE formation (**Figure 14A**). Using this protocol, we replaced Wnt3a treatment with F7L6 and monitored gene expression by RT-qPCR. As expected, expression of the pluripotency marker *OCT4* (*POU5F1*) declined over the 3 days of differentiation with a more potent effect by F7L6 compared to Wnt3a (**Figure 14B**). Concurrently, expression of endodermal markers, *SOX17*, *CXCR4* and *FOXA2*, increased upon treatment with F7L6 to a similar extent as Wnt3a (**Figure 14B**), indicating that activation of FZD7 alone is sufficient to promote DE formation.

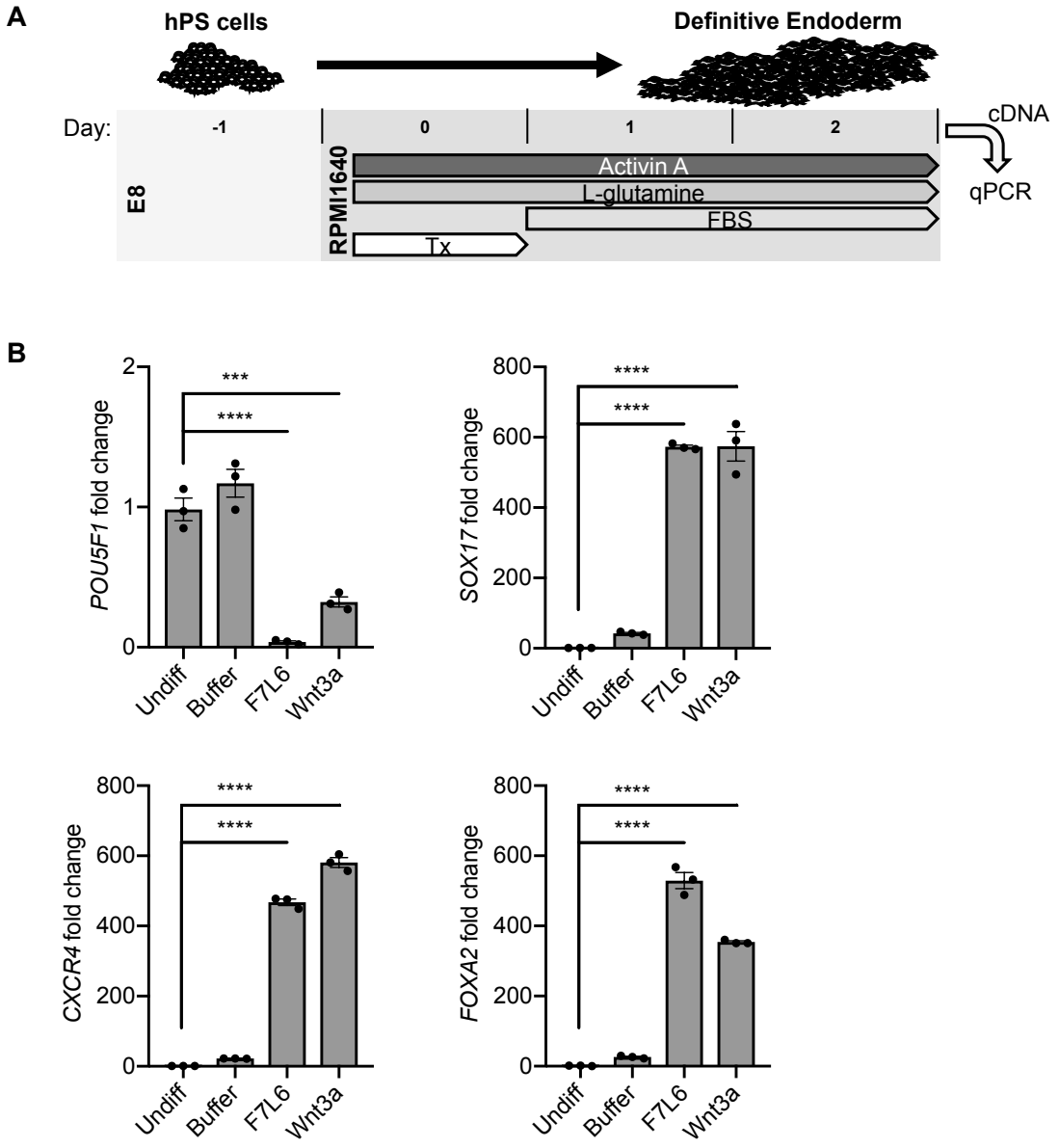

Figure 14. Activation of FZD7 with F7L6 promotes differentiation to definitive endoderm. (**A**) Schematic of definitive endoderm (DE) differentiation protocol. Abbreviations: E8, essential 8 medium; FBS, fetal bovine serum; Tx, treatment. (**B**) RT-qPCR analysis of the differentiation treated with the indicated compounds. Treatment of hPS cells (H9/WA01) with F7L6 or Wnt3a leads to downregulation of the pluripotency marker *POU5F1* and upregulation of the definitive endoderm markers *CXCR4*, *SOX17* and *FOXA2*. Gene expression was normalized to the expression of *RPL13A*. All samples were normalized to undifferentiated (Undiff) samples. For all statistical analyses: one-way ANOVA and Tukey's multiple comparisons test: ****p≤0.0001, ***p≤0.001.

FZD7 activation prevents differentiation towards the hematopoietic lineage.

Hematopoietic stem and progenitor cells can be derived from hPS cells using defined culture conditions [67,68] and can be identified by dual expression of the cell surface markers CD34 and CD45 (**Figure 15A**). We previously showed that a specific WNT signal involving WNT9A and FZD9 increased the efficiency of this differentiation protocol, as monitored by an increase in the yield of CD34/CD45 double positive cells [37,69]. Given this highly selective requirement for WNT9A/FZD9 signaling, we reasoned that activation of FZD7 signaling with F7L6 would likely interfere with the differentiation of hPS cells towards the hematopoietic lineage. We found that F7L6 treatment at days 2-4 of differentiation, the treatment window we previously established to be critical for optimal differentiation, significantly reduced the number of CD34/CD45 double positive cells at day 14 relative to untreated or Wnt3a treated (**Figure 15B**). The percentages of CD34 and CD45 single positive cells were likewise adversely affected by F7L6 (**Figure 15C,D**). RT-qPCR demonstrated that F7L6 failed to induce expression of hematopoietic markers, including MESP1 and MIXL1 at day 4 and KDR at day 11 of differentiation (**Figure 15E**). Therefore, selective activation of FZD7 with F7L6 promotes differentiation into certain lineages, such as DE, but hinders differentiation into other lineages, such as the blood lineage.

Figure 15. Activation of FZD7 with F7L6 blocks differentiation to hematopoietic stem and progenitor cells.

(**A**) Schematic of the APEL hematopoietic stem/progenitor cell (HSPC) differentiation protocol. HPS cells were treated (Tx) with either Wnt3a or F7L6 from Day 2 to 4 of the 14-day differentiation protocol. On day 14, cells were analyzed by flow cytometry for the cell surface markers CD34 and CD45. Quantitation of flow cytometry of CD34/CD45 double positive cells (**B**), CD34 single positive cells (**C**), and CD45 single positive cells (**D**). (**E**) RT-qPCR analysis of MESP1 and MIXL1 at day 4 and of KDR at day 11 of differentiation. For statistical analyses: one-way ANOVA and Tukey's multiple comparisons test: ***p≤0.001, **p≤0.01, *p0.05, ns, not significant.

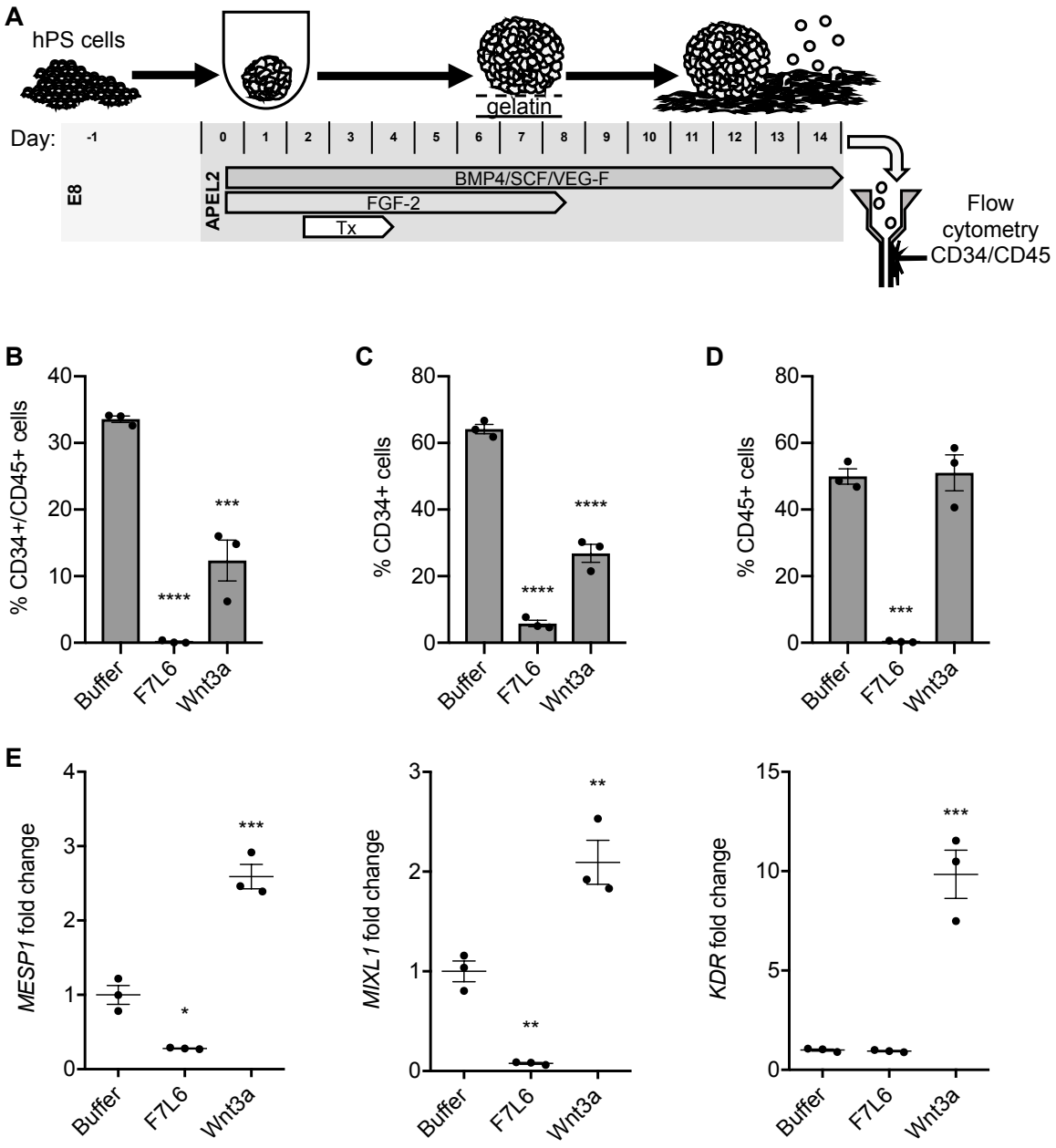
A
hPS cells
gelatin
Day:
-1
0
1
2
3
4
5
6
7
8
9
10
11
12
13
14
E8
APEL2
BMP4/SCF/VEG-F
FGF-2
Tx
Flow cytometry CD34/CD45
B
% CD34+/CD45+ cells
C
% CD34+ cells
D
% CD45+ cells
Buffer
F7L6
Wnt3a
E
MESP1 fold change
MIXL1 fold change
KDR fold change

1.3 DISCUSSION

The WNT/β-catenin signaling pathway is well known for its critical roles in stem cell biology, including maintenance of pluri- and multi-potency and differentiation. However, the study of individual ligand-receptor pairs in regulating stem cell behavior has been complicated by two main factors: first, the apparent promiscuity in WNT-receptor interactions and, second, the large number of *WNT* and *FZD* gene family members. Here we used hPS cells to analyze the role of a single WNT receptor complex, comprised of FZD7 and LRP6, in regulating the transition from undifferentiated and pluripotent stem cell to a mesendodermally restricted cell lineage. Specific activation of signaling was achieved using a WNT mimetic, F7L6, which only engaged and thereby heterodimerized FZD7 and LRP6. In contrast to the widely used Wnt3a protein, which engages multiple cell surface receptors, F7L6 exclusively binds to FZD7 and LRP6.

We demonstrated that selective engagement and heterodimerization of FZD7 and LRP6 with F7L6 is sufficient to drive the differentiation program promoted by Wnt3a in hPS cells. FZD7 is the most abundantly expressed FZD receptor in hPS cells, and its knockdown by RNA interference disrupts expression of pluripotency-associated genes, such as *POU5F1*/*OCT4* and *NANOG* [12,13]. Likewise, inhibition of endogenous WNT processing in hPS cells using PORCN inhibitors also interferes with their pluripotency [12], suggesting that an endogenous WNT signal mediated by FZD7 is required to maintain hPS cells in an undifferentiated and pluripotent state. On the other hand, ectopic activation of WNT/β-catenin signaling, either with Wnt3a or with F7L6, leads to hPS cell differentiation along the mesendodermal lineage.

Whole transcriptome analysis revealed that Wnt3a and F7L6 elicit nearly identical transcriptional responses associated with early embryonic development, including formation of the primitive streak and gastrulation movements. Interestingly, we found that treatment with a GSK3 inhibitor (CHIR98014), which is commonly used interchangeably with Wnt3a, elicits significantly different effects. Most notably, we observed that over a 2-day treatment window,

Wnt3a and F7L6 led to robust expression of the endodermal markers *FOXA2* and *SOX17*, whereas the GSK3 inhibitor did not. Consistent with these observations, Kafri et al. found that GSK3 inhibition elicited significantly different dynamics and kinetics of □-catenin accumulation and localization compared to Wnt3a [70]. These findings indicate that specific activation of WNT/FZD signaling is important to recapitulate developmental processes.

The WNT mimetic F7L6 has several advantages over recombinant WNT proteins. First, native WNT proteins interact promiscuously with multiple receptors. For example, Wnt3a interacts with FZD1, 2, 4, 5, 7, 8, 9, and 10 [55,56]. In addition, the co-receptors LRP5 and LRP6 are functionally redundant [71], indicating that WNT proteins can interact equivalently with either one. In contrast, WNT mimetics can be engineered to interact with greater selectivity for cell surface receptors. In vivo, WNT-FZD signaling specificity is regulated in part by co-receptors. For example, Reck, a glycosylphosphatidylinositol-anchored cell surface protein, acts together with Gpr124, a 7-transmembrane protein, to promote Wnt7a-Fzd-Lrp5/6 signaling to promote angiogenesis in the developing central nervous system [61,62,72,73]. Furthermore, we recently identified a novel function for Egfr in mediating Wnt9a-Fzd9-Lrp5/6 signaling during hematopoietic development in zebrafish [37]. The use of engineered proteins capable of engaging specific WNT receptors, such as F7L6, may overcome the need for the recruitment of specificity-conferring co-receptors, such as Reck, Gpr124 and Egfr, and thus replace the need for purification of biologically active WNT proteins.

A second advantage of WNT mimetics is that they can be assembled using recombinant proteins with favorable biochemical properties. Purification of native WNT proteins has proven extremely difficult, requiring 3 to 4 chromatography steps with yields of approximately 0.1 mg per liter of WNT conditioned medium [74]. Furthermore, WNT proteins are lipid modified [75,76], rendering them highly hydrophobic and necessitating the addition of detergents to maintain their solubility in aqueous conditions. Consistent with its poor physicochemical properties, at low concentrations

the activity of Wnt3a is rapidly extinguished and nearly undetectable. In contrast, F7L6, which is entirely comprised of engineered immunoglobulin sequences and hence is soluble and stable in standard biologically compatible buffers, retains signaling activity at significantly lower concentrations. In addition, by appending tags, such as Fc or 6x-His, F7L6 can be purified using a single affinity binding step, with an approximate yield of 2.5 mg per liter of conditioned media.

Several other groups have described recombinant proteins similar in design to F7L6 and capable of heterodimerizing FZDs and LRP5/6 [40,41,77–79]. In contrast to these other WNT agonists that engage the CRD of FZD, the FZD7-binding arm of F7L6 binds the linker, or neck region, between the CRD and the first transmembrane domain of FZD7. Since this neck region is poorly conserved among the ten FZD receptors, we were able to exclusively engage FZD7 and no other FZD, including mouse Fzd7. This feature of F7L6 allowed us to demonstrate that the CRD is dispensable for signaling, since F7L6, but not Wnt3a, could induce signaling by a CRD-less FZD7. Therefore, aside from docking a WNT protein, the CRD has no additional role in activating the downstream signaling events.

We designed F7L6 as a bi-specific bivalent (= tetravalent) molecule capable of simultaneously binding two FZD7 and two LRP6 cell surface receptors. This design possibly permits WNT receptor oligomerization, which in turn promotes intracellular signalosome formation, as previously proposed [43]. Structural studies have revealed that WNTs can dimerize FZD CRDs either in a 1:2 or a 2:2 stoichiometry [80,81]. These higher order oligomers are hypothesized to promote optimal downstream signaling. Interestingly, a bivalent version, F7L6-sc, capable of forming 1:1 FZD7-LRP6 heterodimers, promotes downstream signaling, indicating that higher order oligomerization is not strictly required for signaling, consistent with previous findings by others [79]. Of note, signal saturation is approximately 2-fold greater for the tetravalent F7L6 version compared to the bivalent F7L6-sc version, indicating that oligomerization may control signal amplitude, possibly by polymerization of the intracellular scaffolding molecules DVL

and AXIN to drive signalosome formation. Therefore, tetrameric ligands, such as F7L6 and those developed by others [40,77], may augment and potentiate signaling by promoting receptor clustering. Additional experiments are needed to resolve the contribution of WNT versus DVL/AXIN to receptor oligomerization and signalosome formation.

Despite their potent stem cell activities in vivo and their potential as therapeutics in regenerative medicine, WNT proteins have not yet been approved for any clinical applications, owing in part to their poor physicochemical properties. Certain formulations, such as liposomal packaging [82], have produced more stable and bioactive WNT3A, which is in early-stage clinical trials to treat patients undergoing posterolateral spinal fusion. However, such formulations will require purification of individual WNTs, which, to date, has only been achieved for WNT3A and WNT5A [76,83]. WNT mimetics, such as the one described here, can be designed to target all WNT receptors and co-receptors and thus offers new opportunities for their development as therapeutics in regenerative medicine.

1.4 MATERIALS AND METHODS

Design of F7, L6 and F7L6

The sequence coding for the heavy (V_H) and light (V_L) chain of the variably fragment (Fv) portion of the FZD7 antibody (F7-Ab) were identified and used to design a single chain variable fragment (F7-Ab scFv) that consists of the heavy chain Fv fused to the light chain Fv with a linker peptide $(GGGGS)_3$. The F7-Ab scFv sequence was cloned into the pFuse-hIgG1-Fc2 mammalian expression vector (Invivogen), containing the IL-2 signal sequence and the IgG1 crystallizable fragment (Fc), to form the F7-Ab scFv-Fc (F7). The domains of the F7 construct are in the following order: IL-2 ss, F7-V_H, $(GGGGS)_3$, F7-V_L, Fc. The coding sequence for the LRP6 scFv (United States Patent No.: US8,883,735, SEQ ID NO: 81 V_L and SEQ ID NO: 82 V_H) was similarly cloned into the pFuse mammalian expression vector to form the LRP6-Ab scFv-Fc (L6). The domains of the L6 construct are in the following order: IL-2 ss, L6-V_L, $(GGGGS)_4$, L6-V_H, Fc. The coding sequence for the two scFv were fused with an additional flexible linker and cloned into the pFuse mammalian expression vector to create a bispecific scFv-Fc (F7L6). The domains of the F7L6 construct are in the following order: IL-2 ss, F7-V_H, $(GGGGS)_3$, F7-V_L, $(GGGGS)_3$, L6-V_L, $(GGGGS)_4$, L6-V_H, Fc. Additional constructs containing a 6xHis tag between the IL-2 ss and the F7-V_H domain with and without the Fc region were generated to express and produce F7L6 and F7L6-sc, respectively.

Expression, purification and characterization of recombinant proteins

CHO cells (RRID:CVCL_0213) were transfected with plasmids encoding F7, L6, F7L6 and F7L6-sc, drug selected (1000 µg/mL zeocin or 4 µg/mL Puromycin, ThermoFisher Scientific) and expanded as clonal stable lines. Conditioned media (CM) were collected from confluent cultures every 3-4 days. Medium was replenished and CM was collected until the cells no longer adhered

to the plate. CM were passed through a 0.22μm filter (Genesee Scientific) and stored at 4°C until time of purification. CHO cells expressing the recombinant Wnt3a protein were similarly cultured and conditioned medium was collected, filtered, and stored. Wnt3a protein used in these studies was purified by 4-step column chromatography as previously described [74]. F7, L6 and F7L6 were purified from CM as follows: CM were applied to a protein G Sepharose (Biovision) column. The column was then extensively washed with phosphate buffered saline (PBS), and bound proteins were eluted with 0.1M glycine pH 2.5 and collected as 1mL fractions into tubes containing 0.1mL 2M Tris-Cl, pH8. Fractions containing the protein of interest were combined and dialyzed against PBS using dialysis tubing with a MWCO of 10kDa (Thermo Scientific). After dialysis, the recombinant proteins were sterile filtered and aliquoted and stored at -80°C. The 6xHis-tagged version of F7L6 and F7L6-sc were purified as follows: CM from CHO cells expressing either F7L6 or F7L6-sc were adjusted to contain 30 mM imidazole and applied to a 1 mL immobilized metal affinity column charged with $NiCl_2$ (HiTrap IMAC HP, Cytiva Lifesciences). The column was washed with 30 mM imidazole in PBS. Bound proteins were eluted with a linear gradient from 30 mM to 300 mM imidazole in PBS into 1 mL fraction. Fractions containing F7L6 were combined and dialyzed against PBS. Fractions containing F7L6-sc were further fractionated by size exclusion chromatography (SEC, Superdex 200 10/300 GL, Cytiva Lifesciences) to remove contaminant proteins. After dialysis or gel filtration, the recombinant proteins were aliquoted and stored at -80°C. SEC of F7L6 and F7L6-sc (as shown in Figure 2 Figure Supplement 3) was performed on a Superdex 200 10/300 GL column (Cytiva Lifesciences) in PBS, and 1 mL fractions were assayed in the presence of RSPO (100 ng/mL) for signaling activity using the STF assay. The previously published Wnt mimetic FLAg F^{P+P}-$L6^{1+3}$ [40] was generously provided by Stephane Angers (University of Toronto, Canada)

Mapping of the F7-Ab epitope

The sequence encoding 42 amino acids (aa) of FZD7 containing the epitope for the F7-Ab (Glycine 168 to Serine 209) was cloned into the bacterial GST expression vector pGEX-4T3 (Cytiva Lifesciences). The epitope was shortened from either end through sequential cloning to produce 10 different length epitopes ranging from the original 42 aa to 8 aa. The GST fusion proteins were expressed in BL21 cells and cell pellets were resuspended in protein sample loading buffer (2% SDS, 5% 2-mercaptoethanol, 10% glycerol, 62.5 mM Tris-Cl pH6.8) and boiled for 5 minutes (min) at 95°C. Proteins were visualized by Coomassie or by immunoblotting using the F7-Ab to determine binding to each epitope length.

Cell lines and culture conditions

All cell lines used in these studies were directly obtained from either ATCC (CHO, HEK293, L) or WiCell Research Institute (H1, H9). Identity of H1 and H9 was authenticated by karyotyping and functional assays, including EB formation and directed differentiation. All HEK293/HEK293T (RRID:CVCL_0045/RRID:CVCL_0063) lines and mouse L-cells (ATCC-CRL-2648) (RRID:CVCL_4536) were cultured in Dulbecco's Modified Eagle's Medium (DMEM) supplemented with 10% fetal bovine serum (FBS) and penicillin/streptomycin. HEK293/HEK293T cells stably transduced with the Wnt reporter Super TOP-Flash (STF, Addgene Plasmid #12456, RRID:Addgene_12456) were previously described (Bauer et al., 2013). HEK293T cells carrying knockout mutations in LRP6 were previously described [37] HEK293T harboring mutations in multiple FZD genes (FZD1,2,7 [F127-KO] and FZD1,2,4,5,7,8) were kindly provided by Professor M. Boutros, Heidelberg University, Germany) [56]. CHO cells overexpressing Wnt3a were cultured in DMEM, 10% FBS and penicillin/streptomycin, and Doxycycline (250 ng/mL) was added to induce Wnt3a expression.

All experiments using human pluripotent stem cell lines (hPS cells) were approved under IRB/ESCRO protocol number 100210 (Principal investigator: K.W.). HPS cell lines H1 (WA01, NIH Registration Number 0043, RRID:CVCL_9771) and H9 (WA09, NIH Registration Number 0062, RRID:CVCL_9773) were obtained from WiCell and cultured in E8 culture medium [84] on Matrigel (BD Biosciences). The H9 reporter lines, H9 SOX17:GFP [64] and H9 T-GFP [63] were cultured in E8 culture medium, passaged with TrypLE Express (Gibco), and seeded with Rock inhibitor Y-27631, 5 μM (Tocris). The H9 SOX17:GFP cell line was kindly provided by material transfer agreement by Dr. Seung Kim (Stanford School of Medicine). Induced pluripotent stem (iPS) cell lines were kindly provided by Dr. Dan Kaufman (UC San Diego) (Li et al., 2018). The iPS cells were cultured in mTeSR™1 (StemCell Technologies), passaged with TrypLE Express, and seeded with Rock inhibitor. All hPS and iPS cells were fed fresh media daily.

Differentiation of hPS cells

Non-directed differentiation: Reporter hPS cell lines, H9 TBXT(T)-eGFP and H9 Sox17-eGFP, were passaged into a Matrigel-coated 12 well plate at 10,000 cells per well. When cells reached 40-60% confluence, media in each plate were replenished and the cells were treated with F7L6 (10 nM), Wnt3a (5 nM), CHIR98014 (250 nM, Sigma-Aldrich), or an equivalent volume of Wnt storage buffer (PBS, 1% CHAPS, 1 M NaCl). Plates were placed in the IncuCyte® Life Cell Analysis System (Sartorius) and cultured without media changes for 5 days at 37°C. Phase and GFP images were recorded every 3 hours for a total of 120 hours after treatment. The IncuCyte software was used to process the images and generate the integrated GFP intensity (GCU x μm2/image).

Endoderm Differentiation: H1 cells were differentiated to endoderm as previously described [32]. Initiated on days 4–6 after passage (depending on culture density), sequential, daily media changes were made for the entire differentiation protocol. After a brief wash in PBS, cells

were cultured in RPMI, Activin A (100 ng/mL, R&D Systems) and a treatment for the first day. Treatments were F7L6 (10nM), Wnt3a (5nM), CHIR (250nM) or an equivalent volume of Wnt storage buffer. The next day the medium was changed to RPMI with 0.2% vol/vol FBS and Activin A (100 ng/mL), and the cells were cultured for 2 additional days. Cells were collected at day 3 and total RNA was isolated and analyzed by RT-qPCR.

Hematopoietic differentiation: HPS cells were differentiated to the hematopoietic lineage as previously described [67,68]. The day prior to differentiation, iPS cells were passaged with TrypLE Express at a high density in mTeSR with Rock inhibitor. On Day 0 of the differentiation, iPS cells were dissociated into a single cell suspension and plated in a 96-well U-bottom plate (Genesee Scientific) at 3,000 cells per well in APEL2 (StemCell Technologies) with 40 ng/mL BMP4 (R&D Systems), 40 ng/mL SCF (R&D Systems), 20 ng/mL VEGF (R&D System), 10 ng/mL FGF-2 (StemCell Technology), and 5 nM Rock inhibitor. On Day 2 of the differentiation, the embryoid bodies (EB) were treated with F7L6 (5 nM), Wnt3a (5 nM), CHIR (250 nM) or an equivalent volume of Wnt storage buffer. On Day 4 of the differentiation, the media was removed from the EBs and replaced with fresh APEL2 with BMP4, SCF, VEGF, and FGF-2. On Day 7 of the differentiation, EBs were transferred to gelatin coated plates. On Day 8 of the differentiation one volume of APEL with BMP4, SCF, and VEGF was added. EBs were dissociated on Day 14 of the differentiation for analysis by flow cytometry.

Immunoblotting by dot blot.

Cells were lysed in TNT buffer (1% Triton X-100, 150 mM NaCl, 50 mM Tris HCl, pH 8) with protease inhibitors (Roche). 5 µL of whole cell lysate (approximately 40 µg) was dotted directly onto nitrocellulose membrane and allowed to dry completely. The nitrocellulose membrane was incubated in blocking buffer (TBST [20 mM Tris-Cl pH8, 150 mM NaCl, 0.2% Tween-20], 1% BSA, 3% non-fat dry milk) for 30-60 min at room temperature (RT), and then

incubated in primary antibody for 1 hour at RT or overnight at 4°C. The conditioned media collected from F7, L6, and F7L6 expressing CHO cells was mixed 1:1 with blocking buffer and used as a primary antibody solution. The nitrocellulose membrane was washed three times in TBST, and then incubated in goat anti-human HRP secondary antibody (ThermoFisher Scientific) at 1:10,000 dilution in blocking buffer for 45-60 min at RT. The nitrocellulose membrane was washed three times in TBST before enhanced chemiluminescent (ECL) detection by SuperSignal West Dura Western Blot Substrate (ThermoFisher Scientific) and exposure to autoradiography film.

Immunoblotting by Western.

To obtain whole cell lysate, cells were lysed in TNT buffer with protease inhibitors. Protein concentrations were determined using Pierce™ Coomassie (Bradford) Protein Assay Kit (ThermoFisher Scientific). Protein sample loading buffer (62.5 mM Tris-Cl pH6.8, 2% SDS, 10% glycerol, 5% 2-mercaptoethanol, bromophenol blue) was added to 20 μg total protein. Samples were denatured at 95°C for 5 min unless samples were intended to be blotted for FZD proteins. Cell lysates were resolved by sodium dodecyl sulfate-polyacrylamide gel electrophoresis (SDS-PAGE), transferred to nitrocellulose membrane, and incubated for 30-60 min in blocking buffer. Primary antibody incubations were done overnight at 4°C. Primary antibodies and dilutions used: anti-FZD7 (F7-Ab) (1:1,000 of 1 mg/mL stock), V5 tag antibody (GeneTex / GTX628529 / 1:4,000), monoclonal anti-β-catenin antibody (Sigma-Aldrich / C7207 / 1:2,000) (RRID_AB_476865) anti-β-actin antibody (Sigma-Aldrich / A2228 / 1:5,000) (RRID:AB_476697). All Western blots were washed three times in TBST prior to incubation in secondary antibody for 45-60 min at RT. Secondary antibodies and dilutions used: goat anti-human IgG HRP-conjugated (ThermoFisher Scientific / 62-8420 / 1:20,000) (RRID:AB_88136), goat anti-mouse IgG HRP-conjugated (Southern Biotech / 1030-05 / 1:20,000) (RRID:AB_2619742). All Western blots were

washed three times in TBST before protein detection by Millipore Sigma Luminata Forte Western HRP substrate and exposure to autoradiography film.

Super TOP-Flash (STF) luciferase assays.

Cells were lysed in luciferase assay buffer (100 mM K-PO_4 buffer pH 7.8, 0.2 % Triton X-100) and transferred to a black-walled 96-well plate. 100 µL of luciferase assay cocktail was added to each well of lysate (25 mM Tris-Cl pH 7.8, 15 mM $MgSO_4$, 10 mM ATP (Sigma-Aldrich), 65 µM BD D-luciferin-Potassium Salt (Fisher Scientific). Luciferase assay readouts were performed on a Promega GloMax Discover Microplate Reader.

Real Time Quantitative Polymerase Chain Reaction (RT-qPCR)

RNA expression was measured by RT-qPCR. RNA was extracted using TRIzol Reagent (ThermoFisher Scientific) and Direct-zol RNA MiniPrep Kit (Zymo Research). cDNA was generated using 50 ng RNA and iScript Reverse Transcription Supermix (Bio-Rad), then diluted 1:10 in UltraPure DNase/RNase-Free Distilled Water (ThermoFisher). RT-qPCR was performed using iTaq Universal SYBR Green Supermix (Bio-Rad) according to the manufacturer's recommendations, and a two-step amplification CFX_2stepAmp protocol on a Bio-Rad CFX384 Touch Real-Time PCR Detection System. Data was analyzed using the $2^{-\Delta\Delta Ct}$ method (Schefe et al., 2006). All gene expression was normalized to the expression of *RPL13A*. The following RT-qPCR primers were used (Gene ID, forward primer, reverse primer):

ARL4A, GGCGATTTAGTCAAGAGGAT, GCTCTTCTCAACACACTACA

AXIN2, TATCCAGTGATGCGCTGACG, CGGTGGGTTCTCGGGAAATG

CXCR4, ACTACACCGAGGAAATGGGCT, CCCACAATGCCAGTTAAGAAGA

FGF18, GAGGAGAACGTGGACTTCCG, ACCTGGATGTGTTTCCCACT

FOXA2, GGAGCAGCTACTATGCAGAGC, CGTGTTCATGCCGTTCATCC

KDR, CCTGTATGGAGGAGGAGGAAGT, CAAATGTTTTTACACTCACAGGCCG

MESP1, CTCTGTTGGAGACCTGGATG, CCTGCTTGCCTCAAAGTG

MIXL1, TCCAGGATCCAGCTTTTATTTTCT, GAGGATAATCTCCGGCCTAGC

NKD1, TCCCAACCTAGAAACCTTAG, AGAAGAAGGAGAAGGAAGAG

NKX1-2, GTAGAAGAGAGGGAATAGGGAGAG, AGCAGCAGAAGTCCAAAGTC

POU5F1, CTTGAATCCCGAATGGAAAGGG, GTGTATATCCCAGGGTGATCCTC

RPL13A, CCTGGAGGAGAAGAGGAAAGAGA, TTGAGGACCTCTGTGTATTTGTCAA

SOX9, GACACAAACATGACCTATCC, GATTCTCCATCATCCTCCAC

SOX17, GTGGACCGCACGGAATTTG, GGAGATTCACACCGGAGTCA

SP5, TCGGACATAGGGACCCAGTT, CTGACGGTGGGAACGGTTTA

Flow cytometry

HPS cell-derived EBs were dissociated with TrypLE Express at 37°C for 5-10 min, periodically triturated using P1000 pipette. Dissociated EBs were resuspended in FACS buffer (PBS, 1 mM EDTA, and 0.5 % FBS) and passed through a cell strainer (Corning). Cell suspensions were pelleted at 200xg for 3 min and resuspended in 100 µL of FACS buffer (approx. $1x10^5$ cells). Cells were incubated on ice for 30 min in the following primary fluorophore-conjugated antibodies (Antibody / Vendor / Catalog# / Concentration): APC anti-human CD34 / Biolegend / 343608 / 1:100 (RRID:AB_2228972); PE anti-human CD45 / Biolegend / 304008 / 1:100 (RRID:AB_314396); APC mouse IgG2a k isotype control / Biolegend / 400222 / 1:100; PE

mouse IgG1, k isotype control / Biolegend / 400112 / 1:100 (RRID:AB_2847828). Cells were washed with 2 mL of FACS buffer and spun down at 200xg for 3 min. Cells were resuspended in 500 mL of FACS buffer with 0.5µg/mL DAPI (Cell Signaling Technology). The cell suspensions were analyzed using the FACS Fortessa (BD Biosciences) and the resulting FSC files were processed with the FlowJo software (BD Biosciences).

Immunofluorescence of overexpressed FZD.

HEK293T F127-KO cells were plated in a 24 well-plate with coverslips. Cells were transfected with V5-tagged FZD receptors and two days post-transfection, cells were fixed with 4% formaldehyde for 15 minutes at RT. Cells were washed twice with 1X PBS and permeabilized with 1X PBS with 0.5% Triton X-100 for one hour at RT. Following permeabilization, cells were blocked with 0.5% BSA in 1X PBS with 0.1% Triton X-100 (1X PBST) for one hour at RT. Cells were stained with V5 antibody (Genetex / GTX628529 / 1:500) in 1X PBST at 4^{o}C overnight. Cells were washed three times with 1X PBST for 10 minutes each. Alexa-Fluor 488 Goat anti-Mouse IgG (Invitrogen / A11001 / 1:1000) (RRID:AB_2534069) in 1X PBST was used as the secondary antibody. Secondary antibody staining was done for 2 hours at RT. Following the secondary staining, cells were washed three times with 1X PBST for 10 minutes each. Coverslips were mounted on glass slides and imaged on Nikon Eclipse Ti2-E microscope with SR HP Apo TIRF 100x NA 1.49 objective.

Transcriptome analysis (RNA-seq)

Total RNA from cells was extracted using TRIzol Reagent and Direct-zol RNA MiniPrep Kit, according to manufacturer recommendations. cDNA library preparation and sequencing were done by Novogene Co., Ltd. A 250-300 bp insert cDNA library was generated by using the

NEBNext® Ultra RNA Library Prep Kit for Illumina® (New England Biolabs, Inc.). Transcriptome sequencing was performed on an Illumina NovaSeq 6000. TopHat (RRID:SCR_013035) and Cufflinks (RRID:SCR_014597) [85,86] were used to perform differential gene expression analysis of RNA-seq experiments. Briefly, sequencing reads were quality filtered, mapped, and aligned to the reference human genome (hg19) with TopHat and Cuffdiff (RRID:SCR_001647) was used to calculate gene expression levels as reads per thousand transcript bases per million reads mapped (RPKM). Statistically significant changes in gene expression were obtained from RPKM values. Genes were clustered by expression pattern and principal component analysis was performed in Genesis [87] (RRID:SCR_015775). Gene ontology was performed using GSEA [59,60] (RRID:SCR_003199).

Data availability

The RNA-seq data discussed in this publication have been deposited in NCBI's Gene Expression Omnibus and are accessible through GEO Series accession number GSE158121. Additional information on these data is available from the corresponding author. Plasmids encoding F7L6 and F7L6-sc will be made available upon request.

Chapter 1, in full, is a reprint of the material as it appears in *eLife*, 2020. Gumber, D.*, Do, M.*, Suresh Kumar, N., Sonavane, P.R., Wu, C.C.N., Cruz, L.S., Grainger, S., Carson, D., Gaasterland, T., Willert, K. The dissertation author was a co-primary investigator and co-author of this paper.

CHAPTER 2:

ANTIBODY-DRUG CONJUGATE SEPTUXIMAB VEDOTIN TARGETS FZD7 TUMORS

2.1 INTRODUCTION

WNT signaling plays critical roles in embryonic development and adult tissue homeostasis by regulating stem cell renewal and differentiation (reviewed in [28]). Consistent with these roles, dysregulation of WNT signaling is frequently found in many human cancers. Known examples of mutated or hyperactive WNT pathway components in cancer include, but are not limited to β-catenin destruction complex components, APC [88] and AXIN [89]; transcription factor, β-catenin [90]; WNT signaling agonists, RSPO2,3 [91]; and E3 ubiquitin ligase, RNF43 [92]. RSPOs, RNF43, and ZNRF3, the latter also an E3 ubiquitin ligase, act by stabilizing the abundance of cell-surface receptors that mediate WNT signals. These receptors include ten mammalian Frizzleds (FZD1-10), all of which have been implicated in multiple cancer types (reviewed in [93,94]).

Clinical trial efforts to drug the WNT pathway in solid tumors have mostly focused on inhibiting WNT receptors or WNT proteins (reviewed in [95]). In particular, the WNT receptors FZD1,2,5,7 and 8 were targeted in pancreatic, metastatic breast, and various other untreatable solid cancers by OMP-18R5 (Vantictumab), a human IgG2 antibody [96–99] (NIH clinical trial numbers: NCT01345201, NCT01957007, NCT01973309, and NCT02005315). Antibody-drug conjugates (ADCs) have also been developed to FZD10 (OTSA101-DTPA; trial NCT04176016) [100] and alternate WNT receptors, ROR1 (VLS-101, NCT03833180, NCT04504916) and PTK7 (PF-06647020; trial NCT03243331) [101]. Inhibition of pan-WNT signaling in the clinic has been achieved by two methods: using FZD8 decoy receptor, OMP-54F28 (Ipafricept), to sequester extracellular WNT proteins [102–104], or by blocking Porcupine (PORCN), a protein critical to WNT secretion from cells. Ipafricept was used in combination therapies to treat hepatocellular, liver, ovarian, and pancreatic cancers (NCT01608867, NCT02050178, NCT02069145, and

NCT02092363). Many small molecule inhibitors have been developed to inhibit PORCN, thereby inhibiting WNT secretion from cells, including WNT974/LGK974 (NCT01351103, NCT02278133, and NCT02649530), ETC-1922159 (ETC-159) (NCT02521844), RXC004 (NCT03447470), and CGX1321 (NCT02675946 and NCT03507998). These PORCN inhibitors potently disrupt growth of Rspo3-translocated cancers [105], which have been observed in 10% of colon cancers [91].

While many of the above WNT-targeting drugs demonstrated efficacy in cancer patients, bone-related adverse effects were commonly observed. These adverse events were likely due to the loss of endogenous WNT signaling, which is required for bone development and homeostasis [25–27]. A pancreatic cancer trial using vantictumab was terminated due to concerns around bone-related safety [96], and similar toxicities were found in an ipafricept trial for epithelial ovarian cancer [104] and ETC-159 trials for various solid tumors [106,107]. To alleviate the bone toxicities caused by these pan-WNT inhibitors, more specific WNT-pathway targeting strategies are required. Frizzled-7 (FZD7), a human cell-surface receptor for WNT proteins, is a strong candidate for targeting due to its restricted expression pattern. FZD7 expression is largely restricted to embryonic development, with absent to modest expression in most normal adult tissues. Of the 10 human FZDs, FZD7 has been the most widely implicated in solid tumors, including but not limited to melanoma, breast, ovarian, hepatocellular, gastric, and colon cancers [16,17,19–22]. Additionally, FZD7 is more highly expressed in glioma, esophageal, gastric, and colorectal tumors compared to adjacent normal tissue, which has led to the proposal that targeting FZD7 is a viable option to treat multiple solid tumors (reviewed in [23,24]).

Here, we describe the development and therapeutic evaluation of a novel FZD7-targeting antibody-drug conjugate, septuximab vedotin (F7-ADC), consisting of a chimeric human-mouse IgG1 antibody and antimitotic payload drug, monomethyl auristatin E (MMAE). We demonstrate that F7-ADC selectively and potently kills ovarian cancer cells that express high levels of FZD7 *in vitro*, as well as FZD7-high ovarian tumor xenografts *in vivo*. Additionally, we did not observe

toxicities following F7-ADC treatment in mice expressing a *Fzd7* gene that has been modified to render the Fzd7 protein reactive with the human-targeting F7-ADC. Our data suggest that the antibody-drug conjugate approach may be a powerful strategy to combat FZD7-expressing ovarian cancers in the clinic.

2.2 RESULTS

FZD7 RNA and protein expression are elevated in ovarian carcinomas.

To evaluate expression of *FZD7* across human cancers, we interrogated bulk RNA-seq patient datasets in The Cancer Genome Atlas (TCGA). We found elevated median *FZD7* expression (shown by X) in breast invasive carcinoma (BRCA), glioblastoma multiforme (GBM), lung squamous cell carcinoma (LUSC), ovarian serous cystadenocarcinoma (OV), prostate adenocarcinoma (PRAD), and uterine carcinosarcoma (UCS) studies. We then further analyzed TCGA OV and BRCA datasets (**Figure 16A**). We separated OV samples into four subtypes defined by "Classification of Ovarian Cancer" (CLOVAR), a prognostic model for high-grade serous ovarian carcinoma [108]. Median *FZD7* expression was higher in the mesenchymal and proliferative subtypes (**Figure 16B**), which correlate with a median survival of ~36 months in patients [108]. In contrast, median survival for the differentiated and immunoreactive subtypes is ~48 months [108]. We also separated BRCA samples based on reported histopathology status and identified a higher trend of *FZD7* expression in triple-negative breast cancer (**Figure 17**), which has been associated with poorer patient outcomes, including prognosis, disease-free survival, and overall survival [109]. Additionally, we analyzed FZD7 protein by immunohistochemistry and observed high expression in ovarian carcinomas, but low expression in normal tissues (**Figure 16C**), indicating that FZD7 may be a tumor-specific antigen. Taken together, these data indicate that FZD7 is a viable candidate for targeted cancer therapies against the WNT pathway in aggressive subtypes of ovarian and breast cancer.

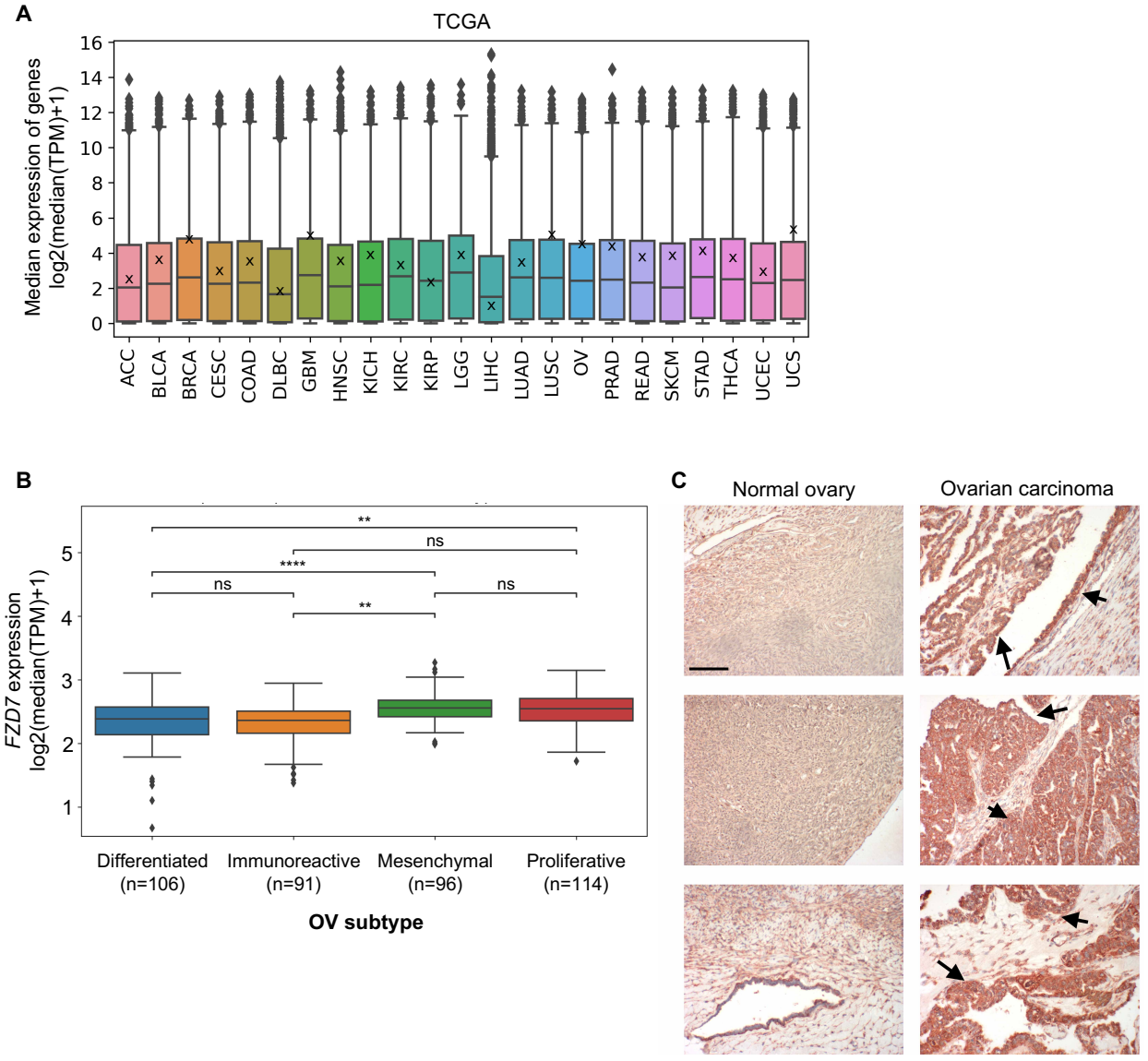

Figure 16. FZD7 RNA and protein expression are elevated in ovarian carcinomas.
(**A**) Median *FZD7* expression in TCGA RNA-seq by cancer type. Data points indicate individual genes; box plots indicate 75% of surveyed genes; X's on box plots indicate *FZD7* expression. (**B**) Median *FZD7* expression in TCGA OV subtypes defined by CLOVAR. Data points indicate individual patient samples; box plots indicate 75% of surveyed patient samples. For statistical analyses: two-sided Mann-Whitney-Wilcoxon test with Bonferroni correction; ****p≤0.0001; **p≤0.01; ns, not significant. (**C**) FZD7 expression is low in normal ovarian tissues but elevated in ovarian carcinomas. Tissues shown at 100X magnification; red-brown staining and arrows: FZD7 staining; scale bar, 500 μm.

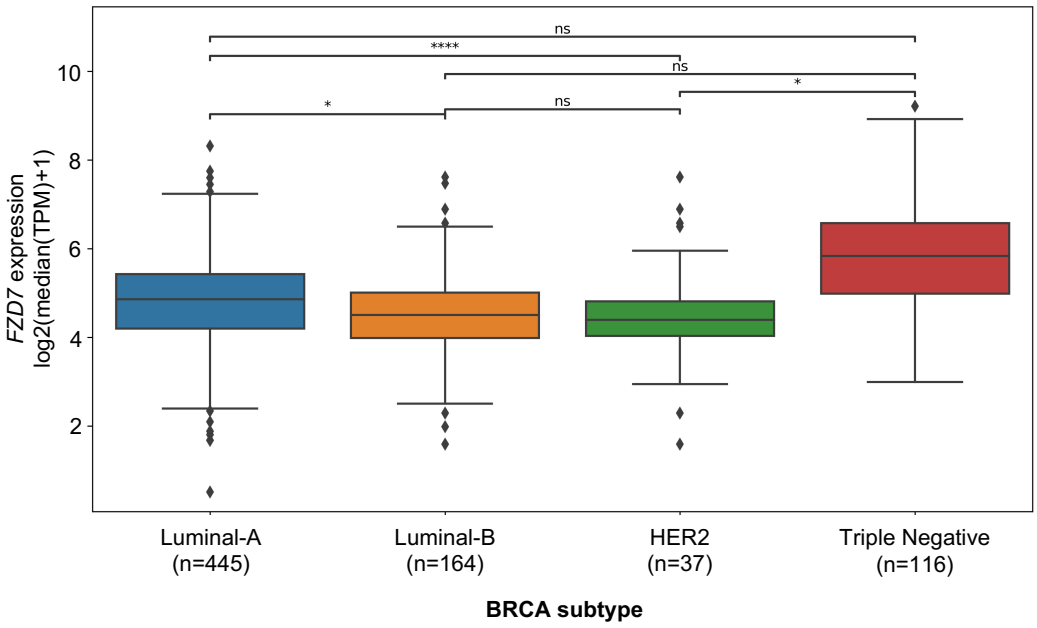

Figure 17. Median *FZD7* expression in TCGA BRCA by histopathological subtype.
Data points indicate individual patient samples; box plots indicate 75% of surveyed patient samples. For statistical analyses: two-sided Mann-Whitney-Wilcoxon test with Bonferroni correction; ****p≤0.0001; *p≤0.05; ns, not significant.

Antibody-drug conjugate septuximab vedotin binds FZD7.

To target human FZD7, we developed an antibody-drug conjugate, septuximab vedotin, hereafter referred to as F7-ADC. We previously demonstrated that the antibody to FZD7 (F7-Ab) binds FZD7 and does not cross-react with the other nine human FZD receptors, FZD(1-6,8-10) [12,15]. F7-ADC consists of a chimeric human-mouse IgG1 antibody (F7-Ab) [15] conjugated to antimitotic drug, monomethyl auristatin E (MMAE), by protease-cleavable maleimidocaproyl-valine-citrulline-para amino benzyl carbamoyl (MC-VC-PABC) linkers (described in [110]) (**Figure 18A**). An average of four MMAE were conjugated to cysteine residues in the antibody hinge region, following reduction of disulfides [110,111]. For non-invasive F7-ADC tracking, we also conjugated a Cy5 fluorophore to a hinge region disulfide via a non-cleavable maleimide linker. We measured loading of MMAE by denaturing reverse-phase high performance liquid chromatography (HPLC) and electro-spray mass spectroscopy (**Figure 19**). By flow cytometry, we confirmed that F7-ADC binds FZD7-expressing human cancer cell lines, MA-148, PA-1, OVCAR-3, and OVCAR-3 FZD7, and does not bind MA-148 FZD7-knockout (KO) cells (**Figure 18B**). We further compared FZD7 protein (**Figure 18C**) and RNA (**Figure 18D**) expression on this panel of cancer cell lines. These data demonstrate that F7-ADC specifically binds human cancer cells that express FZD7.

Figure 18. Antibody-drug conjugate septuximab vedotin binds FZD7.
(**A**) Schematic of antibody-drug conjugate, septuximab vedotin (F7-ADC). MC-VC-PABC-MMAE and Cy5 are conjugated to the IgG1 antibody at cysteine (cys) residues. (**B**) F7-ADC selectively binds FZD7-expressing human cancer cell lines, MA-148, PA-1, OVCAR-3, and OVCAR-3 FZD7. F7-ADC does not bind MA-148 FZD7-KO. Live cells were stained with F7-ADC at the indicated concentrations and analyzed by flow cytometry. (**C**) FZD7 protein expression represented as mean fluorescence intensity (MFI). Live cells were stained with F7-Ab and analyzed by flow cytometry. (**D**) *FZD7* expression by RT-qPCR and normalized to HEK293T (HEK) FZD1,2,7-KO. Data represented as mean ± SEM for three technical replicates.

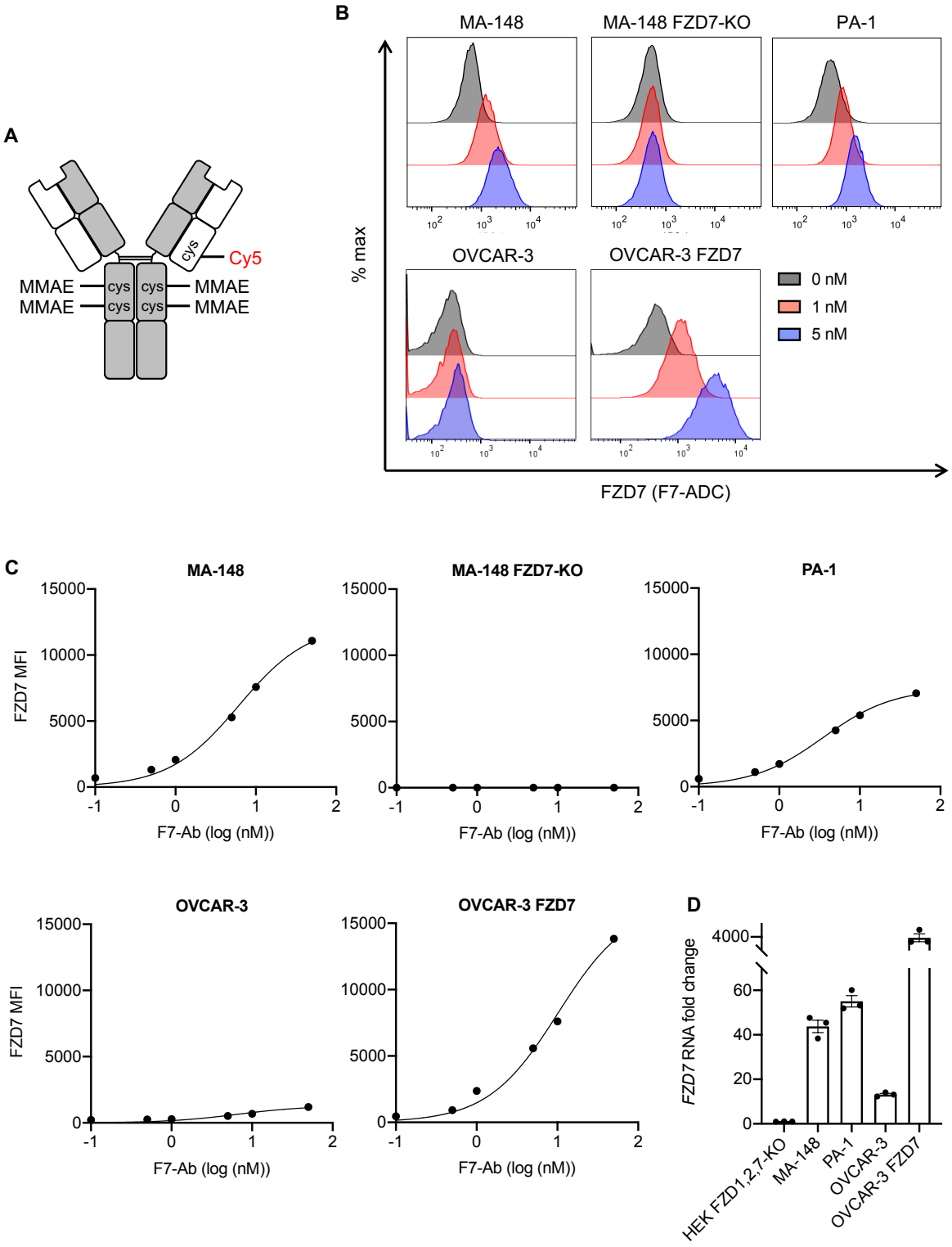
A
Cy5
MMAE
MMAE
cys
B
MA-148
MA-148 FZD7-KO
PA-1
OVCAR-3
OVCAR-3 FZD7
0 nM
1 nM
5 nM
% max
FZD7 (F7-ADC)
C
MA-148
MA-148 FZD7-KO
PA-1
OVCAR-3
OVCAR-3 FZD7
FZD7 MFI
F7-Ab (log (nM))
D
FZD7 RNA fold change
HEK FZD1,2,7-KO
MA-148
PA-1
OVCAR-3
OVCAR-3 FZD7

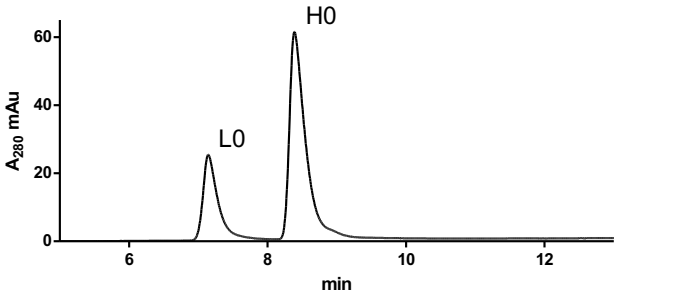

Peak	Ave MW	Assignment
L0	23503	Light chain (LC)[a]
H0	50970	Heavy chain (HC)[a]

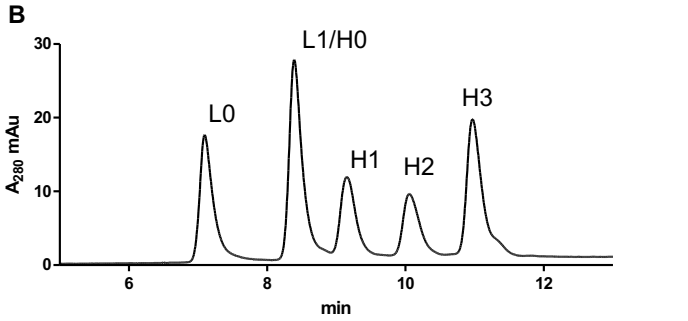

Peak	Ave MW	Assignment
L0	23497	LC
L1/H0	24819 (+1332)	LC-MMAE
	50993	HC
H1	52299 (+1329)	HC-MMAE
H2	53603 (+2633)	HC-(MMAE)2
H3	54931 (+3961)	HC-(MMAE)3

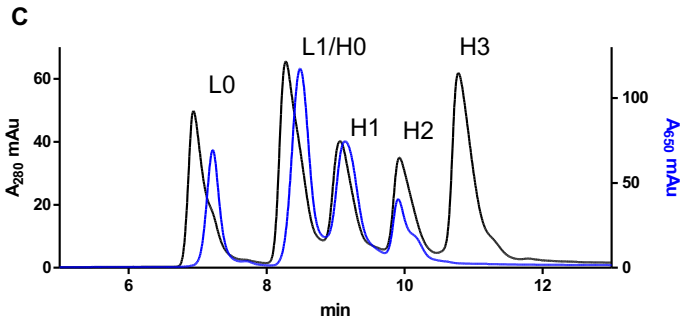

Peak	Ave MW	Assignment
L0	23498	LC
	24273 (+775)	LC-Cy5
L1/H0	24819 (+1332)	LC-MMAE
	50999	HC
	51764 (+794)	HC-Cy5
H1	52313 (+1343)	HC-MMAE,
	53089 (+2119)	HC-MMAE-Cy5
H2	53600 (+2633)	HC-(MMAE)2
	54389 (+3419)	HC-(MMAE)2-Cy5
H3	54930 (+3960)	HC-(MMAE)3

Figure 19. Conjugation of FZD7 antibody with MMAE and Cy5.
Reverse-phase protein chromatograms and electro-spray mass spectroscopy analysis of FZD7 IgG1 antibody (F7-Ab) after (**A**) reduction with excess DTT (**B**) partial reduction with 4 equivalents of TCEP and subsequent reaction with 4 equivalents of MC-VC-PABC-MMAE followed by (**C**) 2 equivalents of Cy5-maleimide, followed by gel filtration and concentration. F7-Ab light and heavy chain reported theoretical MW are 23,503.2 and 49,516.8, respectively, with expected multiple heavy chain glycoforms. Expected addition in mass is 1316.6 and 779.9 for MC-VC-MMAE and Cy5-maleimide respectively.

Septuximab vedotin selectively targets and kills FZD7-expressing cells *in vitro*.

Antibody-drug conjugates with MC-VC-PABC linkers function by binding the target and internalizing to the lysosomes of the target cell, where cathepsin B cleaves the linker from the antibody and releases the payload drug [112]. To confirm that F7-ADC internalizes to the lysosomes of FZD7-expressing cancer cells, we treated FZD7-positive and FZD7-negative cells with a vehicle control (PBS) or F7-ADC and performed confocal live imaging. We observed colocalization of F7-ADC and lysosomes in only FZD7-positive MA-148, PA-1, and OVCAR-3 FZD7 cells (**Figure 20A**).

Next, we demonstrated that F7-ADC induces direct, FZD7-dependent cytotoxicity in a cell viability assay *in vitro* (**Figure 20B**). A single dose of F7-ADC killed MA-148 and PA-1 cells at an IC50 of 5 nM (0.76 ug/mL), and OVCAR-3 FZD7 cells at an IC50 of 0.025 nM (3.9 ng/mL). The IC50 for OVCAR-3 and MA-148 FZD7-KO cells were 25 nM (3.9 ug/mL) and 60 nM (9.6 ug/mL), respectively. F7-Ab treatment did not affect cell viability of FZD7-positive or FZD7-KO cells. In summary, we have shown that F7-ADC selectively internalizes to the lysosomes of FZD7-expressing human cancer cells and induces direct cell death.

Figure 20. Septuximab vedotin specifically targets and kills FZD7-expressing cells *in vitro*. (**A**) Colocalization of F7-ADC and lysosomes were observed after one hour in FZD7-positive MA-148, PA-1, and OVCAR-3 FZD7, but not in MA-148 FZD7-KO. Arrows: colocalization; scale bar: 10 μm; inset scale bars: 5 μm. (**B**) F7-ADC induces direct, FZD7-dependent cytotoxicity in a cell viability assay. Cells were treated with 0.1-100 nM (0.0016-16.4 μg/mL) of indicated drug and all viability were normalized to vehicle. Data represented as mean ± SEM for two independent experiments, three technical replicates per experiment.

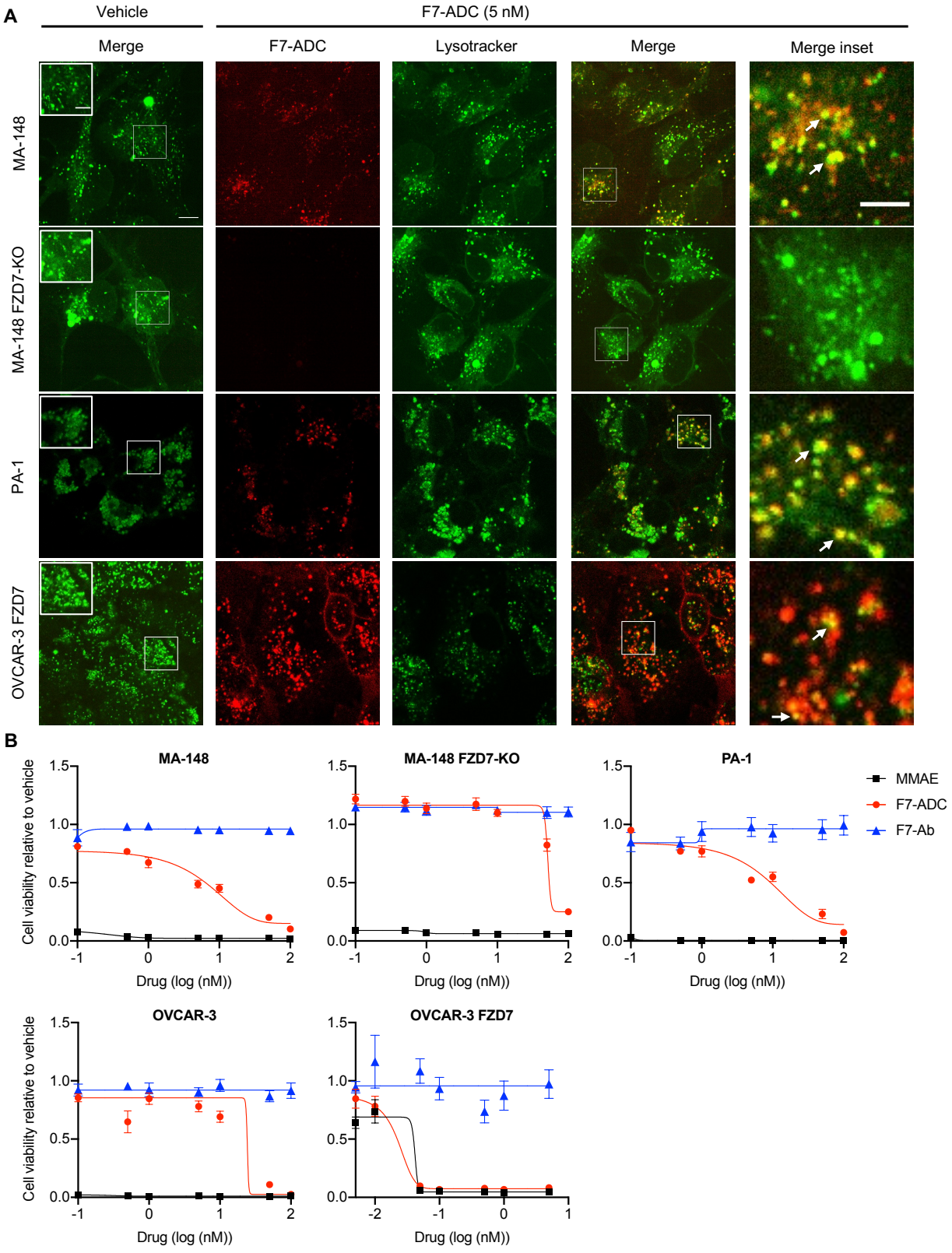
A
Vehicle
F7-ADC (5 nM)
Merge
F7-ADC
Lysotracker
Merge
Merge inset
MA-148
MA-148 FZD7-KO
PA-1
OVCAR-3 FZD7
B
MA-148
MA-148 FZD7-KO
PA-1
OVCAR-3
OVCAR-3 FZD7
Cell viability relative to vehicle
Drug (log (nM))
MMAE
F7-ADC
F7-Ab

Septuximab vedotin induces regression of FZD7 tumors *in vivo*.

To test *in vivo* efficacy of the human-targeting F7-ADC, we utilized a xenograft tumor model (**Figure 21**). We established MA-148, PA-1, or MA-148 FZD7-KO subcutaneous tumors expressing a luciferase reporter, and measured tumor bioluminescence using an In Vivo Imaging System (IVIS). Mice were then treated twice per week with a vehicle control or F7-ADC (3 mg/kg; ~0.5 nmole) by intravenous (tail vein) injection. F7-ADC-treated MA-148-Luciferase and PA-1-Luciferase tumors regressed, while F7-ADC-treated MA-148 FZD7-KO-Luciferase tumors were not statistically different from the control tumors (**Figure 22**). Here, we established a therapeutic F7-ADC dose for tumor regression and demonstrated its specificity to FZD7-expressing tumors *in vivo*. Altogether, our data indicate that intravenous administration of F7-ADC targets and kills implanted tumors that highly express FZD7.

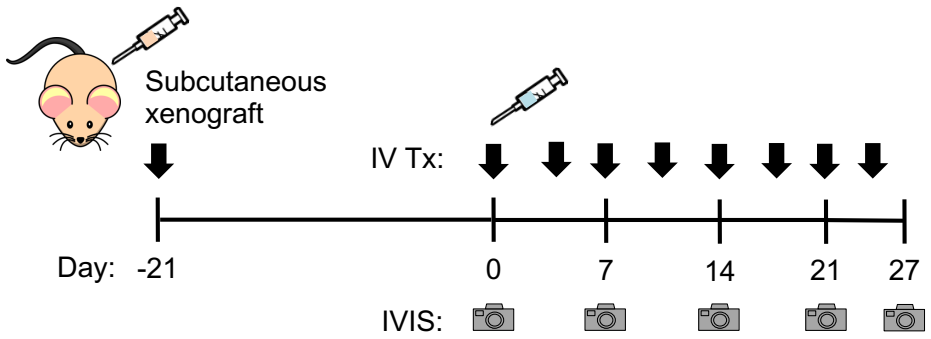

Figure 21. Schematic of *in vivo* tumor xenograft response studies.
Six-week-old female nude mice were injected with cells in the bilateral upper thigh to establish subcutaneous tumor xenografts (MA-148-Luciferase (Luc), PA-1-Luc, or MA-148 FZD7-KO-Luc). Tumor bioluminescence was measured by an IVIS Spectrum after intraperitoneal injection of XenoLight D-luciferin. Mice were randomized into groups once normalized tumor bioluminescence (radiance) reached at least $1x10^7$ photons/s. Treatments were delivered twice per week by bilateral tail vein injection (IV Tx).

Figure 22. Septuximab vedotin induces regression of FZD7 tumors *in vivo*.
(**A**) MA-148-Luciferase and (**B**) PA-1-Luciferase subcutaneous tumor xenografts treated with F7-ADC (3 mg/kg; ~0.5 nmole) regressed after 6 doses of ADC (one vehicle MA-148-Luciferase mouse was euthanized prior to Day 27 due to the tumor diameter exceeding 15mm). (**C**) F7-ADC-treated MA-148 FZD7-KO-Luciferase tumors were not statistically different from vehicle-treated tumors. Tumor IVIS data represented as mean ± SEM; arrows indicate days of treatment (Tx). For statistical analyses: one-way ANOVA and Tukey's multiple comparisons test: ****p≤0.0001; ***p≤0.001; **p≤0.01; *p≤0.05. (**D**) IVIS images for each tumor type.

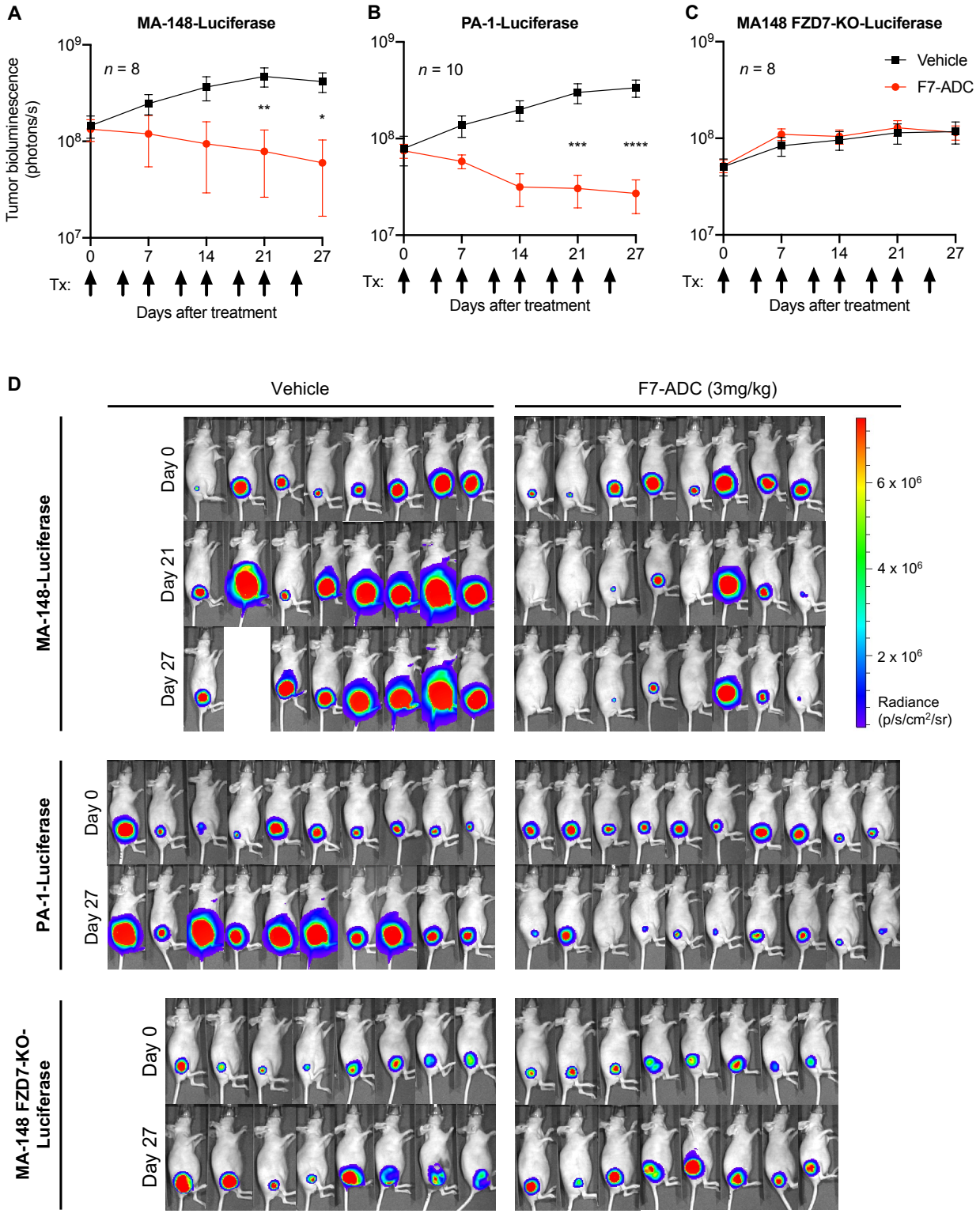
A
MA-148-Luciferase
Tumor bioluminescence (photons/s)
n = 8
**
*
Tx:
Days after treatment
B
PA-1-Luciferase
n = 10
***
****
Tx:
Days after treatment
C
MA148 FZD7-KO-Luciferase
n = 8
Vehicle
F7-ADC
Tx:
Days after treatment
D
Vehicle
F7-ADC (3mg/kg)
MA-148-Luciferase
PA-1-Luciferase
MA-148 FZD7-KO-Luciferase
Day 0
Day 21
Day 27
6 x 10^6
4 x 10^6
2 x 10^6
Radiance (p/s/cm²/sr)

Generation of *Fzd7$^{hF7/hF7}$* mice.

We previously identified the extracellular epitope on human FZD7 to which our antibody (F7-Ab), used in F7-ADC, binds [15]. Moreover, we found that a single amino acid change (proline to leucine at position 188, P188L) in mouse Fzd7 renders Fzd7 reactive with F7-Ab, which we raised to target human FZD7. We used CRISPR-Cas9 to engineer the P188L mutation mouse *Fzd7* (**Figure 23, 24A-B**). The resulting mouse line, *Fzd7$^{hF7/hF7}$*, expresses Fzd7^{P188L} receptors that are recognized by F7-Ab (**Figure 24C**). *Fzd7$^{hF7/hF7}$* mice are viable, fertile, and do not exhibit any of the phenotypic abnormalities previously described in *Fzd7* knockout mice, including tail truncation and kinking [113], suggesting that the *Fzd7$^{hF7/hF7}$* allele produces a functional Fzd7^{P188L} protein.

To further confirm that Fzd7^{P188L} is functional, we tested its ability to transduce Wnt signaling *in vitro*. We derived mouse embryonic fibroblasts (MEFs) from E13.5 *Fzd7$^{+/+}$* (wild type) and *Fzd7$^{hF7/hF7}$* embryos and transduced them with Wnt reporter, 7TGC (TOP-GFP:SV40-mCherry) [114]. To selectively activate Fzd7^{P188L}, we used a previously described WNT mimetic, F7L6 [15], which only interacts with human FZD7. We quantified reporter GFP activity from mCherry-expressing MEFs using flow cytometry after treatment and confirmed that *Fzd7$^{hF7/hF7}$* MEFs responded to F7L6 and Wnt3a. In contrast, Wnt reporter activity in *Fzd7$^{+/+}$* MEFs was only stimulated by Wnt3a and not F7L6 (**Figure 24D**). To summarize, we established a *Fzd7$^{hF7/hF7}$* mouse line expressing Fzd7^{P188L} receptors, which react with our human FZD7-specific F7-ADC and retain Wnt signaling functionality.

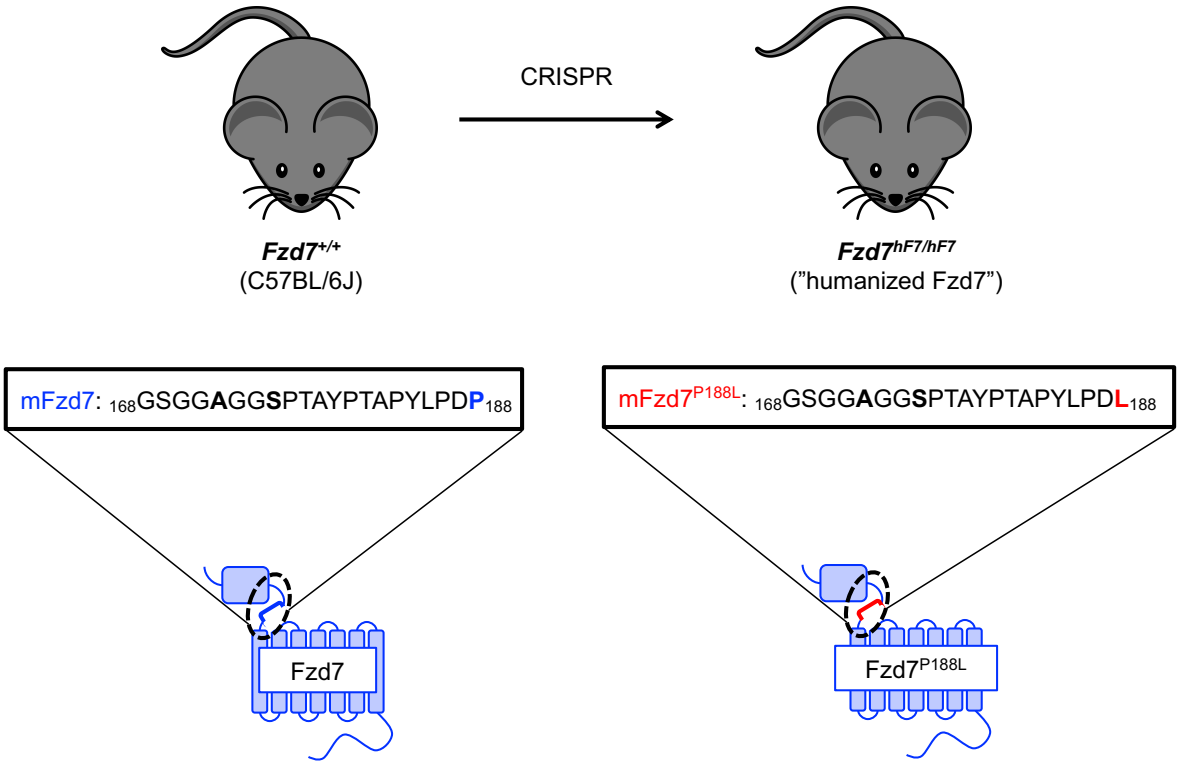

Figure 23. Schematic of Fzd^{P188L} mutation in *Fzd7*$^{hF7/hF7}$ mice.
We mapped the extracellular epitope on human FZD7 to which our antibody, and therefore F7-ADC, binds. The change from proline to leucine at position 188 (P188L) in mouse Fzd7 renders Fzd7 reactive with the antibody. We engineered the mouse *Fzd7* gene such that its protein product expresses a Fzd7 protein carrying the P188L mutation. The resulting *Fzd7*$^{hF7/hF7}$ mice are viable, fertile, and do not exhibit any of the phenotypic abnormalities previously described in Fzd7 knockout mice [113].

Figure 24. Generation of *Fzd7$^{hF7/hF7}$* mice.
(**A**) Schematic of genotyping strategy for *Fzd7$^{hF7/hF7}$* mice. Top: domain structure of mouse Fzd7 protein. Bottom: genomic region of *Fzd7* gene on mouse chromosome 1. Arrows indicate position of polymerase chain reaction (PCR) primers for genotyping. Restriction enzyme BglII digests the PCR product generated from the *Fzd7$^{hF7/hF7}$* allele only. Abbreviations: aa, amino acids; bp, base pairs; CRD, cysteine rich domain; *Fzd7$^{+/+}$*, wild type; ORF, open reading frame; SS, signal sequence; TMD, transmembrane domain. (**B**) Genotyping of *Fzd7$^{+/+}$* and *Fzd7$^{hF7/hF7}$* alleles. PCR and BglII digest of genomic DNA produces a 300-bp fragment for *Fzd7$^{+/+}$* and 250-bp fragment for *Fzd7$^{hF7/hF7}$*. (**C**) Immunoblot of cell lysates of fibroblasts derived from E13.5 *Fzd7$^{+/+}$* and *Fzd7$^{hF7/hF7}$* mice. F7-Ab reacts with the Fzd7^{P188L} protein from *Fzd7$^{hF7/hF7}$* mice but not with wild type Fzd7 protein. (**D**) F7L6 specifically activates Fzd7^{P188L} from *Fzd7$^{hF7/hF7}$* MEFs carrying Wnt reporter, 7TGC. Top: representative flow plots. Bottom: data represented as mean ± SEM from three independent experiments. For statistical analyses: one-way ANOVA and Dunnett's multiple comparisons test: ***p≤0.001; **p≤0.01; *p≤0.05.

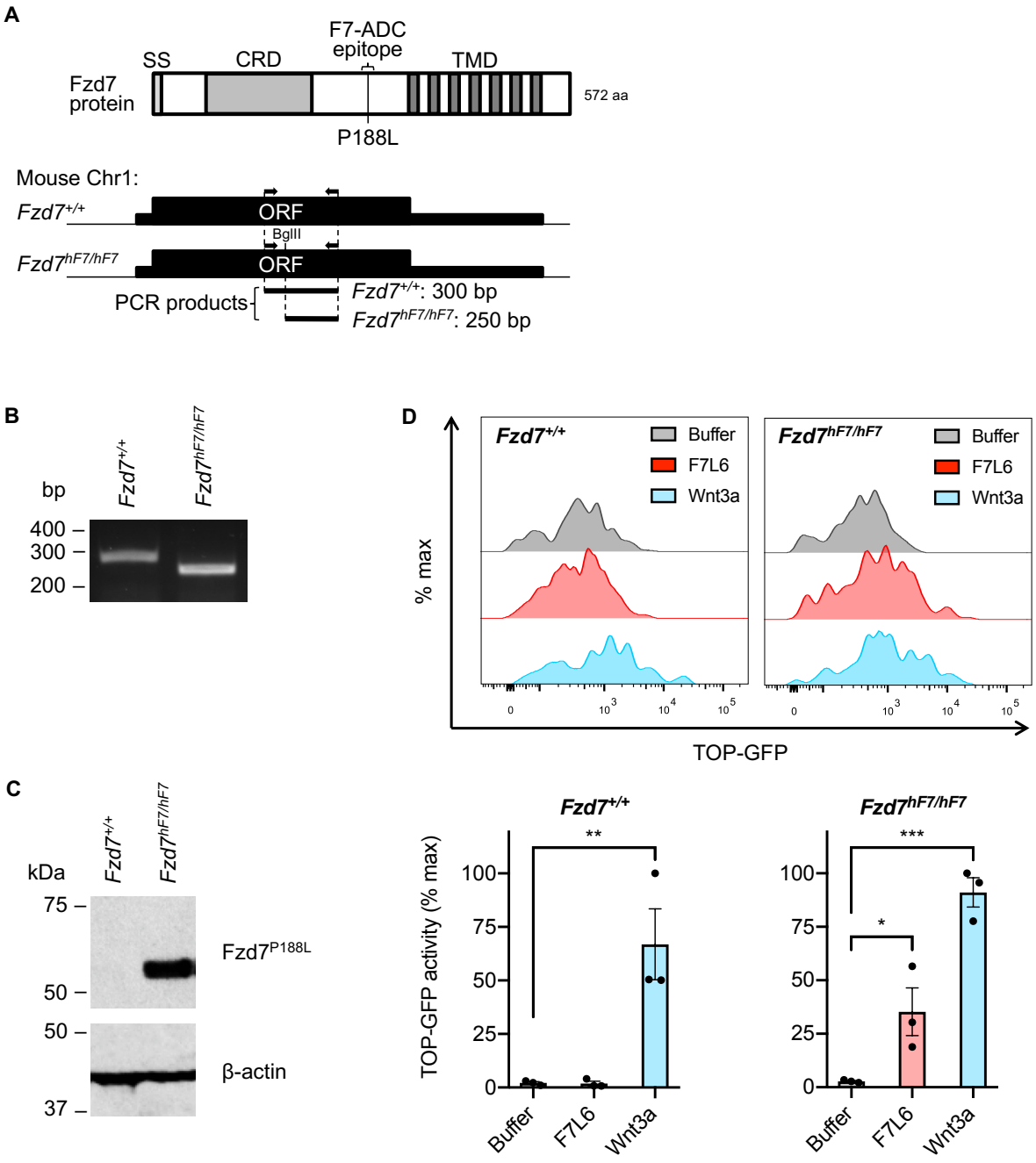
A
SS
CRD
F7-ADC epitope
TMD
Fzd7 protein
572 aa
P188L
Mouse Chr1:
Fzd7+/+
ORF
BglII
Fzd7hF7/hF7
ORF
PCR products
Fzd7+/+: 300 bp
Fzd7hF7/hF7: 250 bp
B
bp
Fzd7+/+
Fzd7hF7/hF7
400 –
300 –
200 –
C
kDa
Fzd7+/+
Fzd7hF7/hF7
75 –
50 –
Fzd7P188L
50 –
37 –
β-actin
D
Fzd7+/+
Buffer
F7L6
Wnt3a
Fzd7hF7/hF7
Buffer
F7L6
Wnt3a
% max
TOP-GFP
Fzd7+/+
Fzd7hF7/hF7
TOP-GFP activity (% max)
**
***
*
100
75
50
25
0
Buffer
F7L6
Wnt3a

Septuximab vedotin does not induce toxicity in *Fzd7$^{hF7/hF7}$* mice.

To evaluate potential toxicities induced by our human-FZD7-targeting F7-ADC, we tested F7-ADC in *Fzd7$^{hF7/hF7}$* mice (**Figure 25**). On Day 0, we administered a single tail vein injection of F7-ADC (10 mg/kg) in twelve-week-old females and males of *Fzd7$^{hF7/hF7}$* and *Fzd7$^{+/+}$* mice (F7-ADC does not recognize wild type mouse Fzd7) (**Figure 26**). None of the F7-ADC-treated *Fzd7$^{hF7/hF7}$* nor of the *Fzd7$^{+/+}$* mice exhibited any changes in activity levels or grooming behavior two hours post-injection and over the following seven days, compared to their respective uninjected controls. Additionally, we did not observe diarrhea or concerning changes in weight during this time, suggesting that the Fzd7+ intestinal stem cells [115,116] were not adversely impacted by the F7-ADC. We further confirmed this finding by examining hematoxylin and eosin (H&E) stained sections of the brain, eye, heart, kidney, liver, ovary or testis, skin, small intestine, and spleen.

Sections of the aforementioned organs from *Fzd7$^{hF7/hF7}$* and *Fzd7$^{+/+}$* mice were reviewed digitally from 2X to 40X magnification. No histopathological abnormalities were noted in any organs: no areas of necrosis, fibrosis, calcification, increased inflammatory infiltrates, edema, dysplastic changes or carcinoma were detected (representative images of the intestine, ovary, skin, and liver in **Figure 27**). Importantly, we did not observe damage to the crypt or villi structures within the small intestine, where Fzd7 is expressed. In sum, we confirmed that a 10 mg/kg dose of F7-ADC (capable of killing implanted tumor xenografts) was not toxic to *Fzd7$^{hF7/hF7}$* mice at the organismal or tissue level.

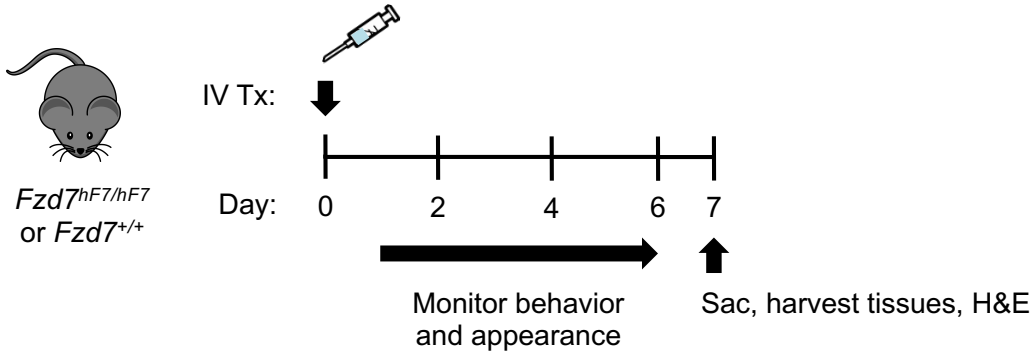

Figure 25. Schematic of septuximab vedotin toxicity study in *Fzd7$^{hF7/hF7}$* mice.
Twelve-week-old mice *Fzd7$^{hF7/hF7}$* and *Fzd7$^{+/+}$* mice were untreated or given a single dose of F7-ADC (10 mg/kg) by tail vein injection. Mice were monitored for two hours post-injection on Day 0 and daily for the following seven days. On Day 7, mice were euthanized (sac) and organs were harvested for hematoxylin and eosin (H&E) staining and histopathological analyses.

				Histopathological changes								
Genotype	**Sex**	**Tx**	**% Weight change**	**Brain**	**Eye**	**Heart**	**Kidney**	**Liver**	**Ovary or testis**	**Skin**	**Small intestine**	**Spleen**
Fzd7$^{hF7/hF7}$	F	None	-1.4%	-	-	-	-	-	-	-	-	-
		ADC	-1.4%	None	None	None	None	None	None	None	None	None
			-1.5%	None	None	None	None	None	None	None	None	None
	M	None	+3.1%	-	-	-	-	-	-	-	-	-
		ADC	-10.8%	None	None	None	None	None	None	None	None	None
			+13.2%	None	None	None	None	None	None	None	None	None
Fzd7$^{+/+}$	F	None	-3.2%	-	-	-	-	-	-	-	-	-
		ADC	-3.7%	None	None	None	None	None	None	None	None	None
			-4.4%	None	None	None	None	None	None	None	None	None
	M	None	-0.8%	-	-	-	-	-	-	-	-	-
		ADC	-2.3%	None	None	None	None	None	None	None	None	None
			-1.9%	None	None	None	None	None	None	None	None	None

Figure 26. Summary of septuximab vedotin toxicity study in *Fzd7*$^{hF7/hF7}$ mice.
Fzd7$^{hF7/hF7}$ and *Fzd7*$^{+/+}$ mice were untreated or given a single intravenous dose of F7-ADC (10 mg/kg). Mice were weighed prior to injection (Day 0) and seven days after (Day 7). H&E staining was performed on the indicated organs harvested on Day 7. The study was blinded for histopathological analyses and no tissue damage was detected.

Figure 27. Septuximab vedotin does not induce tissue damage in *Fzd7*$^{hF7/hF7}$ mice.
Twelve-week-old *Fzd7*$^{hF7/hF7}$ and *Fzd7*$^{+/+}$ were given a single dose of F7-ADC (10 mg/kg) by tail vein injection and organs were harvested seven days later. No histopathological changes were detected in the small intestine, ovary, skin, or liver. Scale bars: 200 µm; blue: nuclei; bright pink: erythrocytes and eosinophilic granules; various shades of pink: cytoplasm.

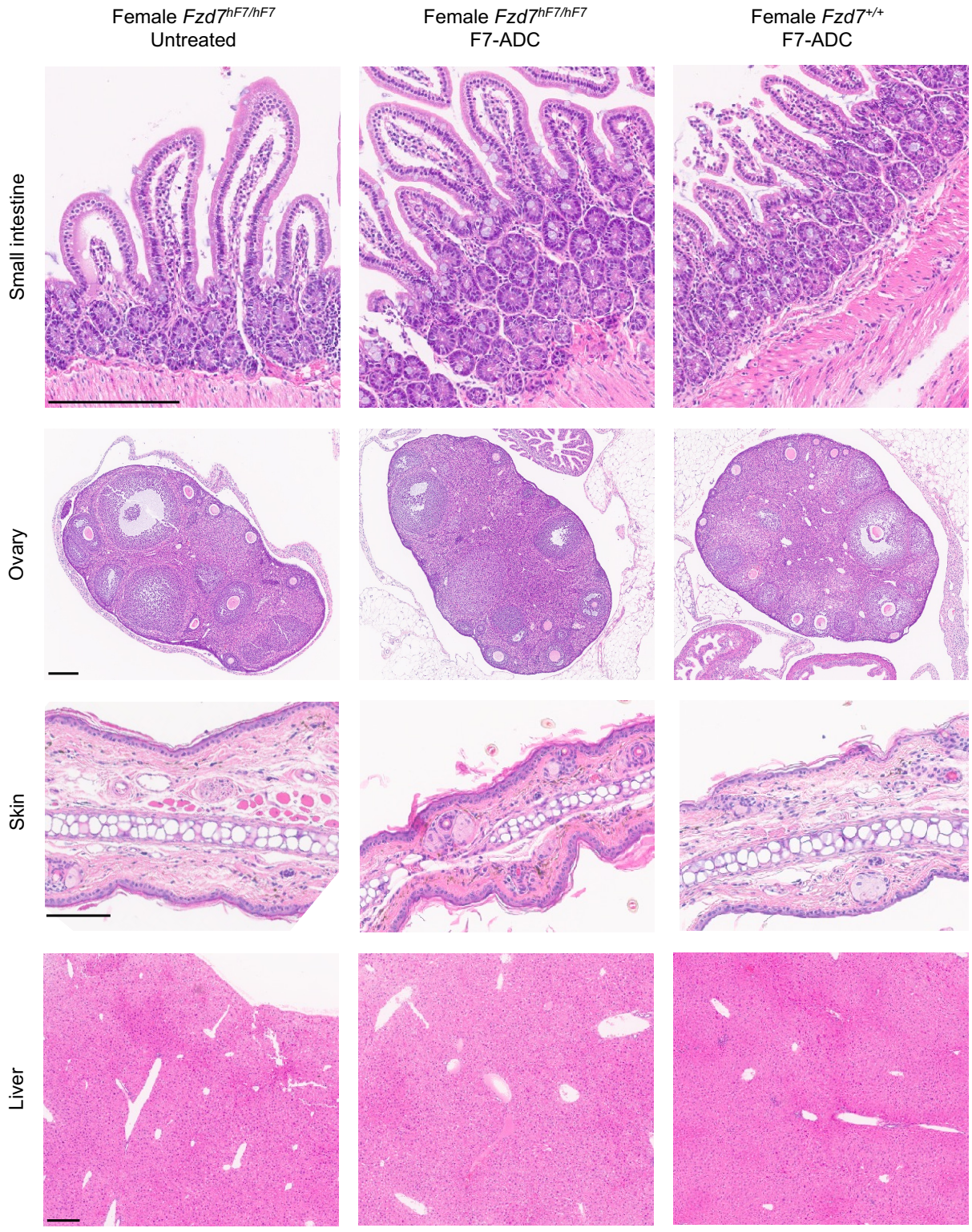
Female Fzd7hF7/hF7
Untreated
Female Fzd7hF7/hF7
F7-ADC
Female Fzd7+/+
F7-ADC
Small intestine
Ovary
Skin
Liver

2.3 DISCUSSION

Although aberrant WNT signaling is observed in many classes of solid tumors, drugging the WNT pathway in the clinic has proved to be a challenge. Most WNT-targeting therapies are designed to globally inhibit WNT signaling, frequently resulting in bone-related adverse effects in patients. In an effort to mitigate the bone toxicities associated with WNT inhibition, we developed an antibody-drug conjugate, septuximab vedotin (F7-ADC), to directly kill human cancer cells expressing WNT receptor, FZD7. In bulk RNA-seq analyses of TCGA datasets, we found elevated median *FZD7* expression in breast invasive carcinoma (BRCA), glioblastoma multiforme (GBM), lung squamous cell carcinoma (LUSC), ovarian serous cystadenocarcinoma (OV), prostate adenocarcinoma (PRAD), and uterine carcinosarcoma (UCS) studies. Upon closer inspection of TCGA BRCA and OV samples, we identified higher *FZD7* expression in triple-negative breast cancer and mesenchymal and proliferative ovarian cancer subtypes, all of which correlate with poorer median survival. Additionally, we observed high FZD7 protein expression in ovarian carcinomas and low FZD7 in normal ovary tissues by immunohistochemistry, indicating that FZD7 may be a tumor-specific antigen. By mining TCGA data and performing these histological analyses, we confirmed that FZD7 is a viable candidate for targeted cancer therapies against the WNT pathway.

F7-ADC is a chimeric human-mouse IgG1 antibody conjugated by MC-VC-PABC linkers to four MMAE molecules, on average. We confirmed that F7-ADC selectively binds FZD7 on human cancer cells, then internalizes to the lysosomes of target cells, where cathepsin B cleaves the linkers and releases the payload drug, MMAE. F7-ADC treatment of FZD7-high ovarian cancer cells, such as MA-148 and PA-1, induced direct cytotoxicity *in vitro* and tumor xenograft regression in nude mouse models. Furthermore, high-dose F7-ADC treatment did not result in toxicities at the organism or tissue level in *Fzd7*$^{hF7/hF7}$ mice, which we engineered to express Fzd7 receptors carrying the P188L mutation necessary for F7-ADC binding. In future studies, it may be worth exploring the tumor-killing performance of F7-ADC in immunocompetent mouse models,

such as the MMTV-Wnt1 mouse tumor model where Fzd7 expression is upregulated [117]. In this setting, F7-ADC may engage host innate immunity to enhance tumor regression, through mechanisms such as antibody-dependent cellular cytotoxicity (ADCC) or antibody-dependent cellular phagocytosis (ADCP). Because F7-ADC does not recognize mouse Fzd7, developing a syngeneic mouse model would require engineering the $Fzd7^{P188L}$ mutation in mouse tumor cells or crossing our *Fzd7*$^{hF7/hF7}$ mice with an existing genetically engineered mouse tumor model. Generating such *in vivo* models would provide further valuable insight into F7-ADC efficacy and potential adverse effects in an immunocompetent system.

In contrast to vantictumab, we did not observe inhibitory effects of our unmodified FZD7 antibody on cancer cell growth (**Figure 3B** and unpublished observations). This lack of effect may be attributed to the fact that our antibody engages FZD7 in the linker region between the cysteine rich domain (CRD) and the first transmembrane domain. Although FZD7-antibody (F7-Ab) complexes are effectively internalized, and an essential feature for antibody and antibody-drug conjugate efficacy, F7-Ab does not block WNT binding to the CRD. Vantictumab, on the other hand, binds the CRD and effectively blocks WNT binding and signaling [97]. Additionally, vantictumab's tumor inhibitory effects may be attributable to its ability to bind multiple FZD receptors (FZD1, 2, 5, 7 and 8) that singly or collectively may play crucial roles in cell proliferation.

In summary, our preclinical F7-ADC data has demonstrated therapeutic efficacy and exquisite specificity to FZD7 *in vitro* and *in vivo*, as well as no toxicity in the *Fzd7*$^{hF7/hF7}$ mouse model. By directly killing FZD7-positive cancer cells, rather than globally inhibiting WNT signaling, we anticipate that the bone-related adverse events frequently associated with WNT-targeting drugs will be alleviated or prevented. Moreover, FZD7 has been implicated in many cancers with poor prognosis. In ovarian cancer, FZD7 expression has correlated with resistance to platinum-based chemotherapy, tumor initiation, and cancer stem cell (CSC) proliferation [118,119]. In additional examples, FZD7 was associated with epithelial-mesenchymal transition in triple-negative breast cancer [120], cisplatin and paclitaxel resistance in uterine cancer [121], and tumor proliferation in

gastric cancer [122]. As such, the F7-ADC approach may be a powerful clinical strategy to combat a variety of aggressive solid tumors that express high levels of FZD7.

2.4 MATERIALS AND METHODS

Cell lines and culture conditions

MA-148 and MA-148 FZD7-KO were cultured in RPMI-1640, 10% fetal bovine serum (FBS), and 1% penicillin/streptomycin. MA-148 line was kindly provided by Dr. Sundaram Ramakrishnan (University of Miami). PA-1 were obtained from ATCC and cultured in Dulbecco's Modified Eagle's Medium (DMEM), 20% FBS, Glutamax, nonessential amino acids (NEAA), and penicillin/streptomycin. OVCAR-3 and OVCAR-3 FZD7 were cultured in RPMI-1640, 20% FBS, Glutamax, NEAA, and penicillin/streptomycin. OVCAR-3 cell line was obtained from ATCC. HEK293T FZD1,2,7-KO were kindly provided by Dr. Michael Boutros (Heidelberg University) and cultured in DMEM, 10% FBS, and penicillin/streptomycin. Mouse embryonic fibroblasts (MEFs) were cultured in DMEM, 10% FBS, Glutamax, NEAA, 25 mM HEPES, and penicillin/streptomycin.

MA-148 FZD7-KO was generated by CRISPR/Cas9 knockout and screened for FZD7 expression by immunoblot and flow cytometry. MA-148 was transfected with pCas9-EGFP and two modified pGRNA plasmids (kindly provided by Dr. Chad Cowan, Harvard University). OVCAR-3 FZD7 was generated by transfecting OVCAR-3 cells with pPB–EF1α:FZD7–IRES:H2B-mCherry–BlastR and pCS2-PiggyBac-Transposase.

gRNA sequence #1 for FZD7-KO: GGCCGCTCCGCTTTCGTCCC

gRNA sequence #2 for FZD7-KO: GGGCATGAGAAGGGGAAGG

Expression vectors and cloning

7TGC (Addgene 24304); Cas9-EGFP and pGRNA (kindly provided by Dr. Chad Cowan, Harvard University; pcDNA3.4-TOPO FZD7 IgG1 antibody (F7-Ab) heavy chain; pcDNA3.4-TOPO F7-Ab light chain; pCS2-PiggyBac-Transposase; pLVX-Luciferase-PuroR (kindly provided by Drs. Ian Huggins and Steve Dowdy, UC San Diego); pPB–EF1α:FZD7–IRES:H2B-mCherry–BlastR.

Antibody-drug conjugate synthesis

F7-Ab-MMAE drug conjugate was synthesized using methods previously described [110,111]. A solution (2 mL, 10.2 mg/mL) of F7-Ab was treated with sodium bicine buffer (200 µL, 1M pH 8.3) and sodium diethylenetriaminepentaacetic acid (20 µL, 100 mM pH 7). Following reduction with 4 equivalents of tris(carboxyethyl)phosphine (TCEP) at 37°C for 2h, the solution was added to 4 equivalents of maleimidocaproyl-valine-citrulline-PABC-MMAE (MC-VC-PABC-MMAE, Levena Biopharma). After 30 min. at room temperature, Cy5-maleimide (2 equivalents) was added and after a further 30 min., gel-filtered (Sephadex G25, 1.0 g) eluting with phosphate buffered saline (PBS). Following centrifugal concentration (Centricon 30 kD MWCO) to about 500 µL, the concentrations of antibody and Cy5 were determined by absorbance using extinction coefficients of 251,000 $M^{-1}cm^{-1}$ (F7-Ab) at 280 nm and 12500 $M^{-1}cm^{-1}$ and 250,000 $M^{-1}cm^{-1}$ at 280 nm and 650 nm respectively for Cy5. Drug loading was measured by denaturing reverse-phase HPLC of the reaction mix prior to addition of Cy5 maleimide, following reduction of any remaining intersubunit disulfides with 50 mM DTT for 30 min. Peaks corresponding to light or heavy chains with 0-3 MMAE were identified by electro-spray mass spectroscopy (**Figure 19**) and peak areas at 280 nm were integrated and weighted to calculate the drug loading. Modified light chain (L1) and unmodified H chain (H0) were not resolved so MMAE loading is an underestimate. No free MC-VC-PABC-MMAE was detected by HPLC following gel filtration.

Flow cytometry

Cells were dissociated using Accutase, pelleted, resuspended in fluorescence-activated cell sorting (FACS) buffer (PBS, 5 mM EDTA, and 2% FBS), and passed through a 40-µm cell strainer (Corning). $1x10^5$ cells were incubated on ice for 30 min. with the indicated concentrations of F7-ADC or F7-Ab-Alexa Fluor 647. Cells were washed with 3 mL of FACS buffer, pelleted, and resuspended in FACS buffer with 0.5 µg/mL DAPI (Cell Signaling Technology). Cells were

analyzed on an LSRFortessa (BD Biosciences) and FSC files were processed using FlowJo (BD Biosciences).

Real Time Quantitative Polymerase Chain Reaction (RT-qPCR)

RT-qPCR methods and primer sequences (*FZD7*, *RPL13A*) were used as previously described [15].

Confocal live imaging

Cells were seeded on a glass-bottom plate for imaging. Cells were washed with PBS, then treated with a vehicle control (PBS) or F7-ADC in 1% FBS media at 37°C for 3 hr. Cells were washed with PBS and replenished with regular 10% FBS media and 50 nM Lysotracker Green (Invitrogen). Live imaging was performed 1 hr. after media replenishment on a Nikon Eclipse Ti2-E or Nikon CSU-W1 microscope with a Plan Apo Lambda 60x 1.4NA objective.

Cytotoxicity assay

Cells were seeded in a 96-well plate the day before drug treatment. MA-148, PA-1, and MA-148 FZD7-KO were incubated with the indicated drugs for 3 days. OVCAR-3 and OVCAR-3 FZD7 were incubated for 5 days due to slower doubling time compared to the other three cell lines. Drug-containing media was then removed, replaced with 100 µL RPMI-1640 and 100 µL of CellTiter-Glo2.0 per well, and incubated in the dark for 25 min. CellTiter-Glo2.0 luciferase readouts were performed on a Promega GloMax Discover Microplate Reader.

***Fzd7$^{hF7/hF7}$* mouse line generation**

Fzd7$^{hF7/hF7}$ mice were generated by standard CRISPR/Cas9 methods by Transgenic Mouse Services at UC San Diego (UCSD) and in compliance with UCSD Institutional Animal Use

and Care Committee (IACUC). C57BL/6NHsd mouse embryos were injected with a Fzd7 repair oligo, Fzd7 guide RNA (gRNA), and Cas9 mRNA (Invitrogen). The repair oligo was ordered from Integrated DNA Technologies. The *in vitro* transcribed gRNA was generated using a MEGAscript™ T7 Transcription Kit (ThermoFisher).

Fzd7 repair oligo (Underlined: new BglII site; bolded: changed nucleotides):
GACGGCTCCGGGGGCGCGGGCGGCAGTCCCACCGCCTACCCTACTGCTCCCTACCTGCC
AGA**T**C**T**ACCTTTCACTGCGATGTCCCCCTCAGATGGCAGAGGCCGCTTGTCTTTCCCCTTC
TCGTGTCCGCGC

Fzd7 guide RNA (Underlined: PAM sequence): GGGGACATCGCAGTGAAAGG(TGG)

MEF generation

All animal work was done in compliance with UCSD IACUC. MEFs were generated from decapitated E13.5 embryos. 7-8 embryos per genotype were minced in warm trypsin for 10 min., washed with trypsin, and pipetted up and down. DNase (Promega) was added to the embryo suspension, pipetted up and down three times, and incubated at 37°C for 5 min. MEF media was added to the suspension, pipetted up and down, and centrifuged at 1000 x g. Supernatant was removed and the embryo pellet was resuspended in MEF media and plated for cell expansion.

Immunoblot

Immunoblot methods and antibody dilutions were used as previously described [15].

TOP-GFP assay

Primary MEFs at passage 3 (P3) were transduced with third-generation lentivirus containing 7TGC (Addgene 24304) and then passed. P4 MEFs were treated with Wnt3a buffer, 5 nM Wnt3a, or 5 nM F7L6. Cells were dissociated using Accutase, pelleted, resuspended in FACS buffer with 0.5 µg/mL DAPI (Cell Signaling Technology), and passed through a 40-µm cell

strainer (Corning). Cells were analyzed on an LSRFortessa (BD Biosciences) and FSC files were processed using FlowJo (BD Biosciences).

In vivo tumor xenograft response studies

All animal work was done in compliance with UCSD IACUC. Six-week-old female nude mice were purchased from the UC San Diego Animal Care Program breeding colony. MA-148-Luciferase (Luc), PA-1-Luciferase, or MA-148 FZD7-KO-Luciferase cells were injected in the bilateral upper thigh to establish subcutaneous tumors. For MA-148-Luciferase or MA-148 FZD7-KO-Luciferase tumors, $3x10^6$ cells were suspended in 100 µL of a 1:1 mix of Matrigel and 10% FBS media. For PA-1-Luciferase tumors, $5x10^6$ cells were suspended in 100 µL of a 1:1 mix of Matrigel (BD Biosciences) and 10% FBS media. Tumor bioluminescence was measured by an IVIS Spectrum after intraperitoneal injection of XenoLight D-luciferin (Perkin Elmer; 200 µL of a 15 mg/mL stock). Tumor bioluminescence was normalized to background bioluminescence of a non-tumor-bearing mouse injected with luciferin. Mice were randomized into groups once normalized tumor bioluminescence (radiance) reached at least $1x10^7$ photons/second. IVIS analyses were performed using Living Image software (Perkin Elmer). Treatments were delivered twice per week by bilateral tail vein injection. To prevent unnecessary morbidity, mice were euthanized if tumor length exceeded 15 mm by caliper measurement.

In vivo toxicity study

All animal work was done in compliance with UCSD IACUC. Twelve-week-old *Fzd7*$^{hF7/hF7}$ and *Fzd7*$^{+/+}$ mice were treated with F7-ADC (10 mg/kg) by bilateral tail vein injection. Seven days after injection, mice were euthanized and tissues collected. All tissues were fixed in 4% PFA for 24 hr. at 4°C. Brains were transferred to a 30% sucrose solution and all other tissues were transferred to 70% ethanol (EtOH) and stored at 4°C.

H&E staining

Hematoxylin and eosin (H&E) staining was done by UCSD Tissue Technology Shared Resource (TTSR) on a Thermo Gemini AS Stainer. Tissues were baked at 60°C for 1 hr. and transferred to solutions in the following order: Clearite-3 (ThermoFisher), 100% EtOH, 95% EtOH, diH_2O, hematoxylin (ThermoFisher), diH_2O, Clarifier 1 (ThermoFisher), diH_2O, Bluing Solution (ThermoFisher), diH_2O, 70% EtOH, Eosin-Y (ThermoFisher), 70% EtOH, 95% EtOH, 100% EtOH, Clearite-3, mounting medium (VWR).

Immunohistochemistry

OV801a ovarian cancer tissue array with matched or unmatched adjacent normal tissue was purchased from US Biomax. Immunohistochemistry (IHC) was done by UCSD TTSR. Tissues were baked at 60°C for 1 hr., then cleared and rehydrated through successive solutions: xylene, 100% EtOH, 95% EtOH, 70% EtOH, diH_2O. Antigen retrieval was performed in Antigen Unmasking Solution (Vector) at 95°C for 30 min. Staining was performed on Intellipath Automated IHC Stainer (Biocare): tissues were blocked in Peroxidase Bloxall (Vector), washed in TBST, and blocked in 3% donkey serum for 10 min. Primary stain was F7-Ab (2.5 µg/mL) for 1 hour. Tissues were then processed as follows: TBST washes, anti-rabbit HRP Polymer (Cell IDX) for 10 min., TBST washes, anti-mouse EnVision+ System-HRP Labelled Polymer (Dako) for 5 min.; diH_2O washes, Mayer's Hematoxylin (Sigma) for 5 min., TBST washes, diH_2O washes, cleared and mounted in xylene-based mounting media.

The Cancer Genome Atlas analyses

RNA-sequencing (RNA-seq) counts (TPM normalized) were obtained from [123]. The median TPM value of each gene in each cancer type was computed and log2-normalized values are plotted. For the OV dataset, classification of samples was obtained from [108]. The BRCA

dataset was classified by the reported histopathology status of each patient. For a reproducible version of the code used for these analyses, visit:

https://notebook.genepattern.org/services/sharing/notebooks/409/preview/

https://notebook.genepattern.org/services/sharing/notebooks/410/preview/

https://notebook.genepattern.org/services/sharing/notebooks/411/preview/

https://notebook.genepattern.org/services/sharing/notebooks/412/preview/

Chapter 2, in full, is currently being prepared for submission for publication of the material. Do, M., Wu, C.C.N., Sonavane, P.R., Juarez, E.F., Adams, S.R., Ross, J., Rodriguez y Baena, A., Patel, C., Mesirov, J.P., Carson, D.A., Advani, S.J., Willert, K. The dissertation author was the primary investigator and author of this paper.

CHAPTER 3:

CONCLUSION AND FUTURE DIRECTIONS

WNT signaling has extensive roles in modulating embryonic development, stem cell biology, and adult disease. But until recently, targeting and studying the roles of individual WNT receptors were complicated by two factors: the inherent ability of WNTs to engage multiple receptors, and the vast number of WNT ligands and FZD receptors encoded by the mammalian genome. My co-authors and I addressed these issues by engineering an activating, bispecific antibody (F7L6) to WNT receptors, FZD7 and LRP6, to further investigate the role of FZD7 signaling in human pluripotent stem (hPS) cells. While we previously established a role for FZD7 in maintaining pluripotency [12,124], here, we also found that FZD7 can induce stem cell differentiation towards mesendodermal lineages [15]. Almost identically to Wnt3a, a known driver of differentiation, F7L6 elicited a transcriptome response associated with early development, including formation of the primitive streak and gastrulation movements. Furthermore, we validated *in vitro* that F7L6 treatment of hPS cells directed mesoderm and definitive endoderm differentiation.

Wnt signaling agonists have incredible potential in regenerative medicine as they are potent activators of stem cell differentiation. However, Wnt proteins themselves have not been approved for clinical applications, due in part to difficulties in protein stability, purification, and solubility. Wnts are frequently produced from the conditioned media of cell lines (e.g. CHO, HEK293T, or L fibroblasts) that stably express and secrete the Wnt of interest. Protein stability in 4°C conditioned media over time can be variable between Wnt species; for example, mouse Wnt3a and human WNT3A are stable for up to one year, while human WNT9A can degrade within a month (unpublished observations for WNT9A). In addition to the issues of producing and storing stable Wnts is the challenge of purifying them, by methods such as fast protein liquid chromatography (FPLC). Published Wnt purifications are multi-step protocols that require elution with detergents (e.g. CHAPS) since most, if not all Wnts possess hydrophobic post-translational

modifications [74,76]. At times, these complex and harsh protein purifications may yield Wnts that are no longer biologically active. Additionally, established purification processes for some Wnt species do not apply to all Wnts. For example, the protocols for Wnt3a and human WNT5A purification [74,76] do not apply to WNT9A, for reasons not yet identified (unpublished observations).

To circumvent the hurdles of protein stability and developing unique purification methods for dozens of Wnt species, we and other members of the Wnt field have instead turned to generating bispecific antibodies to Fzd/FZD and Lrp/LRP receptors, which we refer to as Wnt mimetics [40,41,77–79]. Like naturally occurring Wnt proteins, these engineered Wnt mimetics heterodimerize Fzds/FZDs and Lrps/LRPs to activate Wnt signaling. However, mimetics present many benefits over Wnts. Mimetics often utilize an antibody-based IgG Fc scaffold [15,40] that enables high protein stability, water solubility, and straightforward FPLC purifications without detergent-containing elution steps. Importantly, the single chain variable fragments (scFv) of mimetics can be designed to engage FZDs of our choosing, allowing us to study FZD-specific functions. While previous Wnt mimetics targeted FZD1,2,4,5,7,8 [40,41], F7L6 selectively activates FZD7-mediated WNT signaling and induces mesendodermal differentiation of hPS cells.

Because F7L6 and Wnt3a/WNT3A promote similar transcriptional changes in hPS cells, F7L6 may replace Wnt3a/WNT3A in select contexts of stem cell differentiation and regenerative medicine *in vitro* or *in vivo*. While we observed that F7L6 potently activates mesoderm reporter T-eGFP in H9 hPS cells (**Figure 13**), F7L6 inhibited generation of CD34+/CD45+ hematopoietic stem and progenitor cells (HSPCs) (**Figure 15**). Previous work showed that FZD9 and WNT9A are critical mediators of HSPC formation [37]. Our combined data indicate that FZD7 and FZD9 are not functionally redundant in hPS cells, as FZD7 signaling activates early mesoderm patterning but does not promote blood cell formation. Our work adds to the increasing evidence that select WNT-FZD pairings have specific functions during development and stem cell differentiation.

Like Wnt3a/WNT3A, F7L6 also mediates definitive endoderm (DE) specification of hPS cells, where we observed potent induction of DE markers like *SOX17*, *FOXA2*, *CXCR4*, and *CER1*

(**Figure 9, 14**). Cells of DE lineage form the primitive gut tube, which is further classified into three sections. The foregut gives rise to the esophagus, trachea, lungs, thyroid, stomach, liver, biliary system, and pancreas; the midgut forms the small intestine; and the hindgut forms the colon [125]. Though further investigation is required, F7L6 may be able to replace Wnt3a/WNT3A in early stages of pancreatic or hepatic differentiation, for example, from hPS cells *in vitro* [126,127].

Fzd7/FZD7 signaling not only regulates embryonic and induced pluripotent stem cells, but also adult stem cells. Fzd7 is enriched in Lgr5+ crypt-based columnar (CBC) stem cells in the mouse and human intestine [115]. Conditional deletion of *Fzd7* in CBC stem cells of *Lgr5*$^{EGFP\text{-}IRES\text{-}CreERT2}$ mice impaired intestinal crypt formation and *Fzd7* knockout mice (*Fzd7*$^{NLS/NLS}$) exhibited defects in regenerating intestinal epithelium following a 14-Gy dose of whole-body radiation [113,115]. In another example, the ΔNp63 isoform of the Trp63 transcription factor regulates normal mouse mammary stem cell (MaSC) activity and epithelial homeostasis by activating *Fzd7* transcription to enhance Wnt signaling [117]. Theoretically, F7L6 can be used to activate FZD7 in intestinal CBC stem cells and normal MaSCs to promote cell differentiation and regeneration of damaged tissue. However, we have not yet tested F7L6 *in vivo* nor determined its safety profile. Furthermore, dosing and timing of F7L6 administration *in vivo* would require careful monitoring to prevent uncontrolled tissue growth and tumor-initiating activity.

While critical for normal development and stem cell regulation, WNT signaling can go awry and contribute to the development and progression of diseases such as cancer. FZD7 has been implicated multiple solid tumors, including ovarian and breast cancer, but no FZD7-specific drugs had been developed. To date, the majority of WNT-targeting drugs are inhibitors of global WNT signaling and frequently cause bone-related adverse events in the clinic, despite showing anti-tumor efficacy. To address this unmet need, my co-authors and I developed septuximab vedotin (F7-ADC), an antibody-drug conjugate consisting of a chimeric IgG1 antibody to FZD7 and antimitotic payload drug, MMAE, attached by protease-cleavable MC-VC-PABC linkers. We demonstrated that F7-ADC selectively and potently kills ovarian cancer cells that express high

levels of FZD7 *in vitro*, as well as FZD7-high ovarian tumor xenografts *in vivo*. Moreover, we did not observe acute toxicities following F7-ADC treatment in immunocompetent *Fzd7*$^{hF7/hF7}$ mice, which we engineered to react with our human-targeting F7-ADC. Taken together, the F7-ADC approach may provide a powerful biomarker-driven therapeutic approach to combat a variety of aggressive solid tumors overexpressing FZD7.

While F7-ADC induced regression of cell line derived xenografts in nude immunocompromised mice, further *in vivo* evaluation of tumor-killing efficacy and toxicity are necessary. The MA-148 and PA-1 tumor xenografts used were derived from human cancer cell lines and therefore homogenous in high FZD7 protein expression. In reality, patient tumors are heterogenous, likely with variable expression of FZD7. One method of modeling tumor heterogeneity *in vivo* is to identify patient tumor samples with moderate to high FZD7 protein or RNA expression, and then implant these samples as patient-derived xenograft (PDX) tumors in immunocompromised mice (e.g. NOD *scid* gamma). Once the PDX tumors are established, we can then administer F7-ADC intravenously to determine an efficacious dose for tumor regression. While we have envisioned F7-ADC as a treatment for any FZD7-high solid tumor, we chose to focus on ovarian cancers after identifying a higher trend of *FZD7* RNA in the more aggressive mesenchymal and proliferative subtypes of ovarian serous cystadenocarcinoma in TCGA (**Figure 16B**). Based on our TCGA analyses, additional solid tumor types of interest include breast invasive carcinoma (particularly the triple-negative subtype; **Figure 17**), glioblastoma multiforme, lung squamous cell carcinoma, prostate adenocarcinoma, and uterine carcinosarcoma (**Figure 16A**).

It will also be worth exploring the anti-tumor activity of F7-ADC in immunocompetent animal models. In an immunocompetent system, F7-ADC may engage host innate and adaptive immunity to potentiate tumor regression, through mechanisms such as antibody-dependent cellular cytotoxicity (ADCC) or antibody-dependent cellular phagocytosis (ADCP). Because F7-ADC does not recognize mouse Fzd7, developing a syngeneic mouse model would require

engineering the Fzd7^{P188L} mutation in C57BL/6J mouse-derived cancer cells (e.g. E0771, ID8) or crossing *Fzd7$^{hF7/hF7}$* mice with a genetically engineered mouse model, such as the *MMTV-Wnt1* model for basal-like breast cancer where Fzd7 expression is upregulated [117]. Generating such *in vivo* models would provide further valuable insight into F7-ADC efficacy and potential adverse events in an immunocompetent system.

While we utilized F7-ADC as a monotherapy in tumor xenograft mouse studies, we can better model clinical practice by testing F7-ADC in combination with standard-of-care chemotherapy *in vivo*. For example, ovarian cancer would be treated with taxane- or platinum-based chemotherapeutics [102,104], and breast cancer with doxorubicin, cyclophosphamide, and/or taxanes [128]. Ideally using PDX tumor models or a syngeneic *Fzd7$^{hF7/hF7}$* tumor model, our goal in these studies would be to determine if a combination of F7-ADC and chemotherapy yields better tumor response than chemotherapy alone. Because an ADC and chemotherapy combination may prove to be a toxic combination, we would also need to closely monitor the tumor-bearing mice for adverse events over time. A concern for most WNT-targeting cancer drugs, in particular, has been bone toxicity. As such, we can collect blood from mice weekly and analyze serum levels of P1NP and CTX, biomarkers of bone formation and resorption, respectively. Additionally, we can examine bone structure and density at the study endpoint.

MMAE is a potent anti-tumor payload but MMAE-ADCs can cause adverse events like anemia, neutropenia, thrombocytopenia, hepatic toxicity, and peripheral neuropathy in up to 15% of patients [129]. We demonstrated that F7-ADC, an MMAE-ADC, did not cause acute toxicities or tissue damage in *Fzd7$^{hF7/hF7}$* mice up to seven days after treatment (**Figure 26, 27**). However, we have not yet addressed the possibility of adverse events with twice-per-week treatments over 4+ weeks, which was the dosing strategy used in our tumor xenograft studies. Longer-term treatment with F7-ADC may cause damage to normal tissues where Fzd7/FZD7 is expressed. Immunohistochemical analyses of normal human tissue identified moderate FZD7 expression in the skin, ovarian stroma, intestine, and breast, and low expression in the kidney, muscle, uterus,

testes, eye, and adrenal cortex (unpublished data). In particular, FZD7+ stem cell compartments in the intestine and breast may be damaged by long-term F7-ADC treatment, leading to impaired tissue regeneration capabilities. This type of toxicity has been observed in transgenic mouse models where *Fzd7* knockout or conditional *Fzd7* deletion in *Lgr5*+ intestinal stem cells significantly diminishes crypt formation in the small intestine, especially after whole-body radiation [113,115]. Follow-up toxicity studies in *Fzd7*$^{hF7/hF7}$ mice, ideally a syngeneic *Fzd7*$^{hF7/hF7}$ tumor model, will be required to generate a more comprehensive safety profile of F7-ADC *in vivo*.

In the event that longer-term treatment with F7-ADC is toxic in *Fzd7*$^{hF7/hF7}$ mice, we can replace MMAE in F7-ADC with an alternative payload drug. Other microtubule-inhibitory payloads used in clinically approved ADCs include monomethyl auristatin F (MMAF) and mertansine (DM1). Compared to MMAE, MMAF is less cell-permeable and less cytotoxic as a free drug [111], and used in depatuxizumab mafodotin, an EGFR-targeting ADC for recurrent glioblastoma [130]. Though DM1 has a comparable safety profile to MMAE [129], it has been successfully used in ado-trastuzumab emtansine for HER2-positive breast cancer [131]. Lastly, ravtansine (DM4) is another microtubule inhibitor used in mirvetuximab soravtansine, a folate receptor alpha (FRα)-targeting ADC in Phase 3 trial for platinum-resistant ovarian cancer [132]. Other classes of payloads include topoisomerase I inhibitors (e.g. SN-38 [133]), peptide elongation inhibitors (e.g. exotoxin A [134]), and DNA-alkylating agents (e.g. DGN549/IGN-P1 [135]).

To summarize, the WNT receptor FZD7 has versatile roles in the contexts of development, stem cell regulation, and cancer. Because WNT mimetic F7L6 selectively activates FZD7 signaling and potently directs DE differentiation of hPS cells, it has the potential to become a useful tool in producing endoderm-lineage organs *in vitro*, such as the pancreas and liver. Additionally, F7L6 may stimulate regeneration of intestinal and mammary tissue by activating and inducing differentiation of FZD7+/LGR5+ intestinal stem cells and FZD7+ mammary stem cells in adults. In cancer, we and others have correlated higher FZD7 expression with more aggressive subsets of solid tumors, and so we developed septuximab vedotin (F7-ADC) to directly kill FZD7+

tumors. While we have established an *in vivo* dose for tumor xenograft regression, further preclinical development of F7-ADC is required. The tumor-killing efficacy of F7-ADC needs to be tested in FZD7+ PDX tumor models and a syngeneic, immunocompetent *Fzd7*$^{hF7/hF7}$ mouse tumor model, with the option of using F7-ADC in combination with standard-of-care chemotherapy. Lastly, we need to generate a more comprehensive drug safety profile with longer-term F7-ADC treatment in a syngeneic *Fzd7*$^{hF7/hF7}$ tumor model and monitoring for adverse events.

REFERENCES

(1) Sharma, R. P.; Chopra, V. L. Effect of the Wingless (Wg1) Mutation on Wing and Haltere Development in Drosophila Melanogaster. *Developmental Biology* **1976**, *48* (2), 461–465. https://doi.org/10.1016/0012-1606(76)90108-1.

(2) Nusse, R.; van Ooyen, A.; Cox, D.; Fung, Y. K. T.; Varmus, H. Mode of Proviral Activation of a Putative Mammary Oncogene (Int -1) on Mouse Chromosome 15. *Nature* **1984**, *307* (5947), 131–136. https://doi.org/10.1038/307131a0.

(3) Nusse, R.; Varmus, H. E. Many Tumors Induced by the Mouse Mammary Tumor Virus Contain a Provirus Integrated in the Same Region of the Host Genome. *Cell* **1982**, *31* (1), 99–109. https://doi.org/10.1016/0092-8674(82)90409-3.

(4) Sato, N.; Meijer, L.; Skaltsounis, L.; Greengard, P.; Brivanlou, A. H. Maintenance of Pluripotency in Human and Mouse Embryonic Stem Cells through Activation of Wnt Signaling by a Pharmacological GSK-3-Specific Inhibitor. *Nature Medicine* **2004**, *10* (1), 55–63. https://doi.org/10.1038/nm979.

(5) Hao, J.; Li, T.-G.; Qi, X.; Zhao, D.-F.; Zhao, G.-Q. WNT/β-Catenin Pathway up-Regulates Stat3 and Converges on LIF to Prevent Differentiation of Mouse Embryonic Stem Cells. *Developmental Biology* **2006**, *290* (1), 81–91. https://doi.org/10.1016/j.ydbio.2005.11.011.

(6) Ogawa, K.; Nishinakamura, R.; Iwamatsu, Y.; Shimosato, D.; Niwa, H. Synergistic Action of Wnt and LIF in Maintaining Pluripotency of Mouse ES Cells. *Biochemical and Biophysical Research Communications* **2006**, *343* (1), 159–166. https://doi.org/10.1016/j.bbrc.2006.02.127.

(7) ten Berge, D.; Kurek, D.; Blauwkamp, T.; Koole, W.; Maas, A.; Eroglu, E.; Siu, R. K.; Nusse, R. Embryonic Stem Cells Require Wnt Proteins to Prevent Differentiation to Epiblast Stem Cells. *Nature Cell Biology* **2011**, *13* (9), 1070–1075. https://doi.org/10.1038/ncb2314.

(8) Davidson, K. C.; Adams, A. M.; Goodson, J. M.; McDonald, C. E.; Potter, J. C.; Berndt, J. D.; Biechele, T. L.; Taylor, R. J.; Moon, R. T. Wnt/β-Catenin Signaling Promotes Differentiation, Not Self-Renewal, of Human Embryonic Stem Cells and Is Repressed by Oct4. *PNAS* **2012**, *109* (12), 4485–4490. https://doi.org/10.1073/pnas.1118777109.

(9) Sumi, T.; Tsuneyoshi, N.; Nakatsuji, N.; Suemori, H. Defining Early Lineage Specification of Human Embryonic Stem Cells by the Orchestrated Balance of Canonical Wnt/β-Catenin, Activin/Nodal and BMP Signaling. *Development* **2008**, *135* (17), 2969–2979. https://doi.org/10.1242/dev.021121.

(10) Tsakiridis, A.; Huang, Y.; Blin, G.; Skylaki, S.; Wymeersch, F.; Osorno, R.; Economou, C.; Karagianni, E.; Zhao, S.; Lowell, S.; Wilson, V. Distinct Wnt-Driven Primitive Streak-like Populations Reflect in Vivo Lineage Precursors. *Development* **2014**, *141* (6), 1209–1221. https://doi.org/10.1242/dev.101014.

(11) Niehrs, C. The Complex World of WNT Receptor Signalling. *Nat. Rev. Mol. Cell Biol.* **2012**, *13* (12), 767–779. https://doi.org/10.1038/nrm3470.

(12) Fernandez, A.; Huggins, I. J.; Perna, L.; Brafman, D.; Lu, D.; Yao, S.; Gaasterland, T.; Carson, D. A.; Willert, K. The WNT Receptor FZD7 Is Required for Maintenance of the Pluripotent State in Human Embryonic Stem Cells. *Proc. Natl. Acad. Sci. U.S.A.* **2014**, *111* (4), 1409–1414. https://doi.org/10.1073/pnas.1323697111.

(13) Melchior, K.; Weiss, J.; Zaehres, H.; Kim, Y.; Lutzko, C.; Roosta, N.; Hescheler, J.; Müschen, M. The WNT Receptor FZD7 Contributes to Self-Renewal Signaling of Human Embryonic Stem Cells. *Biol Chem* **2008**, *389* (7), 897–903. https://doi.org/10.1515/BC.2008.108.

(14) Huggins, I. J.; Bos, T.; Gaylord, O.; Jessen, C.; Lonquich, B.; Puranen, A.; Richter, J.; Rossdam, C.; Brafman, D.; Gaasterland, T.; Willert, K. The WNT Target SP5 Negatively Regulates WNT Transcriptional Programs in Human Pluripotent Stem Cells. *Nat Commun* **2017**, *8* (1), 1034. https://doi.org/10.1038/s41467-017-01203-1.

(15) Gumber, D.; Do, M.; Suresh Kumar, N.; Sonavane, P. R.; Wu, C. C. N.; Cruz, L. S.; Grainger, S.; Carson, D.; Gaasterland, T.; Willert, K. Selective Activation of FZD7 Promotes Mesendodermal Differentiation of Human Pluripotent Stem Cells. *Elife* **2020**, *9*. https://doi.org/10.7554/eLife.63060.

(16) Kirikoshi, H.; Sekihara, H.; Katoh, M. Up-Regulation of Frizzled-7 (FZD7) in Human Gastric Cancer. *Int J Oncol* **2001**, *19* (1), 111–115.

(17) Merle, P.; Kim, M.; Herrmann, M.; Gupte, A.; Lefrançois, L.; Califano, S.; Trépo, C.; Tanaka, S.; Vitvitski, L.; de la Monte, S.; Wands, J. R. Oncogenic Role of the Frizzled-7/Beta-Catenin Pathway in Hepatocellular Carcinoma. *J Hepatol* **2005**, *43* (5), 854–862. https://doi.org/10.1016/j.jhep.2005.05.018.

(18) Pode-Shakked, N.; Harari-Steinberg, O.; Haberman-Ziv, Y.; Rom-Gross, E.; Bahar, S.; Omer, D.; Metsuyanim, S.; Buzhor, E.; Jacob-Hirsch, J.; Goldstein, R. S.; Mark-Danieli, M.; Dekel, B. Resistance or Sensitivity of Wilms' Tumor to Anti-FZD7 Antibody Highlights the Wnt Pathway as a Possible Therapeutic Target. *Oncogene* **2011**, *30* (14), 1664–1680. https://doi.org/10.1038/onc.2010.549.

(19) Tiwary, S.; Xu, L. FRIZZLED7 Is Required for Tumor Initiation and Metastatic Growth of Melanoma Cells. *PLoS One* **2016**, *11* (1), e0147638. https://doi.org/10.1371/journal.pone.0147638.

(20) Ueno, K.; Hazama, S.; Mitomori, S.; Nishioka, M.; Suehiro, Y.; Hirata, H.; Oka, M.; Imai, K.; Dahiya, R.; Hinoda, Y. Down-Regulation of Frizzled-7 Expression Decreases Survival, Invasion and Metastatic Capabilities of Colon Cancer Cells. *Br J Cancer* **2009**, *101* (8), 1374–1381. https://doi.org/10.1038/sj.bjc.6605307.

(21) Yang, L.; Wu, X.; Wang, Y.; Zhang, K.; Wu, J.; Yuan, Y.-C.; Deng, X.; Chen, L.; Kim, C. C. H.; Lau, S.; Somlo, G.; Yen, Y. FZD7 Has a Critical Role in Cell Proliferation in Triple Negative Breast Cancer. *Oncogene* **2011**, *30* (43), 4437–4446. https://doi.org/10.1038/onc.2011.145.

(22) Tan, M.; Asad, M.; Heong, V.; Wong, M. K.; Tan, T. Z.; Ye, J.; Kuay, K. T.; Thiery, J. P.; Scott, C.; Huang, R. Y.-J. The FZD7-TWIST1 Axis Is Responsible for Anoikis Resistance and Tumorigenesis in Ovarian Carcinoma. *Mol Oncol* **2019**, *13* (4), 757–780. https://doi.org/10.1002/1878-0261.12425.

(23) King, T. D.; Zhang, W.; Suto, M. J.; Li, Y. Frizzled7 as an Emerging Target for Cancer Therapy. *Cell Signal* **2012**, *24* (4), 846–851. https://doi.org/10.1016/j.cellsig.2011.12.009.

(24) Phesse, T.; Flanagan, D.; Vincan, E. Frizzled7: A Promising Achilles' Heel for Targeting the Wnt Receptor Complex to Treat Cancer. *Cancers (Basel)* **2016**, *8* (5). https://doi.org/10.3390/cancers8050050.

(25) Day, T. F.; Guo, X.; Garrett-Beal, L.; Yang, Y. Wnt/Beta-Catenin Signaling in Mesenchymal Progenitors Controls Osteoblast and Chondrocyte Differentiation during Vertebrate Skeletogenesis. *Dev Cell* **2005**, *8* (5), 739–750. https://doi.org/10.1016/j.devcel.2005.03.016.

(26) Madan, B.; McDonald, M. J.; Foxa, G. E.; Diegel, C. R.; Williams, B. O.; Virshup, D. M. Bone Loss from Wnt Inhibition Mitigated by Concurrent Alendronate Therapy. *Bone Research* **2018**, *6* (1), 1–10. https://doi.org/10.1038/s41413-018-0017-8.

(27) Maeda, K.; Kobayashi, Y.; Udagawa, N.; Uehara, S.; Ishihara, A.; Mizoguchi, T.; Kikuchi, Y.; Takada, I.; Kato, S.; Kani, S.; Nishita, M.; Marumo, K.; Martin, T. J.; Minami, Y.; Takahashi, N. Wnt5a-Ror2 Signaling between Osteoblast-Lineage Cells and Osteoclast Precursors Enhances Osteoclastogenesis. *Nat Med* **2012**, *18* (3), 405–412. https://doi.org/10.1038/nm.2653.

(28) Clevers, H.; Loh, K. M.; Nusse, R. Stem Cell Signaling. An Integral Program for Tissue Renewal and Regeneration: Wnt Signaling and Stem Cell Control. *Science* **2014**, *346* (6205), 1248012. https://doi.org/10.1126/science.1248012.

(29) Nusse, R.; Clevers, H. Wnt/β-Catenin Signaling, Disease, and Emerging Therapeutic Modalities. *Cell* **2017**, *169* (6), 985–999. https://doi.org/10.1016/j.cell.2017.05.016.

(30) Smith, A. Formative Pluripotency: The Executive Phase in a Developmental Continuum. *Development* **2017**, *144* (3), 365–373. https://doi.org/10.1242/dev.142679.

(31) Tesar, P. J.; Chenoweth, J. G.; Brook, F. A.; Davies, T. J.; Evans, E. P.; Mack, D. L.; Gardner, R. L.; McKay, R. D. G. New Cell Lines from Mouse Epiblast Share Defining Features with Human Embryonic Stem Cells. *Nature* **2007**, *448* (7150), 196–199. https://doi.org/10.1038/nature05972.

(32) D'Amour, K. A.; Bang, A. G.; Eliazer, S.; Kelly, O. G.; Agulnick, A. D.; Smart, N. G.; Moorman, M. A.; Kroon, E.; Carpenter, M. K.; Baetge, E. E. Production of Pancreatic Hormone–Expressing Endocrine Cells from Human Embryonic Stem Cells. *Nature Biotechnology* **2006**, *24* (11), 1392–1401. https://doi.org/10.1038/nbt1259.

(33) Blauwkamp, T. A.; Nigam, S.; Ardehali, R.; Weissman, I. L.; Nusse, R. Endogenous Wnt Signalling in Human Embryonic Stem Cells Generates an Equilibrium of Distinct Lineage-Specified Progenitors. *Nat Commun* **2012**, *3*, 1070. https://doi.org/10.1038/ncomms2064.

(34) Jiang, W.; Zhang, D.; Bursac, N.; Zhang, Y. WNT3 Is a Biomarker Capable of Predicting the Definitive Endoderm Differentiation Potential of HESCs. *Stem Cell Reports* **2013**, *1* (1), 46–52. https://doi.org/10.1016/j.stemcr.2013.03.003.

(35) Ross, J.; Busch, J.; Mintz, E.; Ng, D.; Stanley, A.; Brafman, D.; Sutton, V. R.; Van den Veyver, I.; Willert, K. A Rare Human Syndrome Provides Genetic Evidence That WNT Signaling Is Required for Reprogramming of Fibroblasts to Induced Pluripotent Stem Cells. *Cell Rep* **2014**, *9* (5), 1770–1780. https://doi.org/10.1016/j.celrep.2014.10.049.

(36) Ettenberg, S. A.; Charlat, O.; Daley, M. P.; Liu, S.; Vincent, K. J.; Stuart, D. D.; Schuller, A. G.; Yuan, J.; Ospina, B.; Green, J.; Yu, Q.; Walsh, R.; Li, S.; Schmitz, R.; Heine, H.; Bilic, S.; Ostrom, L.; Mosher, R.; Hartlepp, K. F.; Zhu, Z.; Fawell, S.; Yao, Y.-M.; Stover, D.; Finan, P. M.; Porter, J. A.; Sellers, W. R.; Klagge, I. M.; Cong, F. Inhibition of Tumorigenesis Driven by Different Wnt Proteins Requires Blockade of Distinct Ligand-Binding Regions by LRP6 Antibodies. *PNAS* **2010**, *107* (35), 15473–15478. https://doi.org/10.1073/pnas.1007428107.

(37) Grainger, S.; Nguyen, N.; Richter, J.; Setayesh, J.; Lonquich, B.; Oon, C. H.; Wozniak, J. M.; Barahona, R.; Kamei, C. N.; Houston, J.; Carrillo-Terrazas, M.; Drummond, I. A.; Gonzalez, D.; Willert, K.; Traver, D. EGFR Is Required for Wnt9a–Fzd9b Signalling Specificity in Haematopoietic Stem Cells. *Nature Cell Biology* **2019**, *21* (6), 721–730. https://doi.org/10.1038/s41556-019-0330-5.

(38) Veeman, M. T.; Slusarski, D. C.; Kaykas, A.; Louie, S. H.; Moon, R. T. Zebrafish Prickle, a Modulator of Noncanonical Wnt/Fz Signaling, Regulates Gastrulation Movements. *Curr Biol* **2003**, *13* (8), 680–685. https://doi.org/10.1016/s0960-9822(03)00240-9.

(39) Kim, K.-A.; Wagle, M.; Tran, K.; Zhan, X.; Dixon, M. A.; Liu, S.; Gros, D.; Korver, W.; Yonkovich, S.; Tomasevic, N.; Binnerts, M.; Abo, A. R-Spondin Family Members Regulate the Wnt Pathway by a Common Mechanism. *Mol Biol Cell* **2008**, *19* (6), 2588–2596. https://doi.org/10.1091/mbc.E08-02-0187.

(40) Tao, Y.; Mis, M.; Blazer, L.; Ustav, M., Jnr; Steinhart, Z.; Chidiac, R.; Kubarakos, E.; O'Brien, S.; Wang, X.; Jarvik, N.; Patel, N.; Adams, J.; Moffat, J.; Angers, S.; Sidhu, S. S. Tailored Tetravalent Antibodies Potently and Specifically Activate Wnt/Frizzled Pathways in Cells, Organoids and Mice. *eLife* **2019**, *8*, e46134. https://doi.org/10.7554/eLife.46134.

(41) Janda, C. Y.; Dang, L. T.; You, C.; Chang, J.; de Lau, W.; Zhong, Z. A.; Yan, K. S.; Marecic, O.; Siepe, D.; Li, X.; Moody, J. D.; Williams, B. O.; Clevers, H.; Piehler, J.; Baker, D.; Kuo, C. J.; Garcia, K. C. Surrogate Wnt Agonists That Phenocopy Canonical Wnt and β-Catenin Signalling. *Nature* **2017**, *545* (7653), 234–237. https://doi.org/10.1038/nature22306.

(42) Shibamoto, S.; Higano, K.; Takada, R.; Ito, F.; Takeichi, M.; Takada, S. Cytoskeletal Reorganization by Soluble Wnt-3a Protein Signalling. *Genes Cells* **1998**, *3* (10), 659–670. https://doi.org/10.1046/j.1365-2443.1998.00221.x.

(43) DeBruine, Z. J.; Xu, H. E.; Melcher, K. Assembly and Architecture of the Wnt/β-Catenin Signalosome at the Membrane. *Br J Pharmacol* **2017**, *174* (24), 4564–4574. https://doi.org/10.1111/bph.14048.

(44) Martyn, I.; Kanno, T. Y.; Ruzo, A.; Siggia, E. D.; Brivanlou, A. H. Self-Organization of a Human Organizer by Combined Wnt and Nodal Signalling. *Nature* **2018**, *558* (7708), 132–135. https://doi.org/10.1038/s41586-018-0150-y.

(45) Yoney, A.; Etoc, F.; Ruzo, A.; Carroll, T.; Metzger, J. J.; Martyn, I.; Li, S.; Kirst, C.; Siggia, E. D.; Brivanlou, A. H. WNT Signaling Memory Is Required for ACTIVIN to Function as a

Morphogen in Human Gastruloids. *eLife* **2018**, *7*, e38279. https://doi.org/10.7554/eLife.38279.

(46) Klein, P. S.; Melton, D. A. A Molecular Mechanism for the Effect of Lithium on Development. *Proc Natl Acad Sci U S A* **1996**, *93* (16), 8455–8459. https://doi.org/10.1073/pnas.93.16.8455.

(47) Ring, D. B.; Johnson, K. W.; Henriksen, E. J.; Nuss, J. M.; Goff, D.; Kinnick, T. R.; Ma, S. T.; Reeder, J. W.; Samuels, I.; Slabiak, T.; Wagman, A. S.; Hammond, M.-E. W.; Harrison, S. D. Selective Glycogen Synthase Kinase 3 Inhibitors Potentiate Insulin Activation of Glucose Transport and Utilization in Vitro and in Vivo. *Diabetes* **2003**, *52* (3), 588–595. https://doi.org/10.2337/diabetes.52.3.588.

(48) Stambolic, V.; Ruel, L.; Woodgett, J. R. Lithium Inhibits Glycogen Synthase Kinase-3 Activity and Mimics Wingless Signalling in Intact Cells. *Curr Biol* **1996**, *6* (12), 1664–1668. https://doi.org/10.1016/s0960-9822(02)70790-2.

(49) Gertow, K.; Hirst, C. E.; Yu, Q. C.; Ng, E. S.; Pereira, L. A.; Davis, R. P.; Stanley, E. G.; Elefanty, A. G. WNT3A Promotes Hematopoietic or Mesenchymal Differentiation from HESCs Depending on the Time of Exposure. *Stem Cell Reports* **2013**, *1* (1), 53–65. https://doi.org/10.1016/j.stemcr.2013.04.002.

(50) Huang, J.; Guo, X.; Li, W.; Zhang, H. Activation of Wnt/β-Catenin Signalling via GSK3 Inhibitors Direct Differentiation of Human Adipose Stem Cells into Functional Hepatocytes. *Scientific Reports* **2017**, *7* (1), 40716. https://doi.org/10.1038/srep40716.

(51) Kumar, N.; Richter, J.; Cutts, J.; Bush, K. T.; Trujillo, C.; Nigam, S. K.; Gaasterland, T.; Brafman, D.; Willert, K. Generation of an Expandable Intermediate Mesoderm Restricted Progenitor Cell Line from Human Pluripotent Stem Cells. *eLife* **2015**, *4*, e08413. https://doi.org/10.7554/eLife.08413.

(52) Loh, K. M.; Ang, L. T.; Zhang, J.; Kumar, V.; Ang, J.; Auyeong, J. Q.; Lee, K. L.; Choo, S. H.; Lim, C. Y.; Nichane, M.; Tan, J.; Noghabi, M. S.; Azzola, L.; Ng, E. S.; Durruthy-Durruthy, J.; Sebastiano, V.; Poellinger, L.; Elefanty, A. G.; Stanley, E. G.; Chen, Q.; Prabhakar, S.; Weissman, I. L.; Lim, B. Efficient Endoderm Induction from Human Pluripotent Stem Cells by Logically Directing Signals Controlling Lineage Bifurcations. *Cell Stem Cell* **2014**, *14* (2), 237–252. https://doi.org/10.1016/j.stem.2013.12.007.

(53) Naujok, O.; Diekmann, U.; Lenzen, S. The Generation of Definitive Endoderm from Human Embryonic Stem Cells Is Initially Independent from Activin A but Requires Canonical Wnt-Signaling. *Stem Cell Rev Rep* **2014**, *10* (4), 480–493. https://doi.org/10.1007/s12015-014-9509-0.

(54) Teo, A. K. K.; Valdez, I. A.; Dirice, E.; Kulkarni, R. N. Comparable Generation of Activin-Induced Definitive Endoderm via Additive Wnt or BMP Signaling in Absence of Serum. *Stem Cell Reports* **2014**, *3* (1), 5–14. https://doi.org/10.1016/j.stemcr.2014.05.007.

(55) Dijksterhuis, J. P.; Baljinnyam, B.; Stanger, K.; Sercan, H. O.; Ji, Y.; Andres, O.; Rubin, J. S.; Hannoush, R. N.; Schulte, G. Systematic Mapping of WNT-FZD Protein Interactions Reveals Functional Selectivity by Distinct WNT-FZD Pairs. *J. Biol. Chem.* **2015**, *290* (11), 6789–6798. https://doi.org/10.1074/jbc.M114.612648.

(56) Voloshanenko, O.; Gmach, P.; Winter, J.; Kranz, D.; Boutros, M. Mapping of Wnt-Frizzled Interactions by Multiplex CRISPR Targeting of Receptor Gene Families. *The FASEB Journal* **2017**, *31* (11), 4832–4844. https://doi.org/10.1096/fj.201700144R.

(57) D'Amour, K. A.; Agulnick, A. D.; Eliazer, S.; Kelly, O. G.; Kroon, E.; Baetge, E. E. Efficient Differentiation of Human Embryonic Stem Cells to Definitive Endoderm. *Nature Biotechnology* **2005**, *23* (12), 1534–1541. https://doi.org/10.1038/nbt1163.

(58) McGrath, K. E.; Koniski, A. D.; Maltby, K. M.; McGann, J. K.; Palis, J. Embryonic Expression and Function of the Chemokine SDF-1 and Its Receptor, CXCR4. *Dev Biol* **1999**, *213* (2), 442–456. https://doi.org/10.1006/dbio.1999.9405.

(59) Mootha, V. K.; Lindgren, C. M.; Eriksson, K.-F.; Subramanian, A.; Sihag, S.; Lehar, J.; Puigserver, P.; Carlsson, E.; Ridderstråle, M.; Laurila, E.; Houstis, N.; Daly, M. J.; Patterson, N.; Mesirov, J. P.; Golub, T. R.; Tamayo, P.; Spiegelman, B.; Lander, E. S.; Hirschhorn, J. N.; Altshuler, D.; Groop, L. C. PGC-1α-Responsive Genes Involved in Oxidative Phosphorylation Are Coordinately Downregulated in Human Diabetes. *Nature Genetics* **2003**, *34* (3), 267–273. https://doi.org/10.1038/ng1180.

(60) Subramanian, A.; Tamayo, P.; Mootha, V. K.; Mukherjee, S.; Ebert, B. L.; Gillette, M. A.; Paulovich, A.; Pomeroy, S. L.; Golub, T. R.; Lander, E. S.; Mesirov, J. P. Gene Set Enrichment Analysis: A Knowledge-Based Approach for Interpreting Genome-Wide Expression Profiles. *Proc. Natl. Acad. Sci. U.S.A.* **2005**, *102* (43), 15545–15550. https://doi.org/10.1073/pnas.0506580102.

(61) Cho, C.; Smallwood, P. M.; Nathans, J. Reck and Gpr124 Are Essential Receptor Cofactors for Wnt7a/Wnt7b-Specific Signaling in Mammalian CNS Angiogenesis and Blood-Brain Barrier Regulation. *Neuron* **2017**, *95* (5), 1056-1073.e5. https://doi.org/10.1016/j.neuron.2017.07.031.

(62) Eubelen, M.; Bostaille, N.; Cabochette, P.; Gauquier, A.; Tebabi, P.; Dumitru, A. C.; Koehler, M.; Gut, P.; Alsteens, D.; Stainier, D. Y. R.; Garcia-Pino, A.; Vanhollebeke, B. A Molecular Mechanism for Wnt Ligand-Specific Signaling. *Science* **2018**, *361* (6403). https://doi.org/10.1126/science.aat1178.

(63) Kita-Matsuo, H.; Barcova, M.; Prigozhina, N.; Salomonis, N.; Wei, K.; Jacot, J. G.; Nelson, B.; Spiering, S.; Haverslag, R.; Kim, C.; Talantova, M.; Bajpai, R.; Calzolari, D.; Terskikh, A.; McCulloch, A. D.; Price, J. H.; Conklin, B. R.; Chen, H. S. V.; Mercola, M. Lentiviral Vectors and Protocols for Creation of Stable HESC Lines for Fluorescent Tracking and Drug Resistance Selection of Cardiomyocytes. *PLOS ONE* **2009**, *4* (4), e5046. https://doi.org/10.1371/journal.pone.0005046.

(64) Wang, P.; Rodriguez, R. T.; Wang, J.; Ghodasara, A.; Kim, S. K. Targeting SOX17 in Human Embryonic Stem Cells Creates Unique Strategies for Isolating and Analyzing Developing Endoderm. *Cell Stem Cell* **2011**, *8* (3), 335–346. https://doi.org/10.1016/j.stem.2011.01.017.

(65) Touboul, T.; Hannan, N. R. F.; Corbineau, S.; Martinez, A.; Martinet, C.; Branchereau, S.; Mainot, S.; Strick-Marchand, H.; Pedersen, R.; Di Santo, J.; Weber, A.; Vallier, L. Generation of Functional Hepatocytes from Human Embryonic Stem Cells under Chemically Defined Conditions That Recapitulate Liver Development. *Hepatology* **2010**, *51* (5), 1754–1765. https://doi.org/10.1002/hep.23506.

(66) Workman, M. J.; Mahe, M. M.; Trisno, S.; Poling, H. M.; Watson, C. L.; Sundaram, N.; Chang, C.-F.; Schiesser, J.; Aubert, P.; Stanley, E. G.; Elefanty, A. G.; Miyaoka, Y.; Mandegar, M. A.; Conklin, B. R.; Neunlist, M.; Brugmann, S. A.; Helmrath, M. A.; Wells, J. M. Engineered Human Pluripotent-Stem-Cell-Derived Intestinal Tissues with a Functional Enteric Nervous System. *Nature Medicine* **2017**, *23* (1), 49–59. https://doi.org/10.1038/nm.4233.

(67) Ng, E. S.; Davis, R. P.; Azzola, L.; Stanley, E. G.; Elefanty, A. G. Forced Aggregation of Defined Numbers of Human Embryonic Stem Cells into Embryoid Bodies Fosters Robust, Reproducible Hematopoietic Differentiation. *Blood* **2005**, *106* (5), 1601–1603. https://doi.org/10.1182/blood-2005-03-0987.

(68) Ng, E. S.; Davis, R.; Stanley, E. G.; Elefanty, A. G. A Protocol Describing the Use of a Recombinant Protein-Based, Animal Product-Free Medium (APEL) for Human Embryonic Stem Cell Differentiation as Spin Embryoid Bodies. *Nature Protocols* **2008**, *3* (5), 768–776. https://doi.org/10.1038/nprot.2008.42.

(69) Richter, J.; Stanley, E. G.; Ng, E. S.; Elefanty, A. G.; Traver, D.; Willert, K. WNT9A Is a Conserved Regulator of Hematopoietic Stem and Progenitor Cell Development. *Genes (Basel)* **2018**, *9* (2). https://doi.org/10.3390/genes9020066.

(70) Kafri, P.; Hasenson, S. E.; Kanter, I.; Sheinberger, J.; Kinor, N.; Yunger, S.; Shav-Tal, Y. Quantifying β-Catenin Subcellular Dynamics and Cyclin D1 MRNA Transcription during Wnt Signaling in Single Living Cells. *eLife 5*. https://doi.org/10.7554/eLife.16748.

(71) Kelly, O. G.; Pinson, K. I.; Skarnes, W. C. The Wnt Co-Receptors Lrp5 and Lrp6 Are Essential for Gastrulation in Mice. *Development* **2004**, *131* (12), 2803–2815. https://doi.org/10.1242/dev.01137.

(72) Cho, C.; Wang, Y.; Smallwood, P. M.; Williams, J.; Nathans, J. Molecular Determinants in Frizzled, Reck, and Wnt7a for Ligand-Specific Signaling in Neurovascular Development. *eLife* **2019**, *8*, e47300. https://doi.org/10.7554/eLife.47300.

(73) Vallon, M.; Yuki, K.; Nguyen, T. D.; Chang, J.; Yuan, J.; Siepe, D.; Miao, Y.; Essler, M.; Noda, M.; Garcia, K. C.; Kuo, C. J. A RECK-WNT7 Receptor-Ligand Interaction Enables Isoform-Specific Regulation of Wnt Bioavailability. *Cell Rep* **2018**, *25* (2), 339-349.e9. https://doi.org/10.1016/j.celrep.2018.09.045.

(74) Willert, K. H. Isolation and Application of Bioactive Wnt Proteins. *Methods Mol Biol* **2008**, *468*, 17–29. https://doi.org/10.1007/978-1-59745-249-6_2.

(75) Takada, R.; Satomi, Y.; Kurata, T.; Ueno, N.; Norioka, S.; Kondoh, H.; Takao, T.; Takada, S. Monounsaturated Fatty Acid Modification of Wnt Protein: Its Role in Wnt Secretion. *Dev Cell* **2006**, *11* (6), 791–801. https://doi.org/10.1016/j.devcel.2006.10.003.

(76) Willert, K.; Brown, J. D.; Danenberg, E.; Duncan, A. W.; Weissman, I. L.; Reya, T.; Yates, J. R.; Nusse, R. Wnt Proteins Are Lipid-Modified and Can Act as Stem Cell Growth Factors. *Nature* **2003**, *423* (6938), 448–452. https://doi.org/10.1038/nature01611.

(77) Chen, H.; Lu, C.; Ouyang, B.; Zhang, H.; Huang, Z.; Bhatia, D.; Lee, S.-J.; Shah, D.; Sura, A.; Yeh, W.-C.; Li, Y. Development of Potent, Selective Surrogate WNT Molecules and Their

Application in Defining Frizzled Requirements. *Cell Chemical Biology* **2020**, *27* (5), 598-609.e4. https://doi.org/10.1016/j.chembiol.2020.02.009.

(78) Dang, L. T.; Miao, Y.; Ha, A.; Yuki, K.; Park, K.; Janda, C. Y.; Jude, K. M.; Mohan, K.; Ha, N.; Vallon, M.; Yuan, J.; Vilches-Moure, J. G.; Kuo, C. J.; Garcia, K. C.; Baker, D. Receptor Subtype Discrimination Using Extensive Shape Complementary Designed Interfaces. *Nature Structural & Molecular Biology* **2019**, *26* (6), 407–414. https://doi.org/10.1038/s41594-019-0224-z.

(79) Miao, Y.; Ha, A.; de Lau, W.; Yuki, K.; Santos, A. J. M.; You, C.; Geurts, M. H.; Puschhof, J.; Pleguezuelos-Manzano, C.; Peng, W. C.; Senlice, R.; Piani, C.; Buikema, J. W.; Gbenedio, O. M.; Vallon, M.; Yuan, J.; de Haan, S.; Hemrika, W.; Rösch, K.; Dang, L. T.; Baker, D.; Ott, M.; Depeille, P.; Wu, S. M.; Drost, J.; Nusse, R.; Roose, J. P.; Piehler, J.; Boj, S. F.; Janda, C. Y.; Clevers, H.; Kuo, C. J.; Garcia, K. C. Next-Generation Surrogate Wnts Support Organoid Growth and Deconvolute Frizzled Pleiotropy In Vivo. *Cell Stem Cell* **2020**, *27* (5), 840-851.e6. https://doi.org/10.1016/j.stem.2020.07.020.

(80) Hirai, H.; Matoba, K.; Mihara, E.; Arimori, T.; Takagi, J. Crystal Structure of a Mammalian Wnt–Frizzled Complex. *Nature Structural & Molecular Biology* **2019**, *26* (5), 372–379. https://doi.org/10.1038/s41594-019-0216-z.

(81) Nile, A. H.; Mukund, S.; Stanger, K.; Wang, W.; Hannoush, R. N. Unsaturated Fatty Acyl Recognition by Frizzled Receptors Mediates Dimerization upon Wnt Ligand Binding. *Proc Natl Acad Sci U S A* **2017**, *114* (16), 4147–4152. https://doi.org/10.1073/pnas.1618293114.

(82) Morrell, N. T.; Leucht, P.; Zhao, L.; Kim, J.-B.; Berge, D. ten; Ponnusamy, K.; Carre, A. L.; Dudek, H.; Zachlederova, M.; McElhaney, M.; Brunton, S.; Gunzner, J.; Callow, M.; Polakis, P.; Costa, M.; Zhang, X. M.; Helms, J. A.; Nusse, R. Liposomal Packaging Generates Wnt Protein with In Vivo Biological Activity. *PLOS ONE* **2008**, *3* (8), e2930. https://doi.org/10.1371/journal.pone.0002930.

(83) Mikels, A. J.; Nusse, R. Purified Wnt5a Protein Activates or Inhibits Beta-Catenin-TCF Signaling Depending on Receptor Context. *PLoS Biol* **2006**, *4* (4), e115. https://doi.org/10.1371/journal.pbio.0040115.

(84) Chen, G.; Gulbranson, D. R.; Hou, Z.; Bolin, J. M.; Ruotti, V.; Probasco, M. D.; Smuga-Otto, K.; Howden, S. E.; Diol, N. R.; Propson, N. E.; Wagner, R.; Lee, G. O.; Antosiewicz-Bourget, J.; Teng, J. M. C.; Thomson, J. A. Chemically Defined Conditions for Human IPSC Derivation and Culture. *Nature Methods* **2011**, *8* (5), 424–429. https://doi.org/10.1038/nmeth.1593.

(85) Trapnell, C.; Hendrickson, D. G.; Sauvageau, M.; Goff, L.; Rinn, J. L.; Pachter, L. Differential Analysis of Gene Regulation at Transcript Resolution with RNA-Seq. *Nature Biotechnology* **2013**, *31* (1), 46–53. https://doi.org/10.1038/nbt.2450.

(86) Trapnell, C.; Roberts, A.; Goff, L.; Pertea, G.; Kim, D.; Kelley, D. R.; Pimentel, H.; Salzberg, S. L.; Rinn, J. L.; Pachter, L. Differential Gene and Transcript Expression Analysis of RNA-Seq Experiments with TopHat and Cufflinks. *Nature Protocols* **2012**, *7* (3), 562–578. https://doi.org/10.1038/nprot.2012.016.

(87) Sturn, A.; Quackenbush, J.; Trajanoski, Z. Genesis: Cluster Analysis of Microarray Data. *Bioinformatics* **2002**, *18* (1), 207–208. https://doi.org/10.1093/bioinformatics/18.1.207.

(88) Groden, J.; Thliveris, A.; Samowitz, W.; Carlson, M.; Gelbert, L.; Albertsen, H.; Joslyn, G.; Stevens, J.; Spirio, L.; Robertson, M.; Sargeant, L.; Krapcho, K.; Wolff, E.; Burt, R.; Hughes, J. P.; Warrington, J.; McPherson, J.; Wasmuth, J.; Paslier, D. L.; Abderrahim, H.; Cohen, D.; Leppert, M.; White, R. Identification and Characterization of the Familial Adenomatous Polyposis Coli Gene. *Cell* **1991**, *66* (3), 589–600. https://doi.org/10.1016/0092-8674(81)90021-0.

(89) Mazzoni, S. M.; Fearon, E. R. AXIN1 and AXIN2 Variants in Gastrointestinal Cancers. *Cancer Lett* **2014**, *355* (1), 1–8. https://doi.org/10.1016/j.canlet.2014.09.018.

(90) Kim, S.; Jeong, and S. Mutation Hotspots in the β-Catenin Gene: Lessons from the Human Cancer Genome Databases. **2019**, *42* (1), 8–16. https://doi.org/10.14348/molcells.2018.0436.

(91) Seshagiri, S.; Stawiski, E. W.; Durinck, S.; Modrusan, Z.; Storm, E. E.; Conboy, C. B.; Chaudhuri, S.; Guan, Y.; Janakiraman, V.; Jaiswal, B. S.; Guillory, J.; Ha, C.; Dijkgraaf, G. J. P.; Stinson, J.; Gnad, F.; Huntley, M. A.; Degenhardt, J. D.; Haverty, P. M.; Bourgon, R.; Wang, W.; Koeppen, H.; Gentleman, R.; Starr, T. K.; Zhang, Z.; Largaespada, D. A.; Wu, T. D.; de Sauvage, F. J. Recurrent R-Spondin Fusions in Colon Cancer. *Nature* **2012**, *488* (7413), 660–664. https://doi.org/10.1038/nature11282.

(92) Spit, M.; Fenderico, N.; Jordens, I.; Radaszkiewicz, T.; Lindeboom, R. G.; Bugter, J. M.; Cristobal, A.; Ootes, L.; van Osch, M.; Janssen, E.; Boonekamp, K. E.; Hanakova, K.; Potesil, D.; Zdrahal, Z.; Boj, S. F.; Medema, J. P.; Bryja, V.; Koo, B.-K.; Vermeulen, M.; Maurice, M. M. RNF43 Truncations Trap CK1 to Drive Niche-Independent Self-Renewal in Cancer. *The EMBO Journal* **2020**, *39* (18), e103932. https://doi.org/10.15252/embj.2019103932.

(93) Niehrs, C. The Complex World of WNT Receptor Signalling. *Nature Reviews Molecular Cell Biology* **2012**, *13* (12), 767–779. https://doi.org/10.1038/nrm3470.

(94) Zeng, C.-M.; Chen, Z.; Fu, L. Frizzled Receptors as Potential Therapeutic Targets in Human Cancers. *Int J Mol Sci* **2018**, *19* (5). https://doi.org/10.3390/ijms19051543.

(95) Jung, Y.-S.; Park, J.-I. Wnt Signaling in Cancer: Therapeutic Targeting of Wnt Signaling beyond β-Catenin and the Destruction Complex. *Experimental & Molecular Medicine* **2020**, *52* (2), 183–191. https://doi.org/10.1038/s12276-020-0380-6.

(96) Davis, S. L.; Cardin, D. B.; Shahda, S.; Lenz, H.-J.; Dotan, E.; O'Neil, B. H.; Kapoun, A. M.; Stagg, R. J.; Berlin, J.; Messersmith, W. A.; Cohen, S. J. A Phase 1b Dose Escalation Study of Wnt Pathway Inhibitor Vantictumab in Combination with Nab-Paclitaxel and Gemcitabine in Patients with Previously Untreated Metastatic Pancreatic Cancer. *Invest New Drugs* **2020**, *38* (3), 821–830. https://doi.org/10.1007/s10637-019-00824-1.

(97) Gurney, A.; Axelrod, F.; Bond, C. J.; Cain, J.; Chartier, C.; Donigan, L.; Fischer, M.; Chaudhari, A.; Ji, M.; Kapoun, A. M.; Lam, A.; Lazetic, S.; Ma, S.; Mitra, S.; Park, I.-K.; Pickell, K.; Sato, A.; Satyal, S.; Stroud, M.; Tran, H.; Yen, W.-C.; Lewicki, J.; Hoey, T. Wnt Pathway Inhibition via the Targeting of Frizzled Receptors Results in Decreased Growth and Tumorigenicity of Human Tumors. *Proc Natl Acad Sci U S A* **2012**, *109* (29), 11717–11722. https://doi.org/10.1073/pnas.1120068109.

(98) Mita, M. M.; Becerra, C.; Richards, D. A.; Mita, A. C.; Shagisultanova, E.; Osborne, C. R. C.; O'Shaughnessy, J.; Zhang, C.; Henner, R.; Kapoun, A. M.; Xu, L.; Dupont, J.; Brachmann, R. K.; Farooki, A.; Diamond, J. R. Phase 1b Study of WNT Inhibitor Vantictumab (VAN, Human Monoclonal Antibody) with Paclitaxel (P) in Patients (Pts) with 1st- to 3rd-Line Metastatic HER2-Negative Breast Cancer (BC). *JCO* **2016**, *34* (15_suppl), 2516–2516. https://doi.org/10.1200/JCO.2016.34.15_suppl.2516.

(99) Smith, D. C.; Rosen, L. S.; Chugh, R.; Goldman, J. W.; Xu, L.; Kapoun, A.; Brachmann, R. K.; Dupont, J.; Stagg, R. J.; Tolcher, A. W.; Papadopoulos, K. P. First-in-Human Evaluation of the Human Monoclonal Antibody Vantictumab (OMP-18R5; Anti-Frizzled) Targeting the WNT Pathway in a Phase I Study for Patients with Advanced Solid Tumors. *JCO* **2013**, *31* (15_suppl), 2540–2540. https://doi.org/10.1200/jco.2013.31.15_suppl.2540.

(100) Giraudet, A.-L.; Badel, J.-N.; Cassier, P.; Desuzinges, C.; Kriza, D.; Perol, D.; Blay, J.-Y. SYNFRIZZ-A Phase Ia/Ib of a Radiolabelled Monoclonal AB for the Treatment of Relapsing Synovial Sarcoma. *Journal of Nuclear Medicine* **2014**, *55* (supplement 1), 223–223.

(101) Damelin, M.; Bankovich, A.; Bernstein, J.; Lucas, J.; Chen, L.; Williams, S.; Park, A.; Aguilar, J.; Ernstoff, E.; Charati, M.; Dushin, R.; Aujay, M.; Lee, C.; Ramoth, H.; Milton, M.; Hampl, J.; Lazetic, S.; Pulito, V.; Rosfjord, E.; Sun, Y.; King, L.; Barletta, F.; Betts, A.; Guffroy, M.; Falahatpisheh, H.; O'Donnell, C. J.; Stull, R.; Pysz, M.; Escarpe, P.; Liu, D.; Foord, O.; Gerber, H. P.; Sapra, P.; Dylla, S. J. A PTK7-Targeted Antibody-Drug Conjugate Reduces Tumor-Initiating Cells and Induces Sustained Tumor Regressions. *Science Translational Medicine* **2017**, *9* (372). https://doi.org/10.1126/scitranslmed.aag2611.

(102) Fischer, M. M.; Cancilla, B.; Yeung, V. P.; Cattaruzza, F.; Chartier, C.; Murriel, C. L.; Cain, J.; Tam, R.; Cheng, C.-Y.; Evans, J. W.; O'Young, G.; Song, X.; Lewicki, J.; Kapoun, A. M.; Gurney, A.; Yen, W.-C.; Hoey, T. WNT Antagonists Exhibit Unique Combinatorial Antitumor Activity with Taxanes by Potentiating Mitotic Cell Death. *Science Advances* **2017**, *3* (6), e1700090. https://doi.org/10.1126/sciadv.1700090.

(103) Jimeno, A.; Gordon, M.; Chugh, R.; Messersmith, W.; Mendelson, D.; Dupont, J.; Stagg, R.; Kapoun, A. M.; Xu, L.; Uttamsingh, S.; Brachmann, R. K.; Smith, D. C. A First-in-Human Phase I Study of the Anticancer Stem Cell Agent Ipafricept (OMP-54F28), a Decoy Receptor for Wnt Ligands, in Patients with Advanced Solid Tumors. *Clin Cancer Res* **2017**, *23* (24), 7490–7497. https://doi.org/10.1158/1078-0432.CCR-17-2157.

(104) Moore, K. N.; Gunderson, C. C.; Sabbatini, P.; McMeekin, D. S.; Mantia-Smaldone, G.; Burger, R. A.; Morgan, M. A.; Kapoun, A. M.; Brachmann, R. K.; Stagg, R.; Farooki, A.; O'Cearbhaill, R. E. A Phase 1b Dose Escalation Study of Ipafricept (OMP54F28) in Combination with Paclitaxel and Carboplatin in Patients with Recurrent Platinum-Sensitive Ovarian Cancer. *Gynecol Oncol* **2019**, *154* (2), 294–301. https://doi.org/10.1016/j.ygyno.2019.04.001.

(105) Madan, B.; Ke, Z.; Harmston, N.; Ho, S. Y.; Frois, A. O.; Alam, J.; Jeyaraj, D. A.; Pendharkar, V.; Ghosh, K.; Virshup, I. H.; Manoharan, V.; Ong, E. H. Q.; Sangthongpitag, K.; Hill, J.; Petretto, E.; Keller, T. H.; Lee, M. A.; Matter, A.; Virshup, D. M. Wnt Addiction of Genetically Defined Cancers Reversed by PORCN Inhibition. *Oncogene* **2016**, *35* (17), 2197–2207. https://doi.org/10.1038/onc.2015.280.

(106) Ng, M.; Tan, D. S.; Subbiah, V.; Weekes, C. D.; Teneggi, V.; Diermayr, V.; Ethirajulu, K.; Yeo, P.; Chen, D.; Blanchard, S.; Nellore, R.; Gan, B. H.; Yasin, M.; Lee, L. H.; Lee, M. A.; Hill, J.; Madan, B.; Virshup, D.; Matter, A. First-in-Human Phase 1 Study of ETC-159 an Oral PORCN Inhbitor in Patients with Advanced Solid Tumours. *JCO* **2017**, *35* (15_suppl), 2584–2584. https://doi.org/10.1200/JCO.2017.35.15_suppl.2584.

(107) Tan, D.; Ng, M.; Subbiah, V.; Messersmith, W.; Teneggi, V.; Diermayr, V.; Ethirajulu, K.; Yeo, P.; Gan, B.; Lee, L.; Blanchard, S.; Nellore, R.; Yasin, M.; Umrani, D.; Lee, M.; Hill, J.; Madan, B.; Virshup, D. M.; Matter, A. 1427 - Phase 1 Extension Study of ETC-159 an Oral PORCN Inhibitor Administered with Bone Protective Treatment, in Patients with Advanced Solid Tumours.; Annals of Oncology (2018) 29 (suppl_9): ix23-ix27. 10.1093/annonc/mdy430, 2018.

(108) Verhaak, R. G. W.; Tamayo, P.; Yang, J.-Y.; Hubbard, D.; Zhang, H.; Creighton, C. J.; Fereday, S.; Lawrence, M.; Carter, S. L.; Mermel, C. H.; Kostic, A. D.; Etemadmoghadam, D.; Saksena, G.; Cibulskis, K.; Duraisamy, S.; Levanon, K.; Sougnez, C.; Tsherniak, A.; Gomez, S.; Onofrio, R.; Gabriel, S.; Chin, L.; Zhang, N.; Spellman, P. T.; Zhang, Y.; Akbani, R.; Hoadley, K. A.; Kahn, A.; Köbel, M.; Huntsman, D.; Soslow, R. A.; Defazio, A.; Birrer, M. J.; Gray, J. W.; Weinstein, J. N.; Bowtell, D. D.; Drapkin, R.; Mesirov, J. P.; Getz, G.; Levine, D. A.; Meyerson, M.; Cancer Genome Atlas Research Network. Prognostically Relevant Gene Signatures of High-Grade Serous Ovarian Carcinoma. *J Clin Invest* **2013**, *123* (1), 517–525. https://doi.org/10.1172/JCI65833.

(109) Aysola, K.; Desai, A.; Welch, C.; Xu, J.; Qin, Y.; Reddy, V.; Matthews, R.; Owens, C.; Okoli, J.; Beech, D. J.; Piyathilake, C. J.; Reddy, S. P.; Rao, V. N. Triple Negative Breast Cancer - An Overview. *Hereditary Genet* **2013**, *2013* (Suppl 2). https://doi.org/10.4172/2161-1041.S2-001.

(110) Adams, S. R.; Yang, H. C.; Savariar, E. N.; Aguilera, J.; Crisp, J. L.; Jones, K. A.; Whitney, M. A.; Lippman, S. M.; Cohen, E. E. W.; Tsien, R. Y.; Advani, S. J. Anti-Tubulin Drugs Conjugated to Anti-ErbB Antibodies Selectively Radiosensitize. *Nature Communications* **2016**, *7* (1), 13019. https://doi.org/10.1038/ncomms13019.

(111) Hingorani, D. V.; Doan, M. K.; Camargo, M. F.; Aguilera, J.; Song, S. M.; Pizzo, D.; Scanderbeg, D. J.; Cohen, E. E. W.; Lowy, A. M.; Adams, S. R.; Advani, S. J. Precision Chemoradiotherapy for HER2 Tumors Using Antibody Conjugates of an Auristatin Derivative with Reduced Cell Permeability. *Mol Cancer Ther* **2020**, *19* (1), 157–167. https://doi.org/10.1158/1535-7163.MCT-18-1302.

(112) Dubowchik, G. M.; Mosure, K.; Knipe, J. O.; Firestone, R. A. Cathepsin B-Sensitive Dipeptide Prodrugs. 2. Models of Anticancer Drugs Paclitaxel (Taxol®), Mitomycin C and Doxorubicin. *Bioorganic & Medicinal Chemistry Letters* **1998**, *8* (23), 3347–3352. https://doi.org/10.1016/S0960-894X(98)00610-6.

(113) Yu, H.; Ye, X.; Guo, N.; Nathans, J. Frizzled 2 and Frizzled 7 Function Redundantly in Convergent Extension and Closure of the Ventricular Septum and Palate: Evidence for a Network of Interacting Genes. *Development* **2012**, *139* (23), 4383–4394. https://doi.org/10.1242/dev.083352.

(114) Fuerer, C.; Nusse, R. Lentiviral Vectors to Probe and Manipulate the Wnt Signaling Pathway. *PLOS ONE* **2010**, *5* (2), e9370. https://doi.org/10.1371/journal.pone.0009370.

(115) Flanagan, D. J.; Phesse, T. J.; Barker, N.; Schwab, R. H. M.; Amin, N.; Malaterre, J.; Stange, D. E.; Nowell, C. J.; Currie, S. A.; Saw, J. T. S.; Beuchert, E.; Ramsay, R. G.; Sansom, O. J.; Ernst, M.; Clevers, H.; Vincan, E. Frizzled7 Functions as a Wnt Receptor in Intestinal Epithelial Lgr5(+) Stem Cells. *Stem Cell Reports* **2015**, *4* (5), 759–767. https://doi.org/10.1016/j.stemcr.2015.03.003.

(116) Sato, T.; van Es, J. H.; Snippert, H. J.; Stange, D. E.; Vries, R. G.; van den Born, M.; Barker, N.; Shroyer, N. F.; van de Wetering, M.; Clevers, H. Paneth Cells Constitute the Niche for Lgr5 Stem Cells in Intestinal Crypts. *Nature* **2011**, *469* (7330), 415–418. https://doi.org/10.1038/nature09637.

(117) Chakrabarti, R.; Wei, Y.; Hwang, J.; Hang, X.; Andres Blanco, M.; Choudhury, A.; Tiede, B.; Romano, R.-A.; DeCoste, C.; Mercatali, L.; Ibrahim, T.; Amadori, D.; Kannan, N.; Eaves, C. J.; Sinha, S.; Kang, Y. ΔNp63 Promotes Stem Cell Activity in Mammary Gland Development and Basal-like Breast Cancer by Enhancing Fzd7 Expression and Wnt Signalling. *Nat Cell Biol* **2014**, *16* (10), 1004–1015, 1–13. https://doi.org/10.1038/ncb3040.

(118) Wang, Y.; Zhao, G.; Condello, S.; Huang, H.; Cardenas, H.; Tanner, E. J.; Wei, J.; Ji, Y.; Li, J.; Tan, Y.; Davuluri, R. V.; Peter, M. E.; Cheng, J.-X.; Matei, D. Frizzled-7 Identifies Platinum-Tolerant Ovarian Cancer Cells Susceptible to Ferroptosis. *Cancer Res* **2021**, *81* (2), 384–399. https://doi.org/10.1158/0008-5472.CAN-20-1488.

(119) Condello, S.; Sima, L.; Ivan, C.; Cardenas, H.; Schiltz, G.; Mishra, R. K.; Matei, D. Tissue Tranglutaminase Regulates Interactions between Ovarian Cancer Stem Cells and the Tumor Niche. *Cancer Res* **2018**, *78* (11), 2990–3001. https://doi.org/10.1158/0008-5472.CAN-17-2319.

(120) Yin, P.; Bai, Y.; Wang, Z.; Sun, Y.; Gao, J.; Na, L.; Zhang, Z.; Wang, W.; Zhao, C. Non-Canonical Fzd7 Signaling Contributes to Breast Cancer Mesenchymal-like Stemness Involving Col6a1. *Cell Commun Signal* **2020**, *18* (1), 143. https://doi.org/10.1186/s12964-020-00646-2.

(121) Choijamts, B.; Jimi, S.; Kondo, T.; Naganuma, Y.; Matsumoto, T.; Kuroki, M.; Iwasaki, H.; Emoto, M. CD133+ Cancer Stem Cell–like Cells Derived from Uterine Carcinosarcoma (Malignant Mixed Müllerian Tumor). *STEM CELLS* **2011**, *29* (10), 1485–1495. https://doi.org/10.1002/stem.711.

(122) Flanagan, D. J.; Barker, N.; Costanzo, N. S. D.; Mason, E. A.; Gurney, A.; Meniel, V. S.; Koushyar, S.; Austin, C. R.; Ernst, M.; Pearson, H. B.; Boussioutas, A.; Clevers, H.; Phesse, T. J.; Vincan, E. Frizzled-7 Is Required for Wnt Signaling in Gastric Tumors with and Without Apc Mutations. *Cancer Res* **2019**, *79* (5), 970–981. https://doi.org/10.1158/0008-5472.CAN-18-2095.

(123) Rahman, M.; Jackson, L. K.; Johnson, W. E.; Li, D. Y.; Bild, A. H.; Piccolo, S. R. Alternative Preprocessing of RNA-Sequencing Data in The Cancer Genome Atlas Leads to Improved Analysis Results. *Bioinformatics* **2015**, *31* (22), 3666–3672. https://doi.org/10.1093/bioinformatics/btv377.

(124) Melchior, K.; Weiß, J.; Zaehres, H.; Kim, Y.; Lutzko, C.; Roosta, N.; Hescheler, J.; Müschen, M. The WNT Receptor FZD7 Contributes to Self-Renewal Signaling of Human

Embryonic Stem Cells. *Biological Chemistry* **2008**, *389* (7), 897–903. https://doi.org/10.1515/BC.2008.108.

(125) Zorn, A. M.; Wells, J. M. Vertebrate Endoderm Development and Organ Formation. *Annu Rev Cell Dev Biol* **2009**, *25*, 221–251. https://doi.org/10.1146/annurev.cellbio.042308.113344.

(126) D'Amour, K. A.; Bang, A. G.; Eliazer, S.; Kelly, O. G.; Agulnick, A. D.; Smart, N. G.; Moorman, M. A.; Kroon, E.; Carpenter, M. K.; Baetge, E. E. Production of Pancreatic Hormone–Expressing Endocrine Cells from Human Embryonic Stem Cells. *Nature Biotechnology* **2006**, *24* (11), 1392–1401. https://doi.org/10.1038/nbt1259.

(127) Du, C.; Feng, Y.; Qiu, D.; Xu, Y.; Pang, M.; Cai, N.; Xiang, A. P.; Zhang, Q. Highly Efficient and Expedited Hepatic Differentiation from Human Pluripotent Stem Cells by Pure Small-Molecule Cocktails. *Stem Cell Research & Therapy* **2018**, *9* (1), 58. https://doi.org/10.1186/s13287-018-0794-4.

(128) Moo, T.-A.; Sanford, R.; Dang, C.; Morrow, M. Overview of Breast Cancer Therapy. *PET Clin* **2018**, *13* (3), 339–354. https://doi.org/10.1016/j.cpet.2018.02.006.

(129) Masters, J. C.; Nickens, D. J.; Xuan, D.; Shazer, R. L.; Amantea, M. Clinical Toxicity of Antibody Drug Conjugates: A Meta-Analysis of Payloads. *Invest New Drugs* **2018**, *36* (1), 121–135. https://doi.org/10.1007/s10637-017-0520-6.

(130) Lassman, A. B.; van den Bent, M. J.; Gan, H. K.; Reardon, D. A.; Kumthekar, P.; Butowski, N.; Lwin, Z.; Mikkelsen, T.; Nabors, L. B.; Papadopoulos, K. P.; Penas-Prado, M.; Simes, J.; Wheeler, H.; Walbert, T.; Scott, A. M.; Gomez, E.; Lee, H.-J.; Roberts-Rapp, L.; Xiong, H.; Ansell, P. J.; Bain, E.; Holen, K. D.; Maag, D.; Merrell, R. Safety and Efficacy of Depatuxizumab Mafodotin + Temozolomide in Patients with EGFR-Amplified, Recurrent Glioblastoma: Results from an International Phase I Multicenter Trial. *Neuro Oncol* **2019**, *21* (1), 106–114. https://doi.org/10.1093/neuonc/noy091.

(131) Verma, S.; Miles, D.; Gianni, L.; Krop, I. E.; Welslau, M.; Baselga, J.; Pegram, M.; Oh, D.-Y.; Diéras, V.; Guardino, E.; Fang, L.; Lu, M. W.; Olsen, S.; Blackwell, K.; EMILIA Study Group. Trastuzumab Emtansine for HER2-Positive Advanced Breast Cancer. *N Engl J Med* **2012**, *367* (19), 1783–1791. https://doi.org/10.1056/NEJMoa1209124.

(132) Moore, K. N.; Oza, A. M.; Colombo, N.; Oaknin, A.; Scambia, G.; Lorusso, D.; Konecny, G. E.; Banerjee, S.; Murphy, C. G.; Tanyi, J. L.; Hirte, H.; Konner, J. A.; Lim, P. C.; Prasad-Hayes, M.; Monk, B. J.; Pautier, P.; Wang, J.; Berkenblit, A.; Vergote, I.; Birrer, M. J. Phase III, Randomized Trial of Mirvetuximab Soravtansine versus Chemotherapy in Patients with Platinum-Resistant Ovarian Cancer: Primary Analysis of FORWARD I. *Ann Oncol* **2021**, *32* (6), 757–765. https://doi.org/10.1016/j.annonc.2021.02.017.

(133) Bardia, A.; Hurvitz, S. A.; Tolaney, S. M.; Loirat, D.; Punie, K.; Oliveira, M.; Brufsky, A.; Sardesai, S. D.; Kalinsky, K.; Zelnak, A. B.; Weaver, R.; Traina, T.; Dalenc, F.; Aftimos, P.; Lynce, F.; Diab, S.; Cortés, J.; O'Shaughnessy, J.; Diéras, V.; Ferrario, C.; Schmid, P.; Carey, L. A.; Gianni, L.; Piccart, M. J.; Loibl, S.; Goldenberg, D. M.; Hong, Q.; Olivo, M. S.; Itri, L. M.; Rugo, H. S. Sacituzumab Govitecan in Metastatic Triple-Negative Breast Cancer. *New England Journal of Medicine* **2021**, *384* (16), 1529–1541. https://doi.org/10.1056/NEJMoa2028485.

(134) Kowalski, M.; Guindon, J.; Brazas, L.; Moore, C.; Entwistle, J.; Cizeau, J.; Jewett, M. A. S.; MacDonald, G. C. A Phase II Study of Oportuzumab Monatox: An Immunotoxin Therapy for Patients with Noninvasive Urothelial Carcinoma in Situ Previously Treated with Bacillus Calmette-Guérin. *J Urol* **2012**, *188* (5), 1712–1718. https://doi.org/10.1016/j.juro.2012.07.020.

(135) Abu-Yousif, A. O.; Bannerman, B. M.; Cvet, D.; Gallery, M.; Ganno, M. L.; Smith, M. D.; Lai, K. C.; Keating, T. A.; Bolleddula, J.; Stringer, B.; Qian, M. G.; Kamali, A.; Eng, K.; Koseoglu, S.; Xia, C. Q.; Veiby, O. P. Abstract B120: TAK-164, a GCC-Targeted Antibody-Drug Conjugate (ADC) for the Treatment of Colorectal Cancers and Other GI Malignancies. *Mol Cancer Ther* **2018**, *17* (1 Supplement), B120–B120. https://doi.org/10.1158/1535-7163.TARG-17-B120.